AIP | Review of Scientific Instruments

Invited Review Article: Interferometric gravity wave detectors

G. Cella and A. Giazotto

Citation: Rev. Sci. Instrum. **82**, 101101 (2011); doi: 10.1063/1.3652857
View online: http://dx.doi.org/10.1063/1.3652857
View Table of Contents: http://rsi.aip.org/resource/1/RSINAK/v82/i10
Published by the American Institute of Physics.

Related Articles

Characterization of near-terahertz complementary metal-oxide semiconductor circuits using a Fourier-transform interferometer
Rev. Sci. Instrum. 82, 103106 (2011)

Etched multimode microfiber knot-type loop interferometer refractive index sensor
Rev. Sci. Instrum. 82, 095107 (2011)

Demonstration of a self-mixing displacement sensor based on terahertz quantum cascade lasers
Appl. Phys. Lett. 99, 081108 (2011)

Note: High speed optical profiler based on a phase-shifting technique using frequency-scanning lasers
Rev. Sci. Instrum. 82, 086111 (2011)

Bistable transmission of antiferromagnetic Fabry-Perot resonator
J. Appl. Phys. 110, 023512 (2011)

Additional information on Rev. Sci. Instrum.

Journal Homepage: http://rsi.aip.org
Journal Information: http://rsi.aip.org/about/about_the_journal
Top downloads: http://rsi.aip.org/features/most_downloaded
Information for Authors: http://rsi.aip.org/authors

ADVERTISEMENT



Downloaded 02 Nov 2011 to 180.149.51.196. Redistribution subject to AIP license or copyright; see http://rsi.aip.org/about/rights_and_permissions

Invited Review Article: Interferometric gravity wave detectors

G. Cella[1,a)] and A. Giazotto[1,2,b)]
[1]*Istituto Nazionale di Fisica Nucleare Sez. Pisa, Largo Bruno Pontecorvo 3, 56127 Pisa, Italy*
[2]*European Gravitational Observatory (EGO), Via E. Amaldi 56021 S. Stefano di Macerata Cascina (Pi), Italy*

(Received 22 October 2010; accepted 8 August 2011; published online 25 October 2011)

A direct detection of gravitational waves is still lacking today. A network of several earthbound interferometric detectors is currently operating with a continuously improving sensitivity. The window of interest for observation has a lower cut off in the frequency domain below some tens of hertz, determined by the effect of seismic motion. For larger frequencies, the sensitivity is limited by thermal effects below few hundreds of hertz and by the quantum nature of light above that value. Each of these sources of noise pose a big technological challenge to experimentalists, and there are big expectations for the next generation of detectors. A reduction of thermal effects by at least one order of magnitude will be obtained with new and carefully designed materials. At that point the quantum nature of light will become an issue, and the use of quantum non-demolition techniques will become mandatory. In this review, we discuss interferometric detection of gravitational waves from an instrumental point of view. We try to address conceptually important issues with an audience of non-experts in mind. A particular emphasis is given to the description of the current limitations and to the perspectives of beating them. © *2011 American Institute of Physics*. [doi:10.1063/1.3652857]

I. INTRODUCTION

Gravitation is by far the weakest of the known fundamental interactions. In spite of that it has a dominant role in the dynamics of the stars and of the universe in general. The currently accepted theory of gravitation, general relativity, has its roots in the principles of equivalence and general covariance. It has been defined as the most elegant physical theory we have, and it is quite singular in that it was formulated by Einstein on a conceptual basis without the strict necessity of explaining experimental facts.

One of the reasons for this is that the vast majority of the subtle and fascinating phenomena the theory predicts are very difficult to test experimentally as very high precision measurements and technologies are required. These became available only in the last few decades.[1]

The existence of gravitational waves is one of these predictions. They are expected to be produced in phenomena involving large (stellar scale) amounts of accelerating mass, or during the early universe evolution in a wide range of frequencies starting from 10^{-17} Hz and extending at least for 22 orders of magnitudes.

One of the reasons why it is interesting to study gravitational waves is connected to their weakness. Gravitational waves hardly interact with the environment after being produced, so they carry clean information about their source. This is particularly true for waves generated in the earliest instants of the universe: to give an example, while neutrinos are expected to decouple from the environment at a temperature $T_\nu \sim 1$ MeV, in the gravitational case the decoupling temperature is $T_{Pl} \sim 10^{18}$ GeV. This means that the detection of this "fossil" gravitational radiation could give us unique information about the very early universe.[2,3] Signatures of cosmological gravitational waves can be searched at extremely low frequencies by studying anisotropies in the cosmic microwave background,[4] or by analyzing pulsar timing data in the very low frequency range (around 10^{-8} Hz).[5] Detection by means of Doppler tracking of spacecraft[6] or future space detectors[7] becomes possible in the low frequency regime (between 10^{-6} Hz and 1 Hz). At higher frequencies environmental noise becomes small enough to allow for an usable earthbound detector. This is the frequency range of interest from the point of view of this review, from few Hz to few tens of kHz. Detectors for gravitational waves beyond this range have also been proposed.[8–10]

To be fair, it is quite unlikely that the first gravitational waves to be directly detected will be the "fossil" ones. It should be mentioned, however, that current observations started to provide interesting upper limit on cosmological parameters.[11]

The most probable candidates for a first detection are gravitational waves produced by supernovae events,[12] by binary coalescence of very compact objects such as neutron stars or black holes,[13] and by rapidly rotating neutron stars.[14] The study of these gravitational signals will give us extremely important information about the dynamics of the sources.[15,16] In particular, it will be possible to compare the predictions of general relativity and other relativistic theories of gravitation in the strong interacting, nonlinear regime.

On the other hand, detection is quite difficult. The observable effect of a gravitational wave can be understood intuitively as a "deformation" of the space-time, parameterized by a "strain" h which is connected to the variation δL of a reference length L by[17]

$$h = \frac{\delta L}{L}. \tag{1}$$

a)Electronic mail: giancarlo.cella@pi.infn.it. URL: http://www.df.unipi.it/~cella.
b)Electronic mail: adalberto.giazotto@pi.infn.it.

 © 2011 American Institute of Physics

Downloaded 02 Nov 2011 to 180.149.51.196. Redistribution subject to AIP license or copyright; see http://rsi.aip.org/about/rights_and_permissions

The typical expected order of magnitude for the observable h produced by an astrophysical source is given by $h \lessapprox 10^{-21}$. As L is determined by the size of the detector, we see that we have to deal with very tiny length scales: for a km-size detector one should be able to detect a length variation $\delta L = 10^{-18}$ m, which is 10^{-3} the radius of a proton. One of the aims of this review is to explain how this can be possible.

Indirect evidence for the existence of gravitational waves was provided by the well-known work of Hulse and Taylor.[18] With high precision measurements of a binary pulsar system it has been possible to evaluate the rate of energy loss of the system, and to compare them with the expected amount of radiated gravitational energy.

A direct detection is still elusive. First attempts in this direction date to the pioneering work of Weber with his resonant detectors.[19] The technique used in this case is quite different from the interferometric one we will describe later. Weber prepared a large bar of aluminum, which conceptually can be modeled as a harmonic oscillator composed of two masses connected by a spring of rest length L. The two masses will try to stay on geodesics, but the restoring force of the spring does not allow for this when a gravitational wave is present and the spring's length is changed accordingly with Eq. (1). At the end the gravitational wave forces the oscillator, transferring to it some energy which can be detected. This techniques takes advantage of the fact that, if the oscillator has a very high Q, the transfer of energy can be quite efficient near the resonance frequency f_0, providing a large amplification factor. However, this also means that the detection will be possible only for signals in a narrow bandwidth (practically, some tenths of Hz) (Ref. 20) around f_0.

Understanding the sensitivity of this kind of devices requires the evaluation of the noises which can mask the energy gained by the bar. At the end of 1960 Weber declared the evidence of a detection.[21] This claim was never accepted by the scientific community, mainly because attempts to confirm it done by other groups failed. However, Weber's work was the trigger for a very intense activity, based on resonant detectors, which is still alive today.

A. Interferometers

A different approach to the detection of gravitational waves is based on interferometric instruments.[22] Weber himself was well aware about this possibility, but at that time the realization of a real interferometric detector was not realistic because the required technology was too demanding. The situation changed at the start of the 1970s, when the first complete estimation of noises competing with the GW signal was published by Weiss,[23] and a first high sensitivity experimental attempt was done by Robert Forward, a former student of Weber.[24] At the start of the 1980s, the first concrete proposals for an interferometric gravitational wave detector started to appear in the scientific community. In the same period, coherent sources of monochromatic light with powers on the scale of some watts became available, argon-ion lasers at first and neodymium YAG lasers next. Laser power has a direct impact on sensitivity by reducing shot noise. Several prototypes were constructed around the world,[25] starting an effort culminating in the current generation of active detectors.

The basic concept of detection is schematically represented in Figure 1. An input laser beam of amplitude I_L is separated in two parts using a beam splitter of reflectivity R_{BS} and transmissivity T_{BS}. Each part travels along two different paths $\mathcal{P}_N$ and $\mathcal{P}_W$ contained in the interferometer arms, then they are recombined together in an output beam of amplitude O_D looking at how they interfere. The interference

$$O_D = R_{BS}T_{BS}\left(\mathcal{P}_N - \mathcal{P}_W\right) I_L + \left(R_{BS}^2\mathcal{P}_W + T_{BS}^2\mathcal{P}_N\right) I_D \tag{2}$$

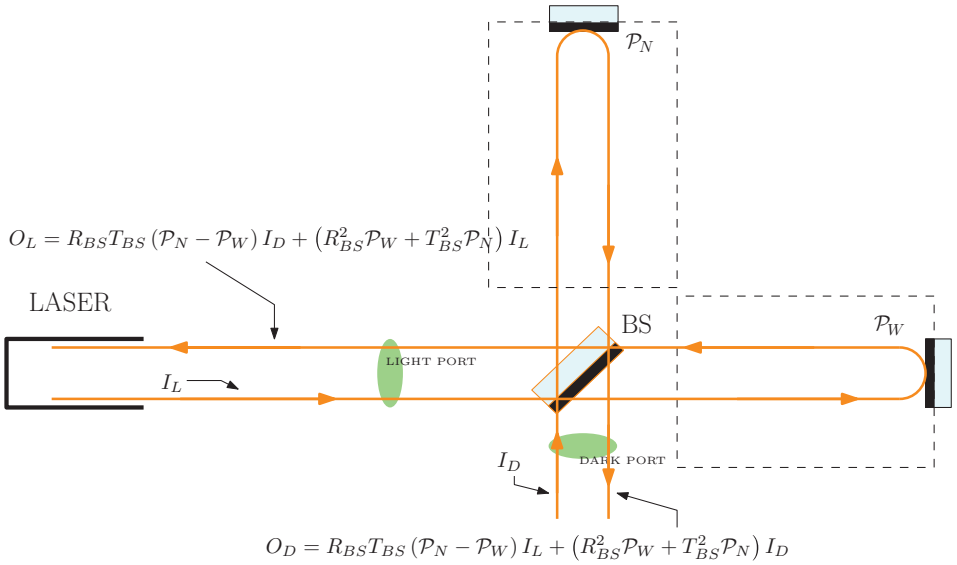


FIG. 1. (Color online) Schematic diagram of a Michelson interferometer. There are two input beams, I_D and I_L, and two output ones, O_D and O_L. $\mathcal{P}_N$ and $\mathcal{P}_W$ represent the transfer functions of each arm, which are the result of the propagation inside the dashed boxes, while R_{BS}, T_{BS} are the reflectivity and the transmissivity of the beam splitter. $\mathcal{P}_N$ and $\mathcal{P}_W$ depend on the specific optical setup of the arm, in the Michelson case they are just free propagations. Whatever they were we get the relations shown between the input and the output beams. Note that if $\mathcal{P}_N = \mathcal{P}_W$ both input fields are completely reflected back.

Downloaded 02 Nov 2011 to 180.149.51.196. Redistribution subject to AIP license or copyright; see http://rsi.aip.org/about/rights_and_permissions

will be a measure of the difference between the phases gained along the two paths (remember that the laser feeds only I_L, so classically $I_D = 0$), which will change when a gravitational wave will cross them. In Eq. (2) we labeled with $\mathcal{P}_N$, $\mathcal{P}_W$ the transfer functions of the two paths with the same name.

Looking at Eq. (1), we see that the sensitivity to a given strain h is proportional to the length of the optical path. In an earthbound detector it is difficult to go beyond a detector size of few kilometers. There are both economic and geographic reasons for this. First of all the laser beam must travel in an ultrahigh vacuum in order to avoid distortions induced by fluctuation of the refraction index. This requires an infrastructure which tends to dominate the economic effort. Concerning the geographic problems, it is interesting to note that earth curvature effects start to be relevant for the length of few kilometers, the difference between vertical directions at two places separated by a distance L becoming non negligible at the requested accuracy level.

In the simplest case, the detector is just a Michelson interferometer, so $\mathcal{P}_N$ and $\mathcal{P}_W$ are simply given by a single back and forth trip to a terminal mirror. The phase ϕ gained is a linear function of the trip length, and for its variation we get

$$\delta\phi = 2 \times \frac{2\pi}{\lambda}\delta L = \frac{4\pi L}{\lambda}h, \tag{3}$$

where λ is the laser's wavelength. With more complicated optical setups for $\mathcal{P}_N$ and $\mathcal{P}_W$ it is possible to obtain a larger proportionality factor between h and $\Delta\phi$. The simplest scheme is given by a delay line, namely, the light is reflected N times back and forth before coming back to the beam splitter. This solution is represented in Figure 3. Also in this case the phase gained scales linearly with the length of the arms, and Eq. (3) changes simply by a factor N.

A different solution is obtained by inserting in the interferometer's arms resonant Fabry-Perot cavities, each being composed of the terminal mirrors and by another semitransparent one added just after the beam splitter. This is represented in Figure 2, the two semitransparent mirrors being *NI* and *WI*. A critical parameter of this setup is the finesse $\mathcal{F}$ of the cavity, which is defined as

$$\mathcal{F} = \pi\frac{\sqrt{r_1 r_2}}{1 - r_1 r_2}, \tag{4}$$

where $r_{1,2}$ are the reflectivities of the two mirrors. Naively, $\mathcal{F}$ can be understood as the typical number of round trips for a photon inside the cavity. However, it must be keep in mind that it would not be correct to interpret the behavior of the laser light inside a Fabry-Perot cavity as a succession of $\mathcal{F}$ reflections, because interference effects dominates. This is the reason why the dependence of the phase gained from the cavity length is no longer linear, but is given instead for $\mathcal{F} \gg 1$ by

$$\delta\phi \simeq \frac{\left(\frac{2\mathcal{F}}{\pi}\right)}{1 + \left(\frac{2\mathcal{F}}{\pi}\sin\frac{2\pi L}{\lambda}\right)^2}\left(\frac{4\pi L}{\lambda}\right)h. \tag{5}$$

Comparing Eqs. (3) and (5) we see that when the cavity is resonating, namely, when its length is an half integer multiple of the laser wavelength, the cavity amplifies the signal by a large factor $2\mathcal{F}/\pi$ which is consistent with the naive interpretation of $\mathcal{F}$ given before. However, as soon as we move away from the resonance by an amount $\delta L_u \gtrapprox \lambda/(2\pi\sqrt{\mathcal{F}})$ this gain is completely lost.

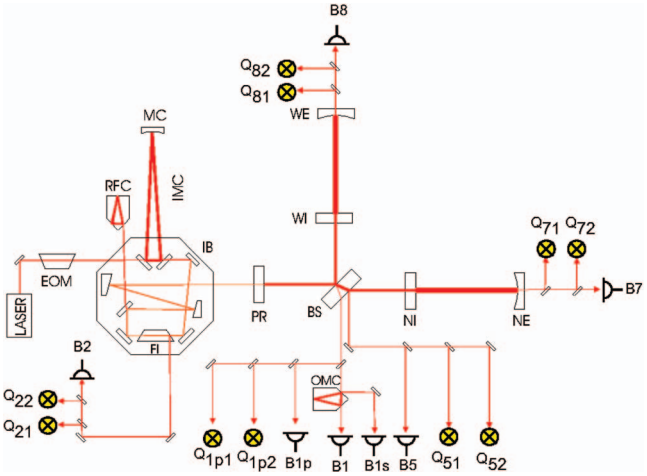


FIG. 2. (Color online) A simplified optical scheme of the Virgo interferometer. The input laser is modulated by an EOM and locked at a RFC, then filtered by a mode cleaner cavity (IMC). It is then injected in the main detector through a power recycling mirror (PR), separated in two parts by a BS. Each split beam resonates inside a Fabry-Perot cavity (WI-WE and NI-NE). The beam is recombined on the beam splitter and is then filtered by an OMC cavity. Small secondary beams are obtained in several points, for example, at the WE and NE mirrors which are not completely reflective and analyzed with photo-diodes (labeled with the letter B) and quadrant photo-diodes (labeled with the letter Q).

It seems that a Fabry-Perot cavity of high finesse is an effective way to increase the sensitivity of an interferometric detectors. However, we must keep in mind two important points. The first is that the relation between $\Delta\phi$ and h does not give us direct information about the sensitivity, because what is really important is the comparison between the signal and the noise amplitude. As will be discussed in Secs. III and IV several noises (the so-called *positional noises*) are directly connected with the interaction between the laser beam and the mirror. This is the case in particular of thermal noise (see Sec. IV) and of the environmental noises (see Sec. III).

Another point is that the length of the cavity must be kept near a resonant value, by an amount comparable with the scale $\delta L_{lin} = \lambda/(4\mathcal{F})$ where its response is linear. Building a rigid enough cavity with $L = O(10^3$ m) is out of question. Beside this, it would not be desirable either. As we saw the interaction of a gravitational wave with a bar is depressed out of mechanical resonance. One of the main advantages of an interferometric detector is its wide band sensitivity. This is obtained by making the mirrors which define the optical path behave as free falling masses.

For an earthbound experiment the realization of a free falling mass concept can only be approximated. The chosen solution is to suspend the mirrors as chains of pendula, which act as harmonic oscillators for horizontal displacements. As detailed in Subsection III A 1 the mirrors can effectively be considered free masses for high enough frequencies. Additionally, the pendula act as attenuators which reduce the

Downloaded 02 Nov 2011 to 180.149.51.196. Redistribution subject to AIP license or copyright; see http://rsi.aip.org/about/rights_and_permissions

environmental noise in the same frequency region (see Subsection III A).

But in the low frequency region seismic motion is not attenuated in any way. The typical rms motion of the ground in this band is around few μm, which is much larger than the typical scale δL_{lin}. In order to reduce this motion to an acceptable level an active control strategy must be implemented, as discussed in Subsection II A.

Coming back to the generic scheme in Figure 1 we see that a device of this kind has really two input and two output fields. The output O_D receives contributions both from fields I_L (coming from the laser, entering through the so-called *light port*) and I_D (entering through the so-called *dark port*). Similar considerations are true for O_L, which is the field reflected back to the laser.

A very important observation is that when the transfer functions $\mathcal{P}_N$ and $\mathcal{P}_W$ are the same O_L is coupled only to I_L and O_D only to I_D. The laser injected in I_L is completely reflected on O_L, no light is present on O_D and for this reason it is said that the interferometer is set at the *dark fringe*.

This allows one to understand better why interferometers are good detectors of gravitational waves.

One could ask why two different arms are needed at all. In principle, the measurement of the ΔL induced by a gravitational wave in a single direction should be enough. This could be obtained by measuring the output O of a single Fabry-Perot cavity. However, a laser beam is not absolutely stable, so the variation δO of the output of a single cavity will be written as

$$\begin{aligned}\delta O &= (\mathcal{P}^{(0)} + \delta\mathcal{P})(I^{(0)} + \delta I) - \mathcal{P}^{(0)} I^{(0)} \\ &\simeq \delta\mathcal{P} I^{(0)} + \mathcal{P}^{(0)} \delta I, \end{aligned} \tag{6}$$

where we split the transfer function of the cavity and the laser field into their average values $\mathcal{P}_0$, I_0, and in their fluctuating part $\delta\mathcal{P}$, δI. The fluctuation $\delta\mathcal{P}$ is generated by the positional noises mentioned before, and hopefully by the gravitational wave. But we see that the fluctuations of the laser act as an additional noise source.

If we repeat the same calculation for an interferometer, we can linearize Eq. (2) obtaining

$$\begin{aligned}\delta O_D = R_{BS} T_{BS} \big[(\delta\mathcal{P}_N - \delta\mathcal{P}_W) I_L^{(0)} + \big(\mathcal{P}_N^{(0)} - \mathcal{P}_W^{(0)}\big)\delta I_L \big] \\ + \big(R_{BS}^2 \mathcal{P}_W^{(0)} + T_{BS}^2 \mathcal{P}_N^{(0)}\big)\delta I_D, \end{aligned} \tag{7}$$

If the unperturbed transfer functions $\mathcal{P}_N^{(0)}$, $\mathcal{P}_W^{(0)}$ of the two arms are the same, the fluctuations of the laser field δI_L are completely ineffective as a noise source. An intuitive way to express this concept is the following: one of the two arms of the interferometer is used as a reference cavity (RFC) to stabilize the laser, the other "senses" the gravitational wave. Gravitational wave and positional noise enters through the variation of the arms' transfer functions $\delta\mathcal{P}_N$, $\delta\mathcal{P}_W$, and their coupling to the apparatus is proportional to the average laser amplitude $I_L^{(0)}$.

Note that in Eq. (7) there is a contribution proportional to δI_D, the fluctuation of the field entering the interferometer through the dark port. Though $\delta I_D = 0$ at the classical level, this term will be present at the quantum level and will be the key to understand optical noise (Sec. II).[26]

Today several interferometric detectors exist, of several scales and sensitivities. A large international scientific collaboration works on both scientific data taking and sensitivity improvement.

There are several bonuses in having more than one detector available. First of all, it will be quite optimistic to think that during the operations detector noise will be completely under control. The rate of unexpected events will never be zero, and a very effective way to reduce them is to use different detectors in coincidence.

In some cases (i.e., the search for a stochastic background of gravitational waves[3]) the correlation between the output of at least a pair of detectors is the only way to reveal the signal. For some non-stochastic sources the confidence of a first detection and the physical information extracted can get a big improvement by finding coincident evidence of an electromagnetic or neutrino counterpart.[27,28] This requires an accurate determination of the source position[29,30] and, once again, a network of detectors.

Finally, after the first detections will be obtained, the activity of gravitational wave experiments will enter a new era which will be characterized by the study of the source's parameters. The accuracy in the determination of these parameters will gain a lot from and in some cases it will possible only by analyzing the data of a network of detectors.[31,32]

The LIGO scientific collaboration (LSC) (Ref. 33) is a community of several hundred of scientists worldwide, which collaborate on the effort to detect gravitational waves. The main detectors used by the collaboration are the 4 km arm's length interferometers located in the United States at Hanford (WA) and Livingston (LA). A shorter interferometer (2 km arm's size) is located in Hanford, sharing the same vacuum enclosure of the largest one. The first scientific data taking started in 2002.

The VIRGO collaboration[34] is a scientific collaboration of groups from Italy, France, the Netherlands, Poland, and Hungary. The detector, located in Italy near Pisa, has an arm length of 3 km. It has been designed to have a good sensitivity in the low frequency region, thanks to a peculiar seismic attenuation system (see Sec. III A) from which the mirrors are suspended.[35] The VIRGO first scientific data taking started in 2007, in coincidence with LIGO detectors.

Both Virgo and LIGO detectors have a very similar optical configuration, using Michelson interferometers with resonant Fabry-Perot cavities added along the arms. In Figure 2, a simplified optical scheme for Virgo is shown. Looking at it we recognize the beam splitter *BS* and the two Fabry-Perot cavities located along the arms, which are delimited by the mirrors *WE*,*WI* and *NE*, *NI*.

There are some other details in the diagram that we did not discuss previously. First of all an additional mirror *PR* is put before the beam splitter. Its role is to send back the light which is reflected by the interferometer to the beam splitter, in order to "recycle" its power. In this way the power of the beam which enters the beam splitter is scaled by a factor which depends on the reflectivity of *PR*. An intuitive way to understand this is the following: the interferometer is equivalent at the dark fringe to a mirror, which together with the mirror *PR* generates a resonant cavity of finesse $\mathcal{F}_{PR}$ and length ℓ_{PR}. The

Downloaded 02 Nov 2011 to 180.149.51.196. Redistribution subject to AIP license or copyright; see http://rsi.aip.org/about/rights_and_permissions

TABLE I. The main parameters of the LIGO, Virgo, GEO600, and TAMA300 detectors. The light source in each case is a Nd:YAG with $\lambda = 1.064$ μm.

			LIGO4k	LIGO2k	Virgo	GEO600	TAMA300
L	Arm length	(m)	4000	2000	3000	600	300
$\mathcal{F}$	Cavity finesse	–	220	220	50	n.a.	520
$f_p \equiv \frac{\Omega_p}{2\pi}$	Cut off frequency	(Hz)	85	170	500	n.a.	481
I_ℓ	Laser power	(W)	10	10	20	10	10
I_0	Laser power at the beam splitter	(W)	500	500	1000	$\lessapprox 10^4$	100

ratio between the input laser power P_{in} and the power inside the cavity P_{cav} will be given by

$$\frac{P_{cav}}{P_{in}} = \frac{4\mathcal{F}_{PR}}{\pi} \frac{1}{1 + \left(\frac{2\mathcal{F}_{PR}}{\pi} \sin \frac{2\pi \ell_{PR}}{\lambda}\right)^2}, \tag{8}$$

which can be quite large if $\mathcal{F}_{PR} \gg 1$ and ℓ_{PR} is maintained at resonance. In Table I it is possible to compare P_{cav} and P_{in} for currently operating detectors.

The triangular cavity IMC and the smaller ones *RFC* and output mode cleaner (*OMC*) are used to stabilize the frequency the laser and to filter it from unwanted higher order modes.[36] We will discuss both higher order modes and frequency stabilization in Sec. II.

In Figure 2 there are several photo-diodes. Apart from the ones used for the detection of the detector output at the dark port (*B1, B1p,* and so on) there are others which are used to measure the field inside the Fabry-Perot cavities on the arms (*B7* and *B8*).This is done by making the terminal mirrors *NE* and *WE* not completely reflective. Another photo-diode (*B2*) is used on the injection bench, *IB,* to monitor the laser to be injected.

There are also quadrant photo-diodes, which can be described as sets of four photo-diodes mounted on the vertices of a small square. They are used to measure not only the intensity of a beam, but also the position of its center in a transverse plane. It is not enough to set the various optical elements of the apparatus in their correct position along the beam, but we need also to align correctly their transverse position and their angular degrees of freedom.[37] In order to do that, we need information about misalignment which are provided by the *Qi*s.

The GEO600 detector,[38] located in Hannover, was built by a British-German scientific collaboration, who subsequently joined the LSC. Its arm length is shorter (600 m), and its optical configuration is quite different. A schematic view of the GEO600 optical setup is in Figure 3.

We note that the injection stage,[39] and the two triangular cavities (*MC1*and *MC2*) are analogous to the *MC* in Figure 2. They are used to give an appropriate transverse spatial shape to the input beam.

There are no resonant cavities along the arms, the light storage time being increased by a four pass delay line setup. In addition to the power recycling technique discussed before (the power recycling mirror is labeled *MPR* in the diagram) a special technique called *signal recycling* (see Subsection II E 3) is implemented,[40] putting a semi-reflective mirror after the beam splitter (labeled *MSR* in the diagram).

A peculiarity of GEO600 is the way in which the mirrors are suspended. In order to reduce as much as possible mechanical dissipations and as a consequence thermal noise the first stage of suspensions for both the mirrors and the beam splitter is implemented as a monolithic triple pendulum entirely made with fused silica.[41] The connection with the optical elements is obtained with the silicate bonding technique.[42] We will comment about that in Sec. IV. Here we want only to remark that similar monolithic suspensions will be used in next generation LIGO and VIRGO detectors.

TAMA300 (Ref. 43) is a Japanese project based on a 300 m interferometer located at the National Astronomical Observatory near Tokyo. This optical configuration is quite similar to the one of LIGO and Virgo. The main aim of the project is to develop advanced techniques needed for a future km-sized interferometer, such as resonant sideband extraction (see Sec. II D).[44,45]

In all the current detectors the sensitivity is limited at low frequency by seismic noise, in the intermediate range by thermal noises and by optical shot noise in the high frequency region. In order to give a precise meaning to this statement we need to define an appropriate quantity to characterize a detector's performance. We will do this in the two subsections which follow. In Subsection I B, we will explain how a gravitational wave can be parameterized, and how it couples to the interferometer. In Subsection I C we will analyze how a noise source can reduce the detector's sensitivity and we will introduce the strain equivalent noise amplitude, which is the most commonly used figure of merit for the detector's sensitivity.

B. The nature of gravitational waves

The Newton's theory of gravitation can be condensed into the law which connects the gravitational potential ϕ to the mass density ρ, namely,

$$\nabla^2 \phi = -4\pi G \rho. \tag{9}$$

This is in analogous to the law in electrostatics that connects the electric potential with the charge density. Being a static law, it cannot be used to describe situations in which ρ changes rapidly with the time. In fact, the force law predicted by Eq. (9) is Newton's famous inverse square action at distance. General relativity theory was introduced by Einstein as an attempt to reconcile the Newtonian theory of gravitation with the principles of special relativity. The gravitational interaction is now mediated by a tensorial field $g_{\mu\nu}$ which plays the role of the space-time metric. It must satisfy the Einstein equation,

$$R^{\rho}_{\mu\rho\nu} - \frac{1}{2} g_{\mu\nu} R^{\rho\sigma}_{\rho\sigma} = \frac{8\pi G}{c^2} T_{\mu\nu}, \tag{10}$$

Downloaded 02 Nov 2011 to 180.149.51.196. Redistribution subject to AIP license or copyright; see http://rsi.aip.org/about/rights_and_permissions

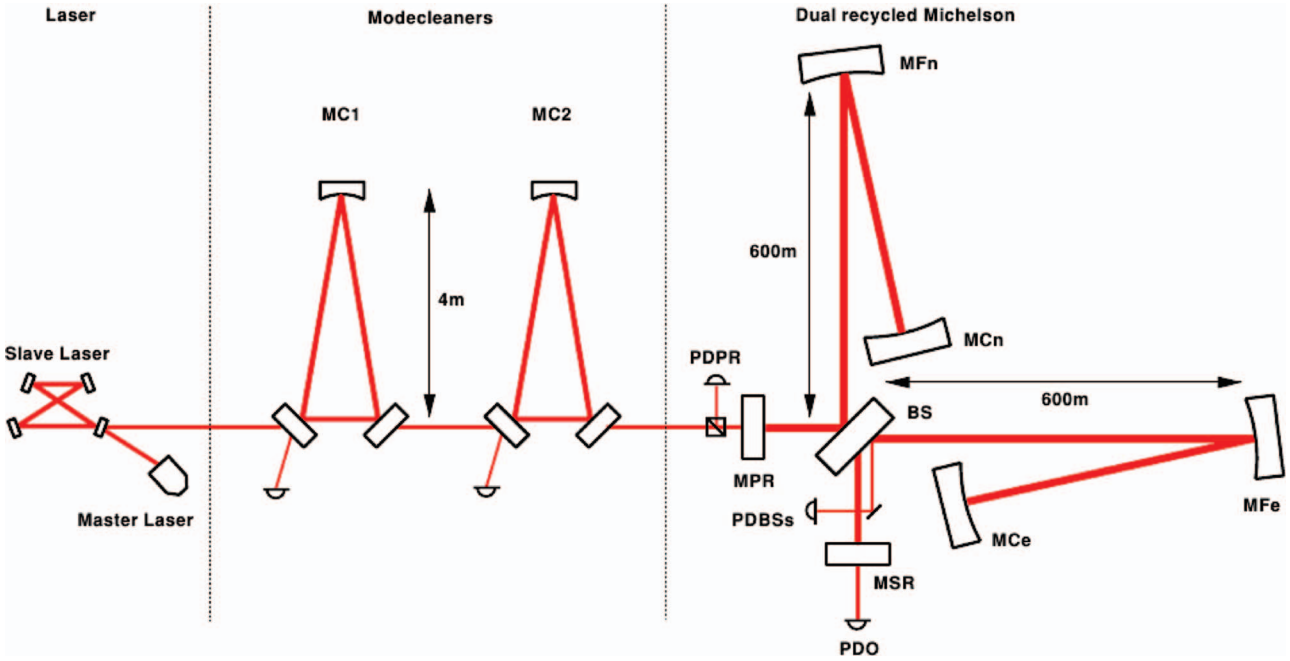


FIG. 3. (Color online) The simplified optical scheme of the GEO600 interferometer.

where the Riemann tensor $R^{\mu}_{\nu\rho\sigma}$ is a particular function of the metric and its first and second derivatives, which describes the space-time curvature in a covariant way. The explicit expression for it can be given as

$$R^{\mu}_{\nu\rho\sigma} = \Gamma^{\mu}_{\nu\sigma,\rho} - \Gamma^{\mu}_{\nu\rho,\sigma} + \Gamma^{\mu}_{\alpha\rho}\Gamma^{\alpha}_{\nu\sigma} - \Gamma^{\mu}_{\alpha\sigma}\Gamma^{\alpha}_{\nu\rho}, \tag{11}$$

where

$$\Gamma^{\mu}_{\nu\rho} = \frac{1}{2}g^{\mu\alpha}(g_{\alpha\nu,\rho} + g_{\alpha\rho,\nu} - g_{\nu\rho,\alpha}) \tag{12}$$

is called the metric connection. $T_{\mu\nu}$ is the energy-momentum tensor, which acts as a source for the gravitation generalizing the role of ρ in Eq. (9). Note that the Riemann tensor has the dimensions of an inverse of a squared length which can be interpreted as a typical curvature scale.

Following the analogy with electromagnetism, it is natural to expect that the presence of time derivatives allows for wavelike solutions. In fact this was recognized early by Einstein himself.[46] However, for a long time a controversy about the physical reality of these *gravitational waves* was present in the literature. The roots of this conceptual difficulty were in the fact that general relativity can be seen as a gauge theory, where the gauge transformations are time and space coordinate reparameterizations. The question was settled 40 years later by Bondi[47] who showed with a *thought experiment* that gravitational waves carry energy and momentum, and cannot be eliminated by a coordinate change.

Equation (10) expresses in a quantitative way the coupling between gravitational field and matter, which is in fact quite weak. This weakness has two consequences. First of all it is difficult to generate gravitational waves. The artificial production with a laboratory scale apparatus is out of question. On the other hand, astrophysical and cosmological scale phenomena seem to be good candidates as gravitational wave sources. The second point is that gravitational waves are very difficult to detect.

In order to obtain the equation for the propagation of a gravitational wave we must linearize the Einstein's equation (10) by supposing that, with an appropriate choice of coordinates, $g_{\mu\nu}$ can be written as

$$g_{\mu\nu} = \eta_{\mu\nu} + h_{\mu\nu}, \tag{13}$$

where $\eta_{\mu\nu}$ is the Minkowski's metric and $h_{\mu\nu}$ is a small correction, $|h_{\mu\nu}| \ll 1$. Retaining only linear terms in $h_{\mu\nu}$ we find that

$$R_{\mu\nu\rho\sigma} = \frac{1}{2}(h_{\sigma\mu,\nu\rho} - h_{\nu\sigma,\mu\rho} - h_{\rho\mu,\nu\sigma} + h_{\rho\nu,\mu\sigma}) \tag{14}$$

from which we obtain, after introducing for convenience the field $\overline{h}_{\mu\nu} = h_{\mu\nu} - 1/2\eta_{\mu\nu}h^{\alpha}_{\alpha}$,

$$R^{\rho}_{\mu\rho\nu} - \frac{1}{2}g_{\mu\nu}R^{\rho\sigma}_{\rho\sigma} = -\overline{h}^{\alpha}_{\mu\nu,\alpha} - \eta_{\mu\nu}\overline{h}^{,\rho\sigma}_{\rho\sigma} + \overline{h}^{\rho}_{\mu\rho,\nu} + \overline{h}^{\rho}_{\nu\rho,\mu} + O(h^2), \tag{15}$$

and setting this quantity equal to zero ($T_{\mu\nu} = 0$) we expect to obtain a candidate for the wave equation in vacuum, which explicitly reads

$$-\overline{h}^{\alpha}_{\mu\nu,\alpha} - \eta_{\mu\nu}\overline{h}^{,\rho\sigma}_{\rho\sigma} + \overline{h}^{\rho}_{\mu\rho,\nu} + \overline{h}^{\rho}_{\nu\rho,\mu} = 0. \tag{16}$$

As it is written, this does not seem a wave equation. However, we must remember that the theory is invariant for arbitrary changes of coordinates. In the linearized framework, this means that we can redefine $x^{\mu} \rightarrow x^{\mu} + \xi^{\mu}(x)$ and $h_{\mu\nu} \rightarrow h_{\mu\nu} - (\xi_{\nu,\mu} + \xi_{\mu,\nu})$ without changing the physics. Here ξ^{μ} is an arbitrary vector field (however, with the constraint that $|\xi_{\nu,\mu} + \xi_{\mu,\nu}| \ll 1$). Note that the linearized Riemann tensor (14) does not change under these transformations.

Downloaded 02 Nov 2011 to 180.149.51.196. Redistribution subject to AIP license or copyright; see http://rsi.aip.org/about/rights_and_permissions

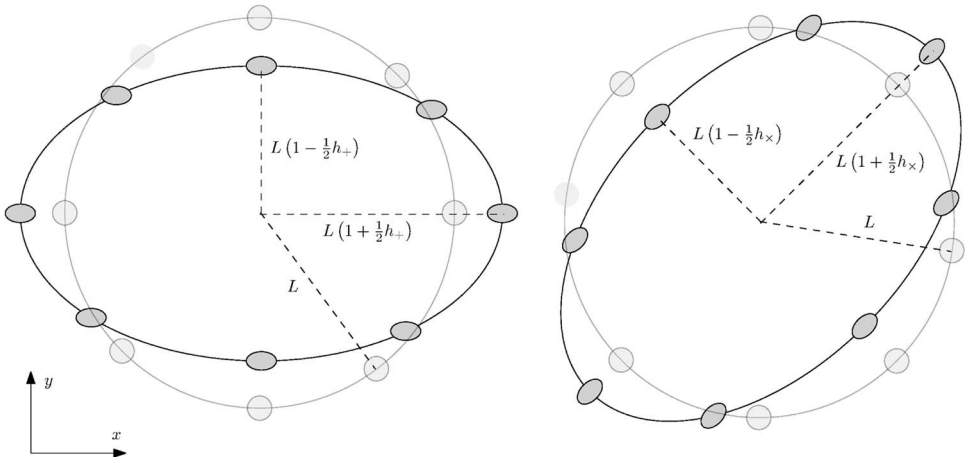


FIG. 4. The effect of a gravitational wave propagating along the z axis on a circular ring of free test masses with radius L. (Left) The displacement induced by the polarization $+$. (Right) The displacement induced by the polarization $\times$. The two polarizations differ for a rotation around the z axis by the angle $\pi/4$.

Using this freedom we can impose some constraints on $h_{\mu\nu}$, in particular we can set

$$\overline{h}^{\mu}_{\mu\nu} = 0 \tag{17}$$

in such a way that Eq. (16) becomes

$$-\overline{h}^{\alpha}_{\mu\nu,\alpha} = 0, \tag{18}$$

which is a wave equation for the field $\overline{h}_{\mu\nu}$. Note that $\overline{h}_{\mu\nu}$ has only six independent components, owing to its symmetry and to the constraint (17).

We are free to do another transformation $\hat{\xi}^{\mu}$, provided that the constraint (17) is preserved which is the case if $\Box\hat{\xi}^{\mu} = 0$.

It is particularly convenient to impose $\overline{h}^{\alpha}_{\alpha} = 0$ (which means $\overline{h}_{\mu\nu} = h_{\mu\nu}$) and $h_{0i} = 0$ $(i = 1, 2, 3)$. This is the so-called transverse traceless (TT) gauge: the constraints over $h_{\mu\nu}$ can be taken as

$$h_{0\mu} = 0, \quad h^{i}_{i} = 0, \quad h^{j}_{ij,} = 0, \tag{19}$$

and we see that there are only two independent components (polarizations) of the field.

We need to understand how a given gravitational wave can modify the output of an interferometer. In Appendix, we discuss this problem in detail, but for the purposes of this review it is enough to quote several results that are valid when the wavelength of the signal is large compared with the detector size, which is quite accurate in the frequency range of interest.

First of all we can describe the action of the gravitational wave on a mass m at coordinates x^j with a force given by Eq. (A28). The quantity $\ddot{h}^{TT}_{ij}$ which appears in the force is a solution of Eq. (18) evaluated at the origin of the coordinate system, which can be chosen for convenience near the beam splitter.

The structure of $\ddot{h}^{TT}_{ij}$ must satisfy the constraints (19), which means that for a wave propagating in the z direction it must be

$$h^{TT}_{ij}(t) = \begin{pmatrix} h_+(t) & h_\times(t) & 0 \\ h_\times(t) & -h_+(t) & 0 \\ 0 & 0 & 0 \end{pmatrix}, \tag{20}$$

which is the linear combination with weights $h_+(t)$, $h_\times(t)$ of the two independent polarizations labeled with $+$ and $\times$. If we consider a ring of free masses in the $z = 0$ plane, and we write their displacement under the action of the force (A28) we find the situation represented in Figure 4.

We see that the space is stretched along a particular direction and contracted along the one orthogonal to it. This is another reason why an interferometer is a good detector for these types of waves: if we imagine the two arms aligned along the x and y axes we see that the variation of corresponding optical paths differs in sign for the h_+ polarization, so that their difference is maximized.

On the other hand, there is no variation induced by the $h_\times$ polarization. As a matter of fact a gravitational wave couples to the detector in a way which depends on both the polarization and direction. This is described in detail in Appendix: in our low frequency approximation the difference between the lengths of the two arms will change for an arbitrary $h^{TT}_{ij}(t)$ accordingly with

$$\frac{\delta L_W - \delta L_N}{L} = h^{TT}_{ij} D^{ij} \equiv h_{\text{eff}}, \tag{21}$$

where D^{ij} is the detector tensors described by Eq. (A30) and we defined an effective strain h_{eff} which takes into account the geometrical response of the detector. Note that it is not mandatory for the two arms to be perpendicular, but this is the case which maximizes the signal in Eq. (21).

We end this subsection by noting that extended theories of gravitation can allow for additional polarizations,[48] and the corresponding displacement patterns will differ from those depicted in Figure 4. For example, "scalar" polarizations, which correspond to an isotropic dilatation of the test mass ring, are much less coupled[49] to the signal exiting the dark port, proportional to the difference in arm lengths (21). In principle, the *common mode* signal present in the beam

Downloaded 02 Nov 2011 to 180.149.51.196. Redistribution subject to AIP license or copyright; see http://rsi.aip.org/about/rights_and_permissions

reflected by the interferometer, which is proportional to the sum $\delta L_W + \delta L_N$, is much more coupled to this kind of wave. However, the reflected beam is strongly contaminated by laser fluctuations, as one can see by writing the analogue of Eq. (7) for δO_L, and the sensitivity will be much worse.

C. The noise budget

We are now in the position to introduce the strain equivalent spectral noise amplitude, which is the most important figure of merit for the detector sensitivity. In order to evaluate the sensitivity of a given detection technique we need to know not only the response of a detector to a given gravitational wave, but also its coupling to each source of noise.

Let us call $\phi(t)$ the output of the detector, in arbitrary units, that we are measuring. It will contain contributions from both the gravitational wave strain and from various noise sources. By choosing $\phi(t)$ in an appropriate way we expect it to depend on the effective strain linearly, so we can write

$$\phi(t) = \int T_{h\to\phi}(t,t')h_{\rm eff}(t')dt' + N_\phi(t), \tag{22}$$

where $N_\phi(t)$ represent additive noise contributions. The kernel $T_{h\to\phi}$ represents the transfer function which connects the effective strain to the output. In the real case, it can depend explicitly on time, because the configuration of the detector can be not completely stationary. In the hypothesis that this effect can be neglected, the transfer function inside the integral will be a function of $t - t'$ only, and we can rewrite Eq. (22) in the frequency domain as

$$\begin{aligned}\tilde{\mathsf{h}}_{\rm eff}(f) &\equiv \tilde{T}_{h\to\phi}(f)^{-1}\tilde{\phi}(f)\\ &= \tilde{h}_{\rm eff}(f) + \tilde{T}_{h\to\phi}(f)^{-1}\tilde{N}_\phi(f).\end{aligned} \tag{23}$$

The quantity $\tilde{\mathsf{h}}_{\rm eff}(f)$ is an estimator of the effective strain, and the quantity

$$\tilde{N}_h(f) \equiv \tilde{T}_{h\to\phi}(f)^{-1}\tilde{N}_\phi(f) \tag{24}$$

in the second member of Eq. (23) is the apparatus noise normalized in such a way to be directly comparable with $\tilde{h}_{\rm eff}$. If we assume that it is possible to model $\tilde{N}_h(f)$ as a stationary stochastic process, we can characterize it with its power spectrum $S_h(f)$, which is formally defined by

$$\langle \tilde{N}_h(f')\tilde{N}_h(f)\rangle = \delta(f-f')S_h(f). \tag{25}$$

We will define the strain equivalent noise spectral amplitude as the square root of $S_h(f)$. Note that it is a dimensioned quantity, with units $\mathrm{Hz}^{-1/2}$. When we integrate $S_h(f)$ over a given frequency interval we obtain the corresponding contribution to the mean square value of the strain equivalent noise.

The theoretical sensitivity of a detector can be estimated by modeling all the expected noise sources. In this way we obtain what is called a "noise budget." As an example, the noise budget of VIRGO is plotted in Figure 5.

The noise sources which limit the sensitivity are given by

- Seismic noise (labeled *Seismic*), which dominates below 2 Hz. This contribution decreases quite rapidly with increasing frequency. There are two reasons for this: first of all the typical spectrum of horizontal displacements of the ground, which is the source of this noise, scales with the frequency roughly as f^{-2}. The second and more important point is that seismic motion is attenuated by inserting an appropriate mechanical filter between the ground and the mirrors. This will be discussed in Subsection III A: for VIRGO the mechanical system is essentially a chain of harmonic oscillators, each of them providing in the high frequency range a factor $\propto f^{-2}$ for the filter in the frequency region of interest.
- Thermal noise generated by dissipation in the suspension chain (labeled *tnPend*). This is the most important effect from 2 Hz to 50 Hz. Each mirror is the bottom stage of an attenuation chain, and the mechanical system is essentially a multiple pendulum. This is coupled to a heat bath at the environmental temperature, and as a consequence the position of the mirror fluctuates. These fluctuations can be estimated at thermal equilibrium using the fluctuation-dissipation theorem, which predicts a power spectrum of the single mirror displacement fluctuations given by

$$S_{\delta L,\rm Mirr}(f) = \frac{4k_BT}{(2\pi f)^2}\frac{\mathrm{ReZ(f)}}{|Z(f)|^2} \simeq \frac{4k_BT}{m}\frac{\phi(f)}{(2\pi f)^3}. \tag{26}$$

Here $Z(f)$ is the mechanical impedance of the multiple pendulum and m is the mirror's mass. The dimensionless function $\phi(f)$ is called the loss angle and parameterizes the dissipation of the system (see Sec. IV B). The approximation used in Eq. (26) is valid in the frequency range we are interested in, which is above the resonances of the chain (the highest one can be found in Figure 5 at $f \simeq 6$ Hz). By summing the uncorrelated contributions of all the four mirrors which compose the cavities and by rescaling by a factor L^{-2} to obtain a strain equivalent power spectrum we find the contribution shown in Figure 5, which shows the expected

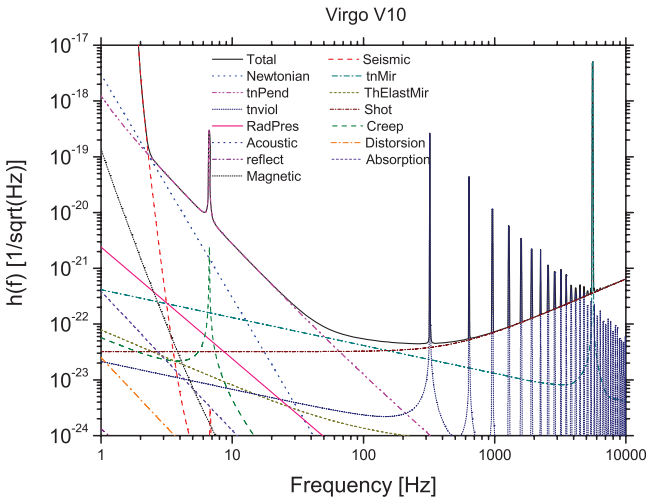


FIG. 5. (Color) The Virgo design noise budget. The sensitivity is limited by seismic noise below 2 Hz, by the thermal noise of the suspension between 2 Hz and 50 Hz, by the thermal noise of the mirror between 50 Hz and 100 Hz and by the shot noise above 100 Hz.

Downloaded 02 Nov 2011 to 180.149.51.196. Redistribution subject to AIP license or copyright; see http://rsi.aip.org/about/rights_and_permissions

power law behavior $\propto f^{-3/2}$. In Figure 5 there are also a set of narrow peaks, the first at $f \simeq 300$ Hz, which can be understood as contributions to $Z(f)$ coming from transverse oscillatory modes of the suspending wires (the so called *violin modes*, labeled *tnviol*).

- Thermal noise generated by dissipation in the mirrors (labeled *tnMir*), which is slightly larger than other noise sources between 50 Hz and 100 Hz. This contribution can also be understood using the fluctuation dissipation theorem. In this case the mechanical oscillators which interact with the heat bath are the internal elastic modes of the mirror's body. Each mode gives a deformation of the mirror's surface, which after being averaged on the laser beam profile is equivalent to a mirror displacement. Summing in quadrature we obtain the contribution shown in Figure 5, which is proportional to $f^{-1/2}$. The reason why this power law is different from the suspension's contribution is that now we are interested in frequencies below the resonances of the oscillators. As a matter of fact the peak at $f \simeq 5.5$ kHz that can be seen in Figure 5 corresponds to the lowest elastic mode of the mirror.
- Shot noise (labeled *Shot*), which is the most important contribution above 100 Hz and is described by the expression

$$\sqrt{S_h(f)} = \sqrt{\frac{\pi\hbar\lambda_\ell}{c}\left(\frac{c^2}{16\mathcal{F}^2L^2} + f^2\right)I_0^{-1}}, \qquad (27)$$

which is valid for an interferometer with resonant cavities along the arm. Equation (27) will be derived in Subsection II E 7. Here λ_ℓ is the laser's wavelength, $\mathcal{F}$ is the finesse of the cavities and L their length. The parameter I_0 is the laser power at the beam splitter. Equation (27) is characterized by the frequency scale

$$f_p = \frac{c}{4\mathcal{F}L}, \qquad (28)$$

and when $f \gg f_p$ the shot noise does not depend on the optical parameters of the cavities, but only on I_0. In this regime, the sensitivity will be proportional to the inverse of the laser power at the beam splitter, which means, taking into account the amplification induced by the power recycling cavity. Looking at Figure 5 we can estimate for Virgo $f_p \simeq 500$ Hz which agrees with the expected value in Table I. When $f < f_p$ the shot noise level will scale with $I_0^{-1/2}$, and we could decrease it by increasing the laser power. This will not improve the sensitivity of Virgo, however, as shot noise is not the dominant factor in this region.

There are many other contributions to the sensitivity which are represented in Figure 5. In this review we will discuss in particular gravity gradient noise (*Newtonian*, Sec. III B), radiation pressure noise (*RadPres*, Sec. II), and mirror thermoelastic noise (*ThElastMir*, Sec. IV A).

The strain equivalent spectral amplitudes of LIGO, Virgo, GEO600, and TAMA300 are compared in Figure 6. The general features of the error budget are quite similar. We see the rapid decrease of the sensitivity moving toward low frequencies. In the Virgo case this "seismic wall" is located at much lower frequencies (around 4 Hz) compared with the other detectors. This is due to the different implementation of the seismic attenuation, which will be discussed in Subsection III A. The peaks that can be seen in the low frequency part of the Virgo curve are as a matter of fact the resonances of the pendula chain in the attenuators. If we rescale the curve of each detector by a factor equal to his arm's length, the seismic dominated part of LIGOs and GEO600 became almost coincident. The reason is that the difference in sensitivity here is completely explained by the larger coupling to the strain allowed by a larger L, in other words the seismic attenuation system of LIGOs and GEO600 have similar performances in term of residual displacement of the mirrors. The "seismic wall" is in this case around 40–50 Hz. For TAMA300 the attenuation starts to be effective at larger frequencies, around 100 Hz.

To understand the differences in the high frequency, shot noise dominated part of the graph we can look at Eq. (27). As we said here the parameters of the cavity do not matter, but only the laser intensity at the beam splitter I_0. If we look at the values in Table I we see that the differences observed in Figure 6 agree with the expectations.

These simple considerations are not applicable to GEO600, which as we said has a different optical configuration. We will come back to this particular case when we will discuss signal recycling (Subsection II E 3). But we remark on a very special feature of the GEO600 setup: by changing the parameters of the signal recycling and power recycling cavities it is possible to tune the sensitivity for a signal of particular type. As an example, it is possible to have a very low noise in a reduced bandwidth, which is optimal for the search of nearly monochromatic waves emitted by rotating neutron stars.[51] This tuning can be done in real time, without interrupting the data taking.[40]

In the intermediate frequency range the sensitivity is limited by thermal noise. If we rescale the sensitivities in Figure 6, multiplying each curve by the arm length of the corresponding interferometer we would see similar values, with two notable differences. First, GEO600 would perform better, owing to his low dissipation monolithic suspensions. Second, the minimum sensitivity of LIGO is better than the VIRGO one. The reason for this is the lower contribution of mirror thermal noise in the former case, due to the different beam profile inside the cavities. This will be discussed in more detail in Sec. IV A.

The noise spectral amplitude is a very important figure of merit for the detector, however, it does not give complete information about its performance. In order to define it we assumed that the noise is a statistically stationary process, but this is rarely strictly true. Nonstationarities can arise at several different time scales.

Drifts of the apparatus parameters generated by its residual coupling to the environment, for example, thermal fluctuations, can slowly change the interferometer behavior, and ultimately destabilize it. If the change is slow enough (its characteristic time scale is large compared with the inverse of the lowest frequency in the detection band) the detector can conveniently be characterized with a time dependent noise

Downloaded 02 Nov 2011 to 180.149.51.196. Redistribution subject to AIP license or copyright; see http://rsi.aip.org/about/rights_and_permissions

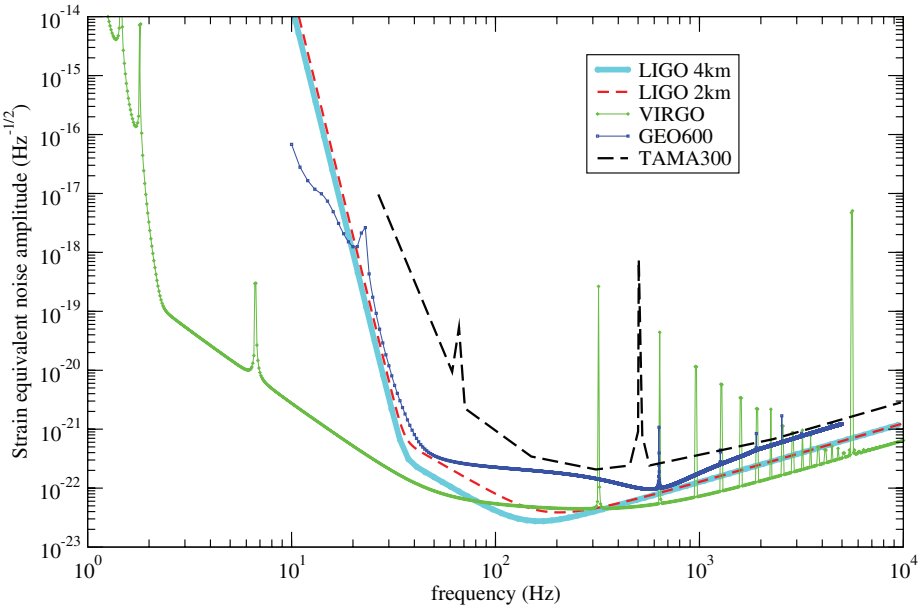


FIG. 6. (Color) The design sensitivities for LIGO 4 km, LIGO 2 km,Virgo, GEO600, and TAMA300. For GEO600 the sensitivity can be tuned by changing the parameters of signal recycling (see Subsection II E 3 and Ref. 50). The plotted curve correspond to a detuning of the recycling cavity of 550 Hz.

amplitude, or with figures of merit derived from it. This leads to the concept of duty cycle, which can be defined as the fraction of the time in which the sensitivity of the apparatus is satisfactory.

Fast nonstationary noise also exists. A typical problem is the presence in the data of short transient events, which can often be modeled as Poisson processes. The discussion of the problems generated by these unwanted features in the data analysis procedures is beyond the scope of this paper, but it is intuitively clear that they can mimic some kind of gravitational wave events. For this reason they should be reduced as much as possible by understanding their physical sources and by removing them. When the reduction of some class of spurious events is not possible, it is very important to characterize them in order to veto the affected segments of data. Typically, this is done by comparing the detector output with the output of additional sensors which monitor the environment.[52–54]

II. OPTICAL ISSUES

Looking at the simplified optical schemes in Figures 2 and 3 we see that, though the basic idea of an interferometric detector is quite simple, there are several issues we should take care of in order to obtain a working detector with the desired sensitivity.

A basic point is that mirrors and other optical elements must be maintained quite near to a convenient operating point in order to work correctly. The external disturbances are so large that this can be done only by implementing an active control strategy. We need to be able to sense the deviations from the chosen operating point, and to apply appropriate forces to correct them. This is discussed in Subsection II A.

In Sec. I we said that when the two arms of the interferometer are perfectly balanced, the fluctuation of the laser beam can be completely neglected. In a real detector this perfect balance can never be obtained, as there are always tolerances in the parameters of the optical elements. Beside that, some asymmetry between the arms can be introduced explicitly for reasons that we will discuss in Subsection II A. As a consequence the laser fluctuations must be reduced, as described in Subsection II B. It is also important to realize that a laser beam is not a simple "light ray" without any geometrical structure.

Apart from "classical" fluctuations induced by external fluctuations, the laser beam and other electromagnetic fields coupled to the apparatus are affected by quantum fluctuations. Phase fluctuations in particular act as a source of noise for the detector. In Subsection II C, we introduce the appropriate formalism to deal with these effects, and we will evaluate the expected contribution of this "quantum optical noise" to the total budget. This evaluation depends on the particular strategy used to detect the phase change of the light exiting the detector. There are several possibilities, we will discuss the most important ones in Subsection II D.

Finally, in Subsection II E we discuss the reduction of this "quantum optical noise." Some techniques have already been implemented in current detectors. The simplest is the power recycling one discussed previously, which as we said amounts to an amplification of the effective laser intensity seen by the mirrors.

This "brute force" approach cannot reduce the noise in an arbitrary way: by increasing the laser power we increase the effect of radiation pressure fluctuations on the mirrors, which also imposes a sensitivity limit. The best compromise between noise induced by phase fluctuations and noise induced by radiation pressure fluctuations have been named

Downloaded 02 Nov 2011 to 180.149.51.196. Redistribution subject to AIP license or copyright; see http://rsi.aip.org/about/rights_and_permissions

standard quantum limit (SQL), and can be understood as a manifestation of the Heisenberg uncertainty principle. Recalling Heisenberg's principle could suggest that SQL is in some sense a fundamental and unavoidable limit. This is not the case: several techniques that can be used to "evade" it have been proposed and we will present some of them. Conceptually, the point is that in order to detect a gravitational wave we do not need really to measure the positions of the mirror repeatedly and with infinite precision, but only to have information about the gravitational "forces" that act on them. As discussed in several works (we suggest, in particular, Refs. 55, 56, and Ref. 57 for a general introduction to the problem) there are no fundamental restriction for doing this. Of course there can be a lot of technological ones.

A possibility is signal recycling, which has been demonstrated in GEO600 and will be also discussed in Subsection II E. More refined techniques are not really important for currently active detectors, which are dominated by thermal noise at intermediate frequencies, but they will be for the future ones.

A. Locking and control

When we describe the coupling of an interferometer to external forces and gravitational waves we implicitly assume that its behavior is linear. However, strictly speaking this is not true, as the phase shift induced by a resonant cavity is a strongly nonlinear function of its length. More precisely, in the quasistatic regime for a cavity with an input mirror of reflectivity r this shift ϕ is given by

$$\phi(\omega_\ell) = \frac{2\omega_\ell L}{c} + 2\arctan\left[\frac{r\sin\left(\frac{2\omega_\ell L}{c}\right)}{1 - r\cos\left(\frac{2\omega_\ell L}{c}\right)}\right] \simeq \frac{2\omega_\ell L}{c} + 2\arctan\left[\frac{\frac{\mathcal{F}}{\pi}\sin\left(\frac{2\omega_\ell L}{c}\right)}{1 + \frac{2\mathcal{F}}{\pi}\sin^2\left(\frac{\omega_\ell L}{c}\right)}\right], \quad (29)$$

where L is the length of the cavity, ω_ℓ is the laser's angular frequency, and the approximation is valid in the large finesse ($r \simeq 1$) regime. This relation is represented graphically in the plot at the center of Figure 7, for several values of r.

Looking at Eq. (29) around the resonance ($L = N\lambda_\ell/2 + \delta L$, where $\lambda_\ell = 2\pi c/\omega_\ell$ is the laser's wavelength) we see that the relevant length scale for the onset of nonlinearities is given by

$$\delta L_{lin} = \frac{\lambda_\ell}{4\mathcal{F}}, \quad (30)$$

which is a small fraction of the wavelength.

As we will see in Sec. III A it is possible to filter the seismic noise in such a way that the spectral amplitude of the mirror's motion is less than 10^{-11} m Hz$^{-1/2}$ above 4 Hz, but in the nonlinear regime the noise spectral amplitude is not a good figure of merit. A more relevant parameter is the total root mean square motion $\sigma_{\rm rms}$ of the mirror, which is the integral of the power spectrum over all the frequencies. The requirement for linearity is that $\sigma_{\rm rms} < \delta L_{lin}$, which is badly violated: the power spectrum integral is dominated by the low frequency region, where the attenuation is not effective and the total rms is typically of the order of several wavelengths. An active feedback system must be used to "lock" the cavities in the linear regime around their requested working point. In GEO600 there are no Fabry-Perot cavities along the arms, but the length of these must be stabilized in any case.

In order to implement an active control for a given degree of freedom we need two ingredients. The first is an error signal, which can be used to know where the system is with respect to the desired configuration. The second is an actuator, which allows us to apply to the system the desired correction.

Let us consider a simple example, the locking of a single, completely reflecting resonant cavity around one of its resonances. Before entering the cavity the phase of the laser of frequency f_ℓ is modulated at a frequency f_{mod}. In this way a series of sidebands are generated, accordingly with the identity

$$e^{i(2\pi f_\ell t + \beta\cos 2\pi f_m t)} = \sum_{n=-\infty}^{\infty} i^n J_n(\beta) e^{2\pi i(f_\ell + n f_{mod})t}, \quad (31)$$

$J_n(\beta)$ being the Bessel function of integer index n. The modulated field $E_{\rm in}$ entering the cavity can be written as

$$E_{\rm in} = E_0\,{\rm Re}\left\{e^{i\omega_\ell t}\sum_{n=-\infty}^{\infty} i^n J_n(\beta) e^{i\omega_n t}\right\}, \quad (32)$$

where $\omega_n = 2\pi n f_{mod}$. The cavity will introduce a different phase shift for each frequency component,

$$E_{\rm out} = E_0\,{\rm Re}\left\{e^{i\omega_\ell t}\sum_{n=-\infty}^{\infty} i^n J_n(\beta) e^{i\omega_n t + i\phi_n}\right\}, \quad (33)$$

where $\phi_n = \phi(\omega_\ell + \omega_n)$ is given by Eq. (29).

The current I_{PD} generated by the photo-diode, *PD*, will be proportional to the intensity of the field,

$$I_{PD} \propto \overline{E_{\rm out}^2} = \frac{E_0^2}{2}\left|\sum_{n=-\infty}^{\infty} i^n J_n(\beta) e^{i\omega_n t + i\phi_n}\right|^2, \quad (34)$$

where the average is over a time scale large compared with f_ℓ^{-1} but small compared with f_m^{-1}. Expanding the squared modulus we get

$$I_{PD} = \frac{E_0^2}{2}\sum_{n,m} i^{n-m} J_n(\beta) J_m(\beta) e^{i\omega_{n-m}t + i(\phi_n - \phi_m)}, \quad (35)$$

and we see that I_{PD} contains all the harmonics of the modulation frequency f_{mod}, each of them weighted by an amplitude which contains information about the resonant cavity through the phase shifts ϕ_k. In the Pound-Drever-Hall technique[58,59] we multiply I_{PD} by a signal which oscillates at the modulation frequency, $\cos(\omega_1 t + \varphi)$, and we average it over a time length which is large compared with f_{mod}^{-1}, but small compared with the time scale of the typical variation of the cavity parameters we are interested to detect. In this way only the terms

Downloaded 02 Nov 2011 to 180.149.51.196. Redistribution subject to AIP license or copyright; see http://rsi.aip.org/about/rights_and_permissions

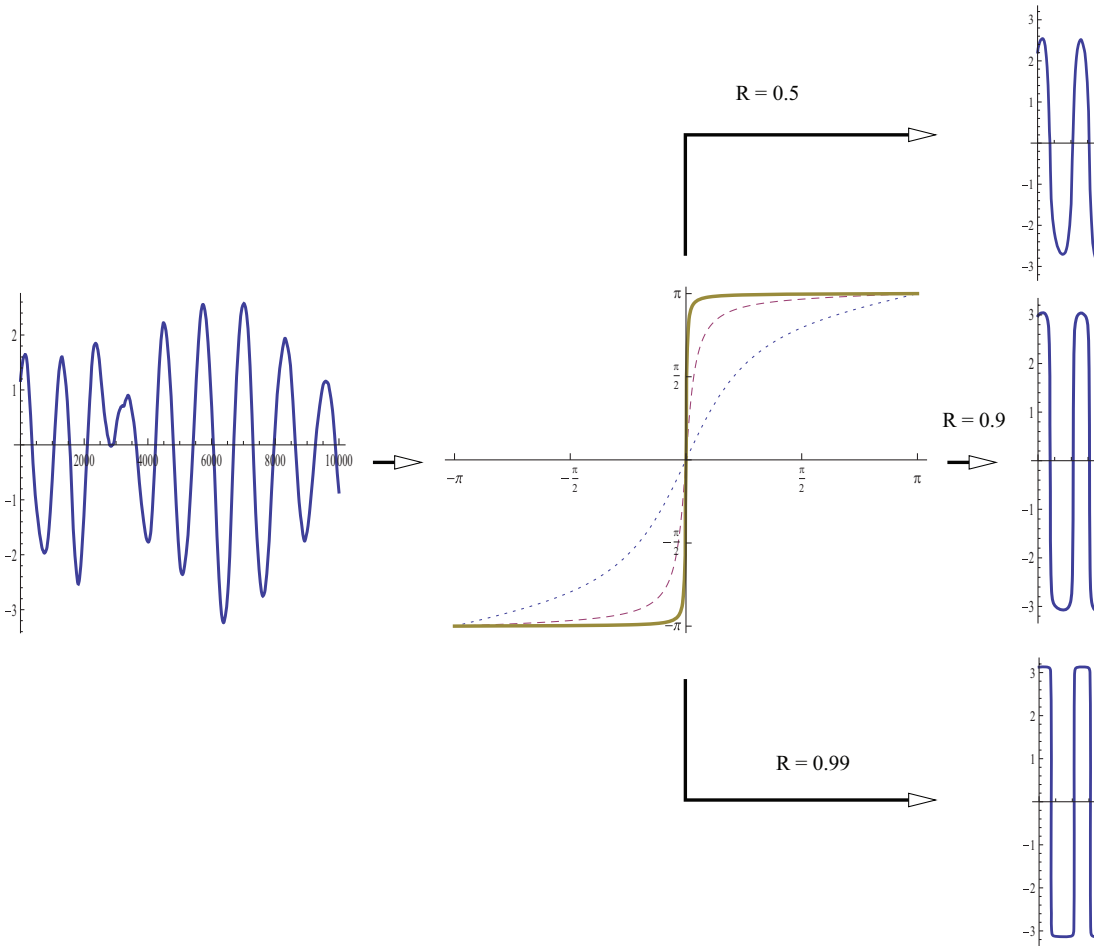


FIG. 7. (Color online) The relation between cavity length and output phase for a resonant cavity. The relation between $\varphi = 2\omega_\ell \delta L/c$ and ϕ (see Eq. (29)) is represented in the center plot, for values of the input mirror's reflectivity which correspond to a cavity finesse of $\mathcal{F} \simeq 4.4$ ($r = 0.5$), $\mathcal{F} \simeq 30$ ($r = 0.9$), and $\mathcal{F} \simeq 312$ ($r = 0.99$). (Left) A qualitative representation of a typical random motion of the cavity, which we suppose is dominated by the pendular mode of the attenuation chain (arbitrary horizontal units, vertical units of $\lambda_\ell/4\pi$). (Right) The resulting phase shift for the chosen values of R (arbitrary horizontal units, vertical units of radians).

with $|m - m| = 1$ survives in the sum (35), and we obtain a signal

$$\begin{aligned} PDH(\varphi) &\equiv \overline{\cos(\omega_1 t + \varphi) I_{PD}} = \mathrm{Re}\,\overline{e^{-i\omega_1 t - i\varphi} I_{PD}} \\ &= -\frac{E_0^2}{2}\sum_{n=0}^{+\infty} J_{n+1}(\beta) J_n(\beta) \mathrm{Im}[e^{i(\phi_{n+1} - \phi_n - i\varphi)} \\ &\quad - e^{-i(\phi_{-(n+1)} - \phi_{-n} + i\varphi)}] \\ &= -\frac{E_0^2}{2}\sum_{n=0}^{+\infty} J_{n+1}(\beta) J_n(\beta) [\sin(\phi_{n+1} - \phi_n - \varphi) \\ &\quad + \sin(\phi_{-(n+1)} - \phi_{-n} + \varphi)]. \end{aligned} \tag{36}$$

From Eq. (29) it follows that when the laser is resonating inside the cavity it is $\phi_{-n} = -\phi_n$ and $PDH(\varphi) = 0$. The important point is that when we move around the resonance $PDH(\varphi)$ changes sign and can be used as an error signal. To get an intuition about that we can choose the modulation frequency f_m in such a way that when f_ℓ resonates $f_\ell \pm f_{mod}$ is anti-resonating, which means in the middle plot of Figure 7 f_ℓ correspond to the center (maximal slope) and $f_\ell \pm f_{mod}$ to the "flat" zone. In less mathematical terms the sidebands $f_\ell \pm f_{mod}$ are directly reflected by the first mirror, so their phase is practically insensitive to changes of the cavity's length, $\phi_{\pm 1} \simeq \pm\pi$, and can be used as a fixed reference.

For a small modulation amplitude $PDH(\varphi)$ is dominated by the $n = 0$ term in the sum (36) (note that the kth term is $O(\beta^{2n+1})$) and we can write

$$PDH(\varphi) \simeq -E_0^2 \frac{\beta}{2} \cos\varphi \sin\phi_0 \simeq -4\mathcal{F} E_0^2 \beta \cos\varphi \frac{\delta L}{\lambda_\ell}, \tag{37}$$

where the second approximation is valid in the linear region $\delta L \ll \frac{\lambda}{\mathcal{F}}$. We conclude that the Pound-Drever-Hall technique allows us to monitor the displacement δL of a cavity from its resonant value and to implement a *longitudinal* control. Similar techniques can be elaborated for cavities with two partially reflective mirrors, using the reflected or the transmitted signal.

The maintaining of the correct length for the cavities is a necessary but not sufficient condition for the correct behavior of the detector. To understand this point we must note that until now we considered a laser beam essentially as a monochromatic plane wave interacting with idealized mirrors and beam splitters. This is a very crude model: in a real laser beam the field is different from zero in a significant way only in a

Downloaded 02 Nov 2011 to 180.149.51.196. Redistribution subject to AIP license or copyright; see http://rsi.aip.org/about/rights_and_permissions

limited area around its axis of propagation. A more correct model will be a solution of the electromagnetic wave equation with this property.

The solution of this problem leads to express the electromagnetic field of a generic beam propagating along the z axis in the positive direction, of frequency f, as a sum over *modes*[36] which looks like

$$E(x, y, z, t) = e^{-i2\pi f(t-z/c)} \sum_{\mu} \mathcal{M}_{\mu}^{A;f}(x, y, z), \tag{38}$$

where E is a generic component of the electromagnetic field (we are ignoring polarizations here) and $\mathcal{M}_{\mu}^{A;f}$ is an appropriate set of mode functions labeled by μ. The expansion for a beam moving in the opposite direction can be obtained by changing sign to z.

A commonly used expansion can be given in term of Hermite-Gauss modes

$$\mathcal{M}_{m,n}^{HG;f}(x, y, z) = \frac{\mathcal{N}_{mn}}{w(z)} H_m\left(\frac{x\sqrt{2}}{w(z)}\right) H_n\left(\frac{y\sqrt{2}}{w(z)}\right) \times \exp\left[-\frac{x^2+y^2}{w(z)^2} + ik\frac{x^2+y^2}{2R(z)} - i\,(m+n+1)\,\phi(z)\right], \tag{39}$$

which are labeled by the pair $\mu \equiv (m, n)$ of non-negative integers. Here $k = 2\pi f/c$, $H_m(x)$ is the mth Hermite polynomial and $\mathcal{N}_{nm}$ is a normalization constant. The function

$$w(z) = w_0\sqrt{1 + \frac{z^2}{z_r^2}} \tag{40}$$

sets the length scale for the amplitude of the field in a plane transverse to the direction of propagation. The free parameter w_0 is the minimum of $w(z)$, its location being the *beam's waist*. The Rayleigh range z_r is related to it by

$$z_r = \frac{\pi w_0^2}{\lambda}. \tag{41}$$

We show the amplitude of the mode for $z = 0$ in some particular cases in Figure 8. We see that the amplitude of the field in the transverse plane has a Gaussian envelope, modulated by the polynomials H_m, H_n. In particular in the *fundamental mode* $\mathcal{M}_{00}^{HG}$ the intensity of the light, proportional to the square of the field, is just a Gaussian of standard deviation $w(z)/2$. When $|z| \gg z_r$ the beam diverges linearly, the divergence angle $\theta_G \equiv \lambda/(\pi w_0)$ being larger and larger when w_0 decrease, a typical diffraction effect.

The phase of the field in a given point depends on the function

$$R(z) = z\left(1 + \frac{z_r^2}{z^2}\right), \tag{42}$$

which is the radius of curvature of the phase front of the beam. We see that the equal phase surfaces are defined for $|z| \gg z_r$ by a paraboloid of rotation with curvature radius $R(z)$. In this region the beam can be described near the axis as a spherical wave. Finally,

$$\phi(z) = \arctan\left(\frac{z}{z_r}\right) \tag{43}$$

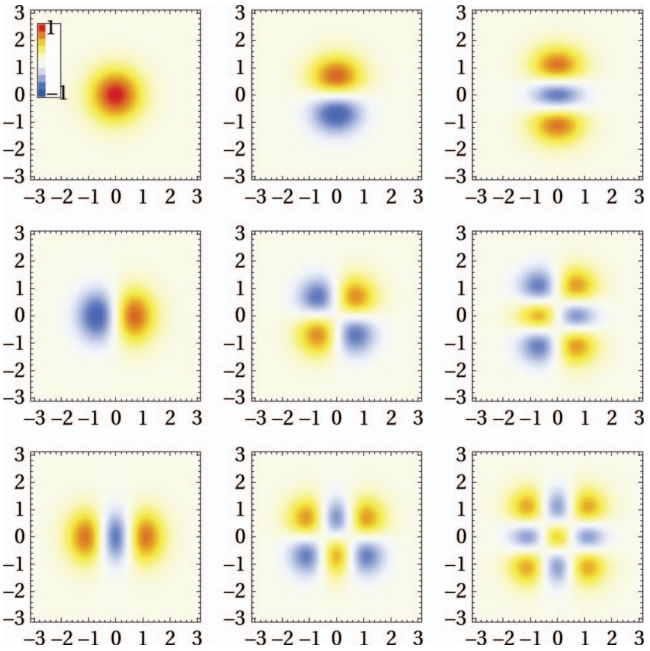


FIG. 8. (Color) The amplitude (in arbitrary units) of the field in the plane transverse to the beam axis for Hermite-Gauss modes $\mathcal{M}_{mn}^{HG}$ with $m = 0, 1, 2$ (rows) and $n = 0, 1, 2$ (columns). We set $w_0 = 1$ and $z = 0$.

is called Gouy phase, and gives an additional mode dependent phase shift of $(m + n + 1)\pi$ radians when the beam propagates through the point of minimal transverse extension w_0 at $z = 0$.

Each mode in Eq. (38) propagates independently from the others. The situation is different when the beam interacts with an optical element. Let us consider, for example, the reflection on a curved mirror: the reflected field can be evaluated and expanded again in modes. It turns out that a given mode is reflected back in the corresponding one with $z \to -z$ only if the phase of the field is the same on all the mirror's surface. If this is not the case the reflected field will contain several different modes. This means that there are two different conditions that must be satisfied for a mode to be able to resonate inside a cavity. First of all the phase cumulated in a round trip must be an integer multiple of 2π. We met this condition before and there is nothing new apart from the fact that the phase must be evaluated taking into account the additional shift induced by the Gouy term (43). This being mode dependent, we expect that only a subset of the modes will be able to resonate.

The new requirement is that the mirror's surface must be *matched* to the equal phase surfaces of the beam. In particular for Hermite-Gauss modes a mirror located at z_M must have a curvature radius $R(z_M)$ and must be normal to the beam axis. Once we fixed the curvature radii of the two mirrors, and their separation, the matching conditions fix the value of w_0 and the position of the $z = 0$ point inside the cavity. In LIGO the $z = 0$ point is chosen in the middle of the cavity, so the mirrors have the same curvature radius. In VIRGO the $z = 0$ point is on the input mirror, which is flat.

The common choice is to arrange the parameters in such a way to have the fundamental mode $\mathcal{M}_{00}^{HG;f_\ell}$ resonating in the cavities. It is mandatory to minimize the fraction of

Downloaded 02 Nov 2011 to 180.149.51.196. Redistribution subject to AIP license or copyright; see http://rsi.aip.org/about/rights_and_permissions

light transferred in a reflection to higher order contributions $\mathcal{M}_{mn}^{HG;f_\ell}$, $m + n > 0$, which is essentially lost and leads to a reduction of sensitivity. This requires the mirrors to be accurately manufactured, with the correct curvature radius and with very low roughness. They must also be maintained aligned, and we need again a control strategy to compensate the effect of external disturbances.

In this case the error signal must contain information about misalignments,[60] which can be generated both by displacements transverse to the beam axis and by rotations.

The signal can be obtained by an extension of the Pound-Drever-Hall technique.[61] The basic idea is the following. Suppose that the $\mathcal{M}_{00}^{HG;f_\ell}$ resonates inside an aligned cavity. In this case only this mode will have an amplitude different from zero. But when a misalignment occurs, part of the field will be converted in other modes. For small nonalignments these will be mainly the $\mathcal{M}_{01}^{HG;f_\ell}$ (for a translation in the vertical direction or a rotation around an horizontal axis) and the $\mathcal{M}_{10}^{HG;f_\ell}$ (for a translation in the horizontal direction or a rotation around a vertical axis). Explicitly the cavity field will be something like

$$E \propto \mathcal{M}_{00}^{HG;f_\ell}(x, y, z) + \left(\frac{\delta x}{w_0} + i\frac{\theta_y}{\theta_G}\right)\mathcal{M}_{10}^{HG;f_\ell}(x, y, z) + \left(\frac{\delta y}{w_0} - i\frac{\theta_x}{\theta_G}\right)\mathcal{M}_{01}^{HG;f_\ell}(x, y, z), \tag{44}$$

where θ_x, θ_y are small rotation angles of the beam around the x, y axis and δx, δy are small displacements of its waist. This equation tells us also what "small" means: the angular deviation must be compared with the beam divergence θ_G and the translation with w_0. It is apparent that the amplitudes of the $\mathcal{M}_{10}^{HG;f_\ell}$ and $\mathcal{M}_{01}^{HG;f_\ell}$ modes contain the information about misalignments we need.

A first method to measure them has been developed by Anderson.[62] The Pound-Drever-Hall modulation frequency is chosen in such a way that both the mode $\mathcal{M}_{00}^{HB;f_\ell}$ at the laser frequency and the modes $\mathcal{M}_{01}^{HG;f_\ell \pm f_{mod}}$, $\mathcal{M}_{10}^{HG;f_\ell \pm f_{mod}}$ at one of the two sideband frequencies are resonating. The modulated incoming beam contains the modes $\mathcal{M}_{00}^{HG;f_\ell}$, $\mathcal{M}_{00}^{HG;f_\ell + f_{mod}}$ and $\mathcal{M}_{00}^{HG;f_\ell - f_{mod}}$ and if the cavity is well aligned the sidebands will be reflected, and only $\mathcal{M}_{00}^{HG;f_\ell}$ will resonate. In presence of a misalignment the reflection of the mirrors will convert a fraction of $\mathcal{M}_{00}^{HG;f_\ell + f_{mod}}$ and $\mathcal{M}_{00}^{HG;f_\ell - f_{mod}}$ in higher order modes, that being resonating will be amplified and sent back. The useful signal will be contained in interference terms proportional to products like

$$\mathcal{M}_{00}^{HG;f_\ell}\mathcal{M}_{01}^{HG;f_\ell - f_{mod}}, \tag{45}$$

which must be detected. But this cannot be done with a single photo-diode, because the integrated value of the intensity will be zero (see Figure 8). Using quadrant diodes, like the Q_i that appear in the diagram 2, we get a signal which is proportional to the difference between the beam intensity integrated on the left and the right part (or on the up and down one) of the diode's surface, which is a measure of the interference. In particular, the difference between left and right part will be of the form

$$I_{diff} \propto \frac{\delta x}{w_0}\cos(2\pi f_{mod}t) + \frac{\theta_y}{\theta_G}\sin(2\pi f_{mod}t) \tag{46}$$

so that it will possible to demodulate separately the information about the translation and the rotation. A completely analogous result holds for the difference between up and down part, which allows the measure of δy and θ_x.

Another approach was suggested by Drever and experimentally demonstrated by Ward.[63] In this case no special condition is imposed on the modulation frequency and only the $\sin(2\pi f_{mod}t)$ part of the difference signal produced by the quadrant diode is used. If the detection is done at a position z along the beam axis the analogous of Eq. (46) is

$$I_{diff} \propto \left[\frac{\delta x}{w_0}\sin\phi(z) + \frac{\theta_y}{\theta_G}\cos\phi(z)\right]\sin(2\pi f_{mod}t), \tag{47}$$

where $\phi(z)$ is the Gouy phase. In order to get separate information for displacements and rotations we need to measure the intensity at two different positions z_1, z_2. This is the reason why simple and quadrant photo-diodes depicted in the diagram 2 are arranged in triplets, for example, Q_{22}, Q_{21}, and B_2. Each triplet provide five error signals, the longitudinal one discussed previously (standard photo-diode) and the four δx, δy, θ_x, and θ_y needed for the alignment.

In a real detector there are several lengths which must be locked to obtain a working detector.[64] There are four important degrees of freedom that must be stabilized, which can be understood by looking at the simplified optical scheme in Figure 2.

We have the lengths of the main Fabry-Perot cavities, L_{WI-WE} and , L_{NI-NE} or better their symmetric and antisymmetric combinations

$$CARM \equiv L_{NI-NE} + L_{WI-WE}, \tag{48}$$

$$DARM \equiv L_{NI-NE} - L_{WI-WE}. \tag{49}$$

L_{WI-WE} is the distance between the WI and WE mirrors, L_{NI-NE} between the NI and the NE ones.

The Michelson interferometer formed by the beam splitter BS and by the mirrors WI and NI must be locked also. The difference between the lengths of its two arms is

$$MICH \equiv L_{WI-BS} - L_{NI-BS} \tag{50}$$

Finally the length relevant for the power recycling cavity is

$$PRCL \equiv L_{BS-PR} + \frac{1}{2}(L_{BS-WI} + L_{BS-NI}). \tag{51}$$

In order to do this the signals provided by several photodiodes (depicted in Figure 2 also) must be used.

An important point is that the actuators used to apply the feedback forces act on the mirrors. As a consequence, it is not possible to control independently *CARM*, *DARM*, *MICH*, and *PRCL*. There will be a non-diagonal *sensing matrix* which connect feedback and actuation.

Feedback forces are needed only at low frequencies, so the mirrors are actively controlled only in the low frequency region, freely moving otherwise. The boundary be-

Downloaded 02 Nov 2011 to 180.149.51.196. Redistribution subject to AIP license or copyright; see http://rsi.aip.org/about/rights_and_permissions

tween the controlled and the free zone is not really sharp, and is determined requiring the total rms to be compatible with the linearity. An interesting consequence of this is that the output signal of the detector must be reconstructed. In the uncontrolled zone it is essentially the calibrated output of the interferometer at the dark fringe. In the controlled one the mirrors are fixed, and information on the gravitational wave strain must be recovered from the control signal used in the feedback. In the intermediate region an appropriate combination of the dark fringe signal and of the control one is constructed.

1. Lock acquisition

The lock acquisition is an independent issue. When the interferometer is not locked the mirrors move freely on a scale of several wavelengths. The typical motion of an uncontrolled mirror is qualitatively represented in the left plot of Figure 7. Its quasi-periodic appearance is due to the fact that, as we said, the total rms is dominated by the low frequency region and by the fundamental pendular mode of the attenuator in particular.

The output of a cavity which moves in that way is represented on the three plots on the right, which correspond to three different finesses. When the cavity's finesse is not small the dynamic of the signal is strongly depressed and will be overwhelmed by the instrumental noise. This means that it is not possible to use it as a control signal, except in the periods when $L = N\lambda/2 \pm \ell_{lin}$. But the cavity will be in this regime only for a typical time $\tau_{lin} = \ell_{lin} v_{rms}^{-1}$. There will be a low probability for the feedback procedure to stabilize the system in this period.

A possible approach is to try to acquire the lock each time the cavity passes through the linear region, and to wait until success.[65] The variable τ_{lin} has in fact a statistical distribution with some finite probability of being larger than some value which allows the locking. This leads to a sequential procedure where the locks of *CARM*, *DARM*, *MICH*, and *PRCL* are obtained one after the other. An additional complication is that the *sensing matrix* that must be used at each step is different, and must be changed dynamically.

An alternative is the variable finesse technique.[66] The basic idea is to acquire the control of the relevant degrees of freedom in an optical working point which is not the final one and is easier to lock. This is obtained by misaligning the power recycling mirror *PR* by some microradians, in such a way to have a large amounts of losses. In this way the finesse of the cavity is lowered, and the corespondent linear range increased. Additionally *MICH* is set in such a way that the transfer functions of the two arms $\mathcal{P}_N$, $\mathcal{P}_W$ are not equal, which means complete cancellation of the light O_D exiting from the dark port, but instead in a regime were $O_L \simeq O_D$ (see Figure 1).

In this configuration *CARM*, *DARM*, *MICH*, and *PRCL* are almost decoupled, and the lock for each of them can be acquired independently and in an easier way due to the reduced finesse. When this is done both the misalignment of *PR* and the offset in *MICH* is removed adiabatically remaining in the locked state, and ending in the required working point. We refer to Ref. 66 for more details.

B. The laser source

A laser source which is at the same time powerful (in order to reduce shot noise) and stable is needed. It is difficult to obtain this because high power lasers are quite sensitive to external perturbations. Beside that, they typically require strong pump sources which are affected by large noises. A possible way to fulfill these requirements is based on a master-slave, injection locked configuration.[67] The basic principle can be described as follows. We start with a "master" laser, which has a reduced power but good stability properties. The idea is to couple it with a high power, "slave" laser. This can be obtained simply as in Figure 9, by injecting the output of the "master" in the resonator of the slave. If the injected power is high enough, and if the frequencies of the "slave" and of the "master" are not too far, the "slave" is forced to operate exactly on the injected frequency. In principle with this method it is possible to come close to the quantum limit for phase and amplitude fluctuations of the final beam (see Sec. II C).

A shift of the natural frequency of the "slave" resonator too far from the frequency of the "master" can be prevented by using a feedback procedure. In Figure 9 the "slave" resonator is a cavity whose optical length can be changed by moving one or more of its mirrors. This is typically obtained with piezoelectric actuators driven by the feedback. The error signal required to implement the control strategy can be obtained by measuring the phase of the output. In Figure 9, this is implemented by using a standard Pound-Drever-Hall procedure, extracting a small fraction of the output light with the partially transmitting mirror M_d.

A standard way to stabilize the frequency of the laser is to lock it to some reference cavity using feedback. Let us consider again for reference the simplified VIRGO optical scheme in Figure 2. The coherent light source is provided by an injection locked master-slave solid state laser ($Nd:YVO_4$).[68] It delivers a power of 20 W at a wavelength of 1064 nm, and enters the vacuum system at the injection bench (*IB*).

A triangular cavity with a round trip length of $L_{RT} = 287$ m (the input mode cleaner, *IMC*) is used for a prestabilisation of the laser frequency. Low frequency stability is obtained by a control system which stabilizes the *IMC* cavity using as a reference the rigid triangular cavity *RFC*.

Another important purpose of the *IMC* cavity is the spatial filtering of the laser beam.[69] As we said the resonant cavities of the interferometer are maintained at the resonance of the fundamental mode $\mathcal{M}_{00}^{HG;f_\ell}$, and it is important for the input beam to be coupled as much as possible to it. However, the intensity profile of the beam provided by the laser source can be different from the desired one, as several spatial distortions can be induced by optical components which are encountered along its path such as electro-optical modulators, or by thermal lensing effects. An equivalent way to express this is the following: a fraction of the laser power will be distributed on modes which are different from $\mathcal{M}_{00}^{HG;f_\ell}$ and must be reduced.

Downloaded 02 Nov 2011 to 180.149.51.196. Redistribution subject to AIP license or copyright; see http://rsi.aip.org/about/rights_and_permissions

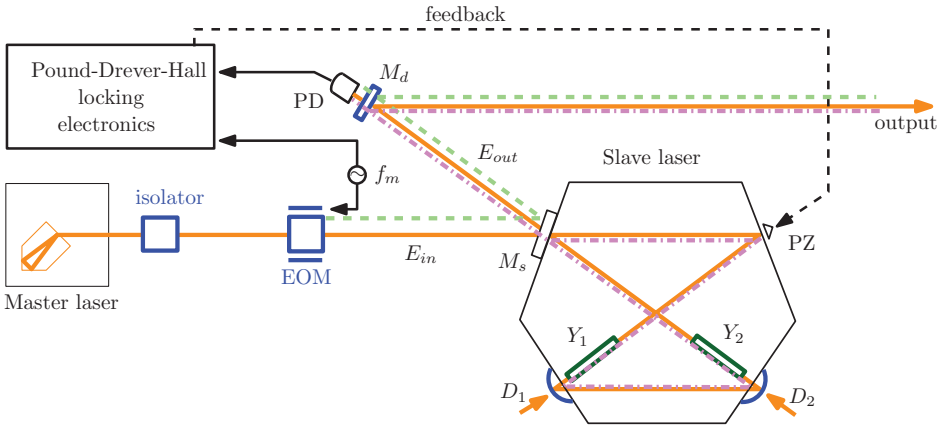


FIG. 9. (Color) Scheme of the high power laser used in Virgo, based on injection locking techniques. The master laser's beam (continuous orange) of frequency f_ℓ is phase modulated by the electro-optical modulator *EOM*, which introduces two sidebands $f_\ell \pm f_m$ (dashed green). The interaction between the master's beam and the mirrors inside the cavity introduce a further modulation (dashed-dotted, pink), which is the noise to be reduced. A fraction of the light produced is transmitted through the reflective mirror M_s, and photodetected. The feedback signal is obtained using a standard Pound-Drever-Hall technique, and used to drive the piezoelectric actuator *PZ*.

This can be done arranging the *IMC* parameters in such a way that $\mathcal{M}_{00}^{HG;f_\ell}$ is maximally transmitted, while other modes are suppressed. The *IMC* has been chosen to be triangular to avoid back reflection of the beam toward the laser source, with initial and final flat mirrors and an intermediate one with a curvature radius R_C. With this geometry the filtering efficiency can be quantified as

$$\frac{T_{mn}}{T_{00}} = \frac{1}{1 + \left(\frac{2\mathcal{F}}{\pi} \sin \frac{2\pi L_{RT}}{c} \Delta_{mn}\right)^2}, \tag{52}$$

where T_{mn} is the power transmission coefficient for the $\mathcal{M}_{mn}^{HG;f_\ell}$ mode and

$$\Delta_{mn} = \frac{c(m+n)}{2\pi L_{RT}} \arccos \sqrt{1 - \frac{L_{RT}}{R_C}}. \tag{53}$$

As Eq. (53) suggests, the filtering principle is based on the fact that different modes, though at the same frequency f_ℓ, can gain a different phase shift in a round trip owing to the Gouy phase contribution (see Eq. (43)). From Eq. (52) it is evident that a good rejection of higher order modes require a large finesse $\mathcal{F}$ of the cavity. It is also mandatory to avoid degenerate cavities where

$$(m+n) \arccos \sqrt{1 - \frac{L_{RT}}{R_C}} = k\pi \tag{54}$$

for some integer k. In other words, the ratio L_{RT}/R_C must be chosen in such a way to avoid that any higher order mode will resonate together with the fundamental one.

C. Optical noise

A correct investigation of the optical noise cannot avoid a quantum description of the laser beam. A considerable simplification is that a linear approximation in the fluctuations is almost always adequate (this does not means that nonlinear effects are always completely negligible, see, for example, Ref. 70). As we saw the effect of the motion of the mirror is the generation of a several symmetric pair of sidebands around the carrier field. It is convenient to introduce a formalism that describes each pair as a single object,[71,72] the quadrature vector. We are not interested in polarization effects, so we can describe the beam with a single component of the electric field which we write as a quantum operator,

$$\hat{E}(t) = \int_0^\infty \sqrt{\frac{2\pi\hbar\omega}{Sc}} [\hat{a}(\omega) e^{-i\omega t} + \hat{a}^\dagger(\omega) e^{i\omega t}] \frac{d\omega}{2\pi}. \tag{55}$$

Here S is the transverse section of the beam and $\hat{a}(\omega)$,$\hat{a}^\dagger(\omega)$ creation and destruction operators with nonzero commutator $[\hat{a}(\omega), \hat{a}^\dagger(\omega')] = 2\pi\delta(\omega - \omega')$.

The first step is to write the positive frequency part $E^{(+)}(t)$ of the electric field as

$$\hat{E}^{(+)}(t) = \frac{1}{2}\left[\hat{E}_1(t) + i\hat{E}_2(t)\right] e^{-i\omega_c t}$$

a relation which defines in an unique way the Hermitian quadrature operators $\hat{E}_1(t)$, $\hat{E}_2(t)$. Note that

$$\hat{E}(t) = \hat{E}_1(t) \cos(\omega_c t) + \hat{E}_2(t) \sin(\omega_c t). \tag{56}$$

The operators $\hat{E}_1(t)$, $\hat{E}_2(t)$ can now be written as

$$\begin{pmatrix} \hat{E}_1(t) \\ \hat{E}_2(t) \end{pmatrix} = \sqrt{\frac{4\pi\hbar\omega_c}{Sc}} \left[\underline{\alpha} + \int_0^{\omega_c} \left(\delta\underline{a}(\Omega) e^{-i\Omega t} + h.c.\right) \frac{d\Omega}{2\pi}\right]. \tag{57}$$

Here we split the field in a "large" part proportional to the real two component vector $\underline{\alpha}$, which represents the carrier field, and in a "small" one proportional to the quadrature vectors

$$\delta\underline{a}(\Omega) = \begin{pmatrix} \delta\hat{a}_1(\Omega) \\ \delta\hat{a}_2(\Omega) \end{pmatrix} \equiv \frac{1}{\sqrt{2}} \begin{pmatrix} \delta\hat{a}_+ + \delta\hat{a}_-^\dagger \\ -i\delta\hat{a}_+ + i\delta\hat{a}_-^\dagger \end{pmatrix}, \tag{58}$$

which represent the fluctuating part, which is defined in term of the usual creation and destruction operators after their expectation value on the state which represents the laser's beam has been subtracted,

$$\delta\hat{a}_\pm \equiv \hat{a}(\omega_c \pm \Omega) - \langle \hat{a}(\omega_c \pm \Omega) \rangle. \tag{59}$$

This fluctuating part will contain information about the gravitational waves, and the detector noises. We omitted from

Downloaded 02 Nov 2011 to 180.149.51.196. Redistribution subject to AIP license or copyright; see http://rsi.aip.org/about/rights_and_permissions

Eq. (57) additional contributions at sideband frequencies $\Omega > \omega_c$ which are not relevant for us, and $O(\Omega/\omega_c) \lesssim 10^{-13}$ corrections. In the same approximation we find the nonzero commutators

$$[\delta\hat{a}_I(\Omega), \delta\hat{a}_J^\dagger(\Omega')] = 2\pi i \epsilon_{IJ} \delta(\Omega - \Omega'). \tag{60}$$

We can rewrite the transfer function of a resonant cavity in this new formalism. The basic rule for the computation is to assume that the modulations induced by the interaction with the interferometer are small, formally of the same order of the input field's fluctuations. In this way the "large" part of the input field will be transformed in the "large" part of the output one by a detector which can be considered unperturbed, which means without noises of any kind and without gravitational waves. The same will be true for the fluctuations: input fluctuations will be converted into output fluctuations by an unperturbed interferometer. The interesting part is of course the effect of perturbations, gravitational waves, and noises. These take the "large" part of the input field converting it in additional "small" contribution to the output field.

It is convenient to derive a set of basic rules for the propagation of the laser beam, which can be used to build the transfer function of a complete detector. The simplest example is the relation between the field freely propagating from point A to point B. This is just a fixed delay,

$$E_B(t) = E_A\left(t - \frac{1}{c}L_{AB}\right), \tag{61}$$

which becomes in the quadrature formalism $\underline{a}_B = \mathcal{D}_{BA}\,\underline{a}_A$, where the "propagator" $\mathcal{D}_{AB}$ is defined by its action on the "large" and "small" component,

$$\begin{bmatrix} \underline{\alpha}_B \\ \delta\underline{a}_B \end{bmatrix} = \mathcal{D}_{BA} \begin{bmatrix} \underline{\alpha}_A \\ \delta\underline{a}_A \end{bmatrix}, \tag{62}$$

where

$$\mathcal{D}_{BA} = \begin{bmatrix} \boldsymbol{R}\left(\frac{\omega_c L_{AB}}{c}\right) & 0 \\ 0 & e^{i\frac{\Omega}{c}L_{AB}}\boldsymbol{R}\left(\frac{\omega_c L_{AB}}{c}\right) \end{bmatrix} \tag{63}$$

and $\boldsymbol{R}(\theta)$ is a rotation of an angle θ.

The second key ingredient is the relation between the field reflected from a moving mirror and the incoming one, which can be written after a linearization in the small mirror's displacement δX along the propagation direction of the beam as

$$\alpha_{out}(t) = R\alpha_{in}(t), \tag{64}$$

$$\delta a_{out}(t) = R\delta a_{in}(t) - \frac{2R}{c}\delta X(t)\dot{\alpha}_{in}(t), \tag{65}$$

where R is the mirror's reflectivity. For the corresponding quadratures this means

$$\begin{bmatrix} \underline{\alpha}_{out} \\ \delta\underline{a}_{out} \end{bmatrix} = \mathcal{R}_\pm \begin{bmatrix} \underline{\alpha}_{in} \\ \delta\underline{a}_{in} \end{bmatrix}, \tag{66}$$

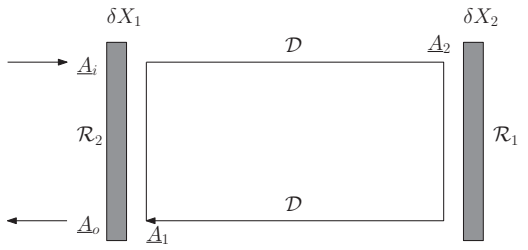


FIG. 10. The schematization of a resonant cavity with moving mirrors, with the naming conventions used in the text.

where in order to describe a reflection on the left side $\mathcal{R}_+$ must be used, $\mathcal{R}_-$ otherwise. Explicitly we get ($\kappa = \omega_c/c$)

$$\mathcal{R}_\pm = \begin{bmatrix} I & 0 \\ \mp 2\kappa\delta\tilde{X}(\Omega)\boldsymbol{R}\left(\frac{\pi}{2}\right) & I \end{bmatrix} R. \tag{67}$$

We can rederive now the transfer function for a resonant cavity. Looking at the schematic diagram in Figure 10 we can write formally

$$\underline{a}_o = -\mathcal{R}_{+,1}\underline{a}_i + T_1\underline{a}_1, \tag{68}$$

$$\underline{a}_2 = \mathcal{D}\left(T_1\underline{a}_i + \mathcal{R}_{-,1}\underline{a}_1\right), \tag{69}$$

$$\underline{a}_1 = \mathcal{D}\mathcal{R}_{+,2}\underline{a}_2, \tag{70}$$

which can be solved as

$$\underline{a}_o = \frac{\mathcal{D}\mathcal{R}_{+,2}\mathcal{D} - \mathcal{R}_{+,1}}{1 - \mathcal{R}_{-,1}\mathcal{D}\mathcal{R}_{+,2}\mathcal{D}}\underline{a}_i. \tag{71}$$

If the carrier resonates inside the cavity this expression can be considerably simplified. We are interested in the regime $R \simeq 1$ (high reflectivity of the input mirror). In the range of signal's frequencies Ω we are interested in it is legitimate to neglect corrections $O(\frac{\Omega L}{c})$ but not $O(\mathcal{F}\frac{\Omega L}{c})$, where $\mathcal{F} = \pi/(1-R)$ is the finesse of the cavity. With this approximation the "small" output component can be written to leading order as

$$\delta\underline{a}_0 = \frac{4\mathcal{F}\kappa}{\pi}\frac{\Omega_p}{\Omega_p - i\Omega}\left(\delta\tilde{X}_2 - \delta\tilde{X}_1\right)\boldsymbol{R}\left(\frac{\pi}{2}\right)\underline{\alpha}_i + \frac{\Omega_p + i\Omega}{\Omega_p - i\Omega}\delta\underline{a}_i, \tag{72}$$

where

$$\Omega_p = \frac{\pi c}{2\mathcal{F}L} \tag{73}$$

is a real parameter with the dimension of a frequency, $i\Omega_p$ being the pole of the transfer function. Owing to this pole the sensitivity will decrease at higher frequencies, with a cutoff which scales as the inverse of the finesse. For an arm length of 3 km and a typical finesse of 50 this cutoff frequency is around 500 Hz. The intuitive explanation of this behavior is that when the finesse is large a photon remains inside the cavity and interacts with the gravitational wave for a longer time (of the order of $\mathcal{F}L/c$). If the period of oscillation of the wave is comparable to this time, its effect will be averaged and suppressed.

Downloaded 02 Nov 2011 to 180.149.51.196. Redistribution subject to AIP license or copyright; see http://rsi.aip.org/about/rights_and_permissions

Using Eq. (72) it is possible now to construct the transfer function of the complete interferometer, in order to evaluate the optical contributions to the noise budget starting from Eq. (74).[73] If we suppose that the cavities in the two arms are optically equivalent this will be simply given by (see Figure (1) for the naming convention)

$$\delta \underline{o}_D = e^{2i\beta}\delta \underline{\imath}_D + e^{i\beta}\sqrt{\frac{2\mathcal{K}}{S_h^{SQL}}}\begin{pmatrix} 0 \\ \tilde{h} + L^{-1}\tilde{\delta}_{NG} \end{pmatrix}. \tag{74}$$

We set for notational simplicity

$$\delta\tilde{L}_N(\Omega) - \delta\tilde{L}_W(\Omega) = \tilde{\delta}_{NG}(\Omega) + L\tilde{h}(\Omega), \tag{75}$$

where $\tilde{h}(\Omega) = \tilde{h}_{ij}(\Omega)D^{ij}$ and $\tilde{\delta}_{NG}(\Omega) = \delta\tilde{L}_{N,NG}(\Omega) - \delta\tilde{L}_{W,NG}(\Omega)$ is the fluctuation of the difference between the length of the two cavities induced by non-gravitational forces. For future convenience we introduced the parameters $\beta = \arctan(\Omega/\Omega_p)$,

$$S_h^{SQL} = \frac{4\hbar}{\mu\Omega^2 L^2}, \tag{76}$$

$$\mathcal{K} = \frac{I_0}{I_{SQL}}\frac{2\Omega_p^4}{\Omega^2\left(\Omega_p^2 + \Omega^2\right)}, \tag{77}$$

where $I_0 = \hbar\omega_c\alpha_L^2/2$ is the laser beam's power, μ is the reduced mass of the two mirrors of each cavity and

$$I_{SQL} = \frac{\mu L^2\Omega_p^4}{2\omega_c}. \tag{78}$$

The suffix *SQL* in previous parameters stands for "standard quantum limit", for reasons that will be explained later.

The carrier is represented in quadrature space by a fixed vector $\underline{\alpha}$, and without loss of generality we choose $\underline{\alpha}_L = (\alpha_L, 0)^T$. When a mirror moves it generates a fluctuation of the reflected field which is perpendicular to $\underline{\alpha}$, which we can interpret as a phase fluctuation, at least when it is much smaller than the modulus of $\underline{\alpha}$.

A fluctuation in the direction parallel to $\underline{\alpha}$ can be interpreted instead as a fluctuation of the field intensity. From Eq. (74) we see that this effect cannot be induced by the mirrors' motion, and is just the amplitude fluctuation of the input field $\delta\underline{\imath}_D$. This is not necessarily true if the cavities are not resonating, if the optical scheme is modified, or if the two cavities are not optically equivalent. Concerning this last point, an important consequence is that the laser's amplitude fluctuations, which can be quite large, are completely suppressed by a symmetric setup.

Finally, note that there is a big conceptual difference between the first and the second term in Eq. (74): the first, which contains the gravitational wave's signal, is amplified by a factor proportional to $\mathcal{F}$. This means that increasing the finesse of the cavities we can suppress the effect of the second on the sensitivity. However, a large $\mathcal{F}$ does not suppress noises connected with the movement of the mirrors, as for example, thermal and seismic ones.

Equation (74) gives us the output quadrature field. In order to measure practically this quantity we must have a strategy that we can apply experimentally. As the two components of $\delta\underline{o}$ are non-commuting operators, a preliminary observation is that it cannot be possible to measure both. It is also apparent that owing to the rotation operator $\boldsymbol{R}(\pi/2)$ the gravitational wave signal is present inside the component of $\delta\underline{o}_D$ which is orthogonal to the carrier $\underline{\alpha}_D = \underline{\alpha}_L$, that is the phase quadrature. In principle the simplest idea could be to measure just this component: assuming that this is possible the estimator of the gravitational strain strain will be

$$e^{-i\beta}\sqrt{\frac{S_h^{SQL}}{2\mathcal{K}}}\delta o_{D,2} = \tilde{h} + e^{i\beta}\sqrt{\frac{S_h^{SQL}}{2\mathcal{K}}}\delta\imath_{D,2} + \frac{1}{L}\tilde{\delta}_{NG}. \tag{79}$$

The covariance C_{ab} of the quantum fluctuations associated with the operators $\hat{a}$, $\hat{b}$ will be given by the expectation value of the symmetrized product

$$\frac{1}{2}\langle\hat{a}(\omega)^\dagger\hat{b}(\omega') + \hat{a}(\omega')\hat{b}(\omega)^\dagger\rangle = \frac{1}{2}2\pi\delta(\omega - \omega')C_{ab}(\omega). \tag{80}$$

For the quadrature operators associated with the input field this means

$$C_{\imath_0\imath_0} = C_{\imath_{\pi/2}\imath_{\pi/2}} = 1, \quad C_{\imath_{\pi/2}\imath_0} = 0,$$

and assuming that $\delta\imath_{D,2}$ and $\tilde{\delta}_{NG}$ are uncorrelated we obtain the strain equivalent noise power spectrum

$$S_h(\Omega) = \frac{1}{2}\frac{S_h^{SQL}}{\mathcal{K}} + \frac{1}{L^2}S_{\delta_{NG}}(\Omega), \tag{81}$$

The first term in Eq. (81) is clearly dependent on the fluctuations of the beam entering in the apparatus from the output port. This beam is in a vacuum state, so these fluctuations are a purely quantum effect. The increase of this term at higher frequency is just an effect of the reduced coupling between a gravitational wave and the detector in this regime. This kind of noise is commonly called shot noise, and can be derived in an alternative but equivalent way considering the counting statistic of photons on the output, which is, of course, connected also to the quantum nature of the electromagnetic field.

The second term is proportional to the power spectrum of all the stochastic forces which drive the mirrors, in particular thermal, seismic, and optical (radiation pressure) ones.

Looking at Eq. (81) we see that in the quantum fluctuation contributions to the strain equivalent power spectrum there is a factor proportional to the inverse of α^2, which measures the laser's intensity. This is the quantitative formulation of the intuitive concept that by increasing the laser's power we reduce the optical shot noise. This can be done directly, trying to implement more powerful laser sources. Another possibility is the *power recycling* technique.

This is implemented in the scheme depicted in Figure 2 by the semitransparent mirror *PR* which is inserted between the laser and the interferometer light port. The path between *PR* and the beam splitter can be seen as a resonant cavity, which amplify the power entering inside the interferometer by a factor proportional to its finesse. In VIRGO the input laser power of 20 W is enhanced by a factor 50 using power recycling.

Downloaded 02 Nov 2011 to 180.149.51.196. Redistribution subject to AIP license or copyright; see http://rsi.aip.org/about/rights_and_permissions

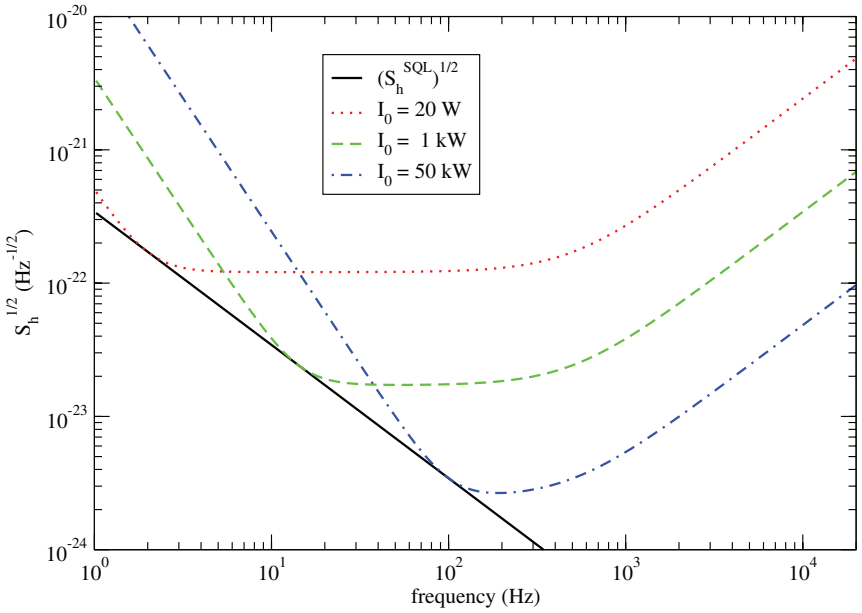


FIG. 11. (Color online) The optical strain equivalent noise spectral amplitude $\sqrt{S_h}$ as a function of the frequency, for selected values of the laser power at the beam splitter. The mirror mass is $m = 20$ kg and the cavity finesse $\mathcal{F} = 50$, the values chosen in Virgo. Taking into account the power recycling the laser power at the beam splitter is $I_0 = 10^3$ W.

One might expect that it was possible to suppress optical noise at an arbitrary level, simply by increasing the laser power. This is not the case in fact, the reason being that there is (at least) another contribution of laser's quantum fluctuations hidden in Eq. (79).

The electromagnetic field inside the main resonant cavities acts with its radiation pressure on the mirrors. As the radiation pressure is proportional to the field amplitude, quantum fluctuations generates a fluctuating force proportional to $\underline{\alpha}^T \delta\underline{a}$. Inside a cavity the carrier is amplified by a factor $\sqrt{2\mathcal{F}/\pi}$. In the low frequency approximation we are using the fluctuating fields at the two mirrors are the same (we neglect delays), and they are amplified too by a factor

$$\frac{T}{1 - Re^{2i\Omega L/c}} \simeq \sqrt{\frac{2\mathcal{F}}{\pi}} \frac{1}{1 - i\Omega/\Omega_p}, \tag{82}$$

so each mirror feels the same radiation pressure, pushing in opposite directions. This gives a length fluctuation which can be written as

$$\delta\tilde{L}^{(RP)} = \left(-\frac{1}{\mu\Omega^2}\right)\left(\frac{2\hbar\omega_c}{c}\right)\left(\frac{2\mathcal{F}}{\pi}\right)\frac{\alpha\imath_1}{1 - i\Omega/\Omega_p}, \tag{83}$$

where $-\mu\Omega^2$ is the mechanical transfer function between radiation pressure force and cavity length. Note that the two mirrors are schematized as free falling bodies, which is a good approximation in the frequency range of interest: the general case can easily be considered by inserting a more refined transfer function.

The field entering in each cavity comes from the beam splitter, so the carrier amplitude gets a factor $1/\sqrt{2}$, and the fluctuating field is a linear combination of the fluctuations entering from the light and dark ports. For the relative length difference fluctuation we get

$$\tilde{\delta}_{NG}^{(RP)} = \left(-\frac{1}{\mu\Omega^2}\right)\left(\frac{2\hbar\omega_c}{c}\right)\left(\frac{2\mathcal{F}}{\pi}\right)\frac{\alpha/\sqrt{2}}{1 - i\Omega/\Omega_p} \times \left[\frac{1}{\sqrt{2}}(\imath_{L,1} + \imath_{D,1}) - \frac{1}{\sqrt{2}}(\imath_{L,1} - \imath_{D,1})\right]. \tag{84}$$

We see that the laser's fluctuations cancel again. This contribution is proportional to $\imath_1$, and can be inserted in Eq. (74) obtaining

$$\delta\underline{o}_D = e^{2i\beta}\begin{pmatrix} 1 & 0 \\ -\mathcal{K} & 1 \end{pmatrix}\delta\underline{\imath}_D + e^{i\beta}\sqrt{\frac{2\mathcal{K}}{S_h^{SQL}}}\begin{pmatrix} 0 \\ \tilde{h} + L^{-1}\tilde{\delta}_{TH} \end{pmatrix}, \tag{85}$$

where $\tilde{\delta}_{TH}$ is the residual fluctuation induced by non-optical and non-gravitational forces. If we assume a measurement of the phase quadrature we obtain

$$S_h(\Omega) = \frac{1}{2}S_h^{SQL}\left(\frac{1}{\mathcal{K}} + \mathcal{K}\right) + \frac{1}{L^2}S_{\delta_{TH}}(\Omega), \tag{86}$$

where the first term is our final estimate of optical noise. As $\mathcal{K}$ is proportional to the laser power we see that increasing it reduces shot noise but increases radiation pressure. For a given I_0 the lower noise power spectrum S_h^{SQL} is reached when $\mathcal{K} = 1$, which means at the particular frequency given by

$$\Omega_{opt}^2 = \frac{\Omega_p^2}{2}\left[\sqrt{1 + \frac{8I_0}{I_{SQL}}} - 1\right], \tag{87}$$

and $\Omega_{opt} = \Omega_p$ when $I_0 = I_{SQL}$.

In Fig. 11 we plotted $\sqrt{S_h}$ for selected values of I_0, a cavity finesse $\mathcal{F} = 50$ and a mirror mass $m = 20$ kg, which are the appropriate values for Virgo. It seems that S_h^{SQL} (the

Downloaded 02 Nov 2011 to 180.149.51.196. Redistribution subject to AIP license or copyright; see http://rsi.aip.org/about/rights_and_permissions

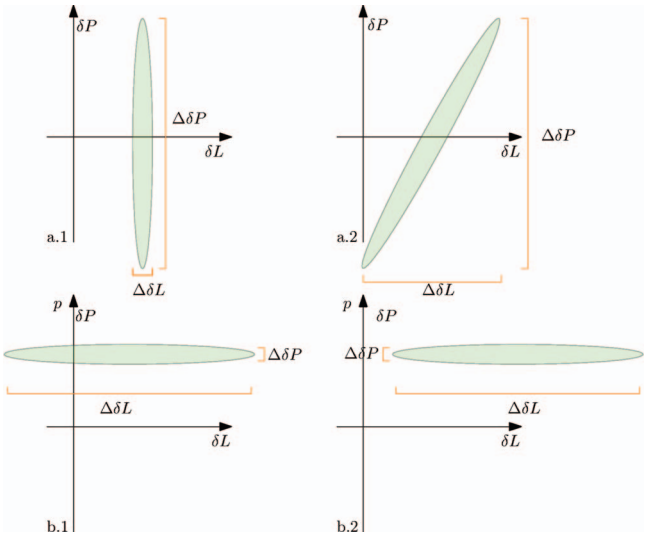


FIG. 12. (Color online) The evolution of a probability distribution for the relative distance between two masses in the phase space during a repeated measurement of position (a.1-a.2) and velocity (b.1-b.2). In the upper part, there is a large indetermination δP and a small one in δL. In the lower part the situation is reversed.

so-called *standard quantum limit*) plays the role of a fundamental lower bound for the detector's noise. This can be interpreted as a consequence of the quantum uncertainty principle in the following sense. When we try to increase the precision of a position measurement δL at $t = t_1$ by increasing the laser power, we increase also the back action force introducing a large uncertainty of the conjugate momentum δP.

We can get an intuitive understanding of the quantum limit looking at the evolution of the probability distribution in the phase space spanned by δL, δP (Figure 12). We start with a first measure of the cavity length, and we find $\delta L(t_1)$, with an uncertainty $\Delta\delta L(t_1)$ which in principle can be very small. The uncertainty in the momentum will be at least $\Delta\delta P(t_1) = \frac{\hbar}{2\Delta\delta L(t_1)}$: a possible probability distribution after the measurement is depicted in Figure 12(a.1).

Before we measure again the system will evolve. The probability distribution will be dragged by the classical motion[74] and deformed as shown in Figure 12(a.2): the main feature of this transformation is that the indetermination $\Delta(\delta L)$ increases, because the dragging depends on the velocity. Using the Heisenberg equation of motion

$$\delta\hat{L}(t_2) = \delta\hat{L}(t_1) + \frac{1}{\mu}\hat{P}(t_1)\,(t_2 - t_1)\,, \tag{88}$$

where μ is the reduced mass of the two mirrors of the cavity we find that

$$\begin{aligned}\Delta\delta L(t_2)^2 &= \Delta\delta L(t_1)^2 + \frac{1}{\mu}\Delta\delta P(t_1)^2\,(t_2 - t_1)^2 \\ &= \Delta\delta L(t_1)^2 + \frac{\hbar^2\,(t_2 - t_1)^2}{4\mu}\frac{1}{\Delta\delta L(t_1)^2}.\end{aligned} \tag{89}$$

Ultimately, we are interested in getting information about a classical force which acts on the test masses (the gravitational wave), and in order to do that we compare the position of the mirror at $t = t_2$ with the one which is expected for a free evolution. The best we can do is to choose $\Delta\delta L(t_1)^2$ in such a way to minimize Eq. (89), obtaining

$$\Delta\delta L(t_2)^2_{min} = \sqrt{\frac{\hbar^2\,(t_2 - t_1)^2}{\mu}}, \tag{90}$$

which gives a lower limit for the accuracy. Another way to derive this result is to notice that from Eq. (88) it follows the commutation relation

$$[\delta\hat{L}(t_1), \delta\hat{L}(t_2)] = i\hbar\frac{(t_2 - t_1)}{\mu}, \tag{91}$$

which enforces an indetermination relation between repeated position measurements. Though there are some delicate points in the interpretation of this result[75] the physical picture is quite simple: a position measurement introduces an indeterminacy of the momentum, which in turn acts back on the position during the time evolution which follows. A rigorous and complete discussion of the accuracy achievable with continuous measurements can be found, for example, in Ref. 57.

D. Detection techniques

In the previous subsection, we assumed the ability to measure the phase quadrature of the output beam. This can in fact be done by using the homodyne technique, which is based on the optical setup depicted in Figure 13. The basic idea is to split the input the laser obtaining a field $\underline{l}$ which is recombined with with the output using a beam splitter (*BS* in the figure). The intensity of the two final beams is measured with two photo-diodes (*PD1* and *PD2*) and the two measured values are subtracted to get the output signal.

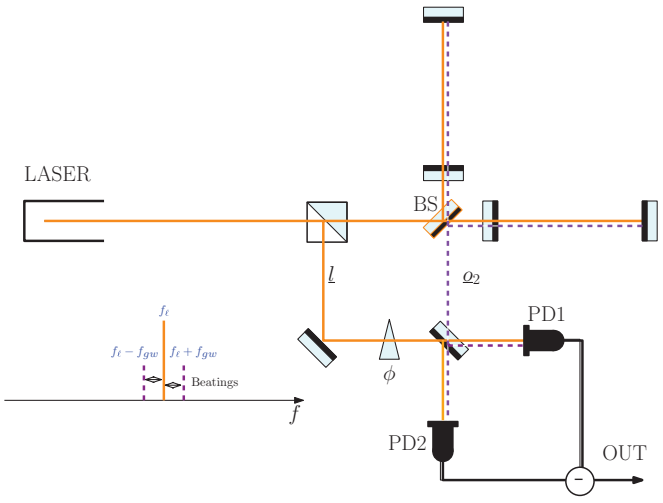


FIG. 13. (Color online) The homodyne detection technique. The continuous line corresponds to the carrier field, the dashed one to the modulation sidebands induced by the differential motion of the cavities. In this case the interferometer is maintained in the "dark fringe" condition, so the carrier entering the light port is completely reflected back. In the output field the carrier frequency f_ℓ and the sidebands corresponding to a gravitational signal $f_\ell \pm f_{gw}$ are present, and the photo-diode detects the beat (black arrows) between carrier and sidebands.

Downloaded 02 Nov 2011 to 180.149.51.196. Redistribution subject to AIP license or copyright; see http://rsi.aip.org/about/rights_and_permissions

The final result can be constructed starting from Eq. (74). The fields which enters the photo-diodes are given by

$$\underline{o}_{PD1} = \frac{1}{\sqrt{2}}\underline{o}_2 - \frac{1}{\sqrt{2}}\mathcal{D}_\phi \underline{l}, \tag{92}$$

$$\underline{o}_{PD2} = \frac{1}{\sqrt{2}}\underline{o}_2 + \frac{1}{\sqrt{2}}\mathcal{D}_\phi \underline{l}, \tag{93}$$

where $\mathcal{D}_\phi$ is an additional optical path for the initially split field which can be varied using a phase shifter. Note that both contains the carrier field and the sidebands generated by the motion of the mirrors. The ac part intensity of a field $\underline{A}$ can be written in the quadrature formalism as (the $\star$ operation represents a convolution and a scalar product between quadrature vectors)

$$I[\underline{a}](\Omega) = \underline{a} \star \underline{a} = 2\underline{\alpha} \cdot \delta\underline{a} + O(\delta\underline{a}^2), \tag{94}$$

which is proportional to the amplitude fluctuations as expected. Now the output signal will be proportional to

$$I[\underline{o}_2 - \mathcal{D}_\phi \underline{l}] - I[\underline{o}_2 + \mathcal{D}_\phi \underline{l}] \propto \underline{o}_2 \star \mathcal{D}_\phi \underline{l}, \tag{95}$$

but this means

$$\underline{o}_2 \star \mathcal{D}_\phi \underline{l} = \delta\underline{o}_2 \cdot R_\phi \underline{\beta} + O(\delta\underline{l}\delta\underline{o}), \tag{96}$$

where $\underline{\beta}$ is the "large" carrier component of the split field. We see that by choosing appropriately the phase shift ϕ we can project the field $\underline{O}_2$ in the preferred direction in the quadrature space. Note that there is no additional contribution to the fluctuations coming from the $\underline{l}$ field, because the "large" carrier component is not present in $\underline{O}_2$.

The homodyne technique is very appealing from a conceptual point of view. However, its experimental implementation is quite delicate. The shift $\mathcal{D}_\phi$, which is given not only by the shifter ϕ depicted in Figure 13 but also by the propagation along its optical path, must be highly stabilized. This means that all the optical elements involved must be stabilized and isolated from environmental fluctuations.

For this reason the detection scheme that was implemented initially in first generation interferometers was quite different, and is represented schematically in Figure 14.

This solution is based on the modulation of the laser which feeds the interferometer.[58] An electro-optical modulator (EOM) generates a pair of sidebands of the carrier field at $f = f_{laser} \pm f_{mod}$, where f_{mod} is in the radio frequency range. When the intensity of the output beam is detected at the photodiode, the signal sidebands $f_{laser} \pm f_{gw}$ beat with the modulation sidebands generating a signal at $f_{mod} \pm f_{gw}$, which is then demodulated in the mixer.

The modulation sidebands must be present at the photodiode, and this is not the case if the two arms of the detector have the same optical transfer function. This is solved by introducing the so-called Schnupp asymmetry,[76,77] which can be realized with a delay τ in one of the two arms. Looking at the expressions in Figure 1 we see that this gives an output signal which is proportional to $(e^{2\pi i f\tau} - 1)$, and we want this to be large for $f = f_{mod}$ but small for $f = f_{gw}$. This can be obtained by choosing a delay of the order of the inverse of f_{mod}, which correspond to a length of the order of few meters for a typical f_{mod} around 10^8 Hz.

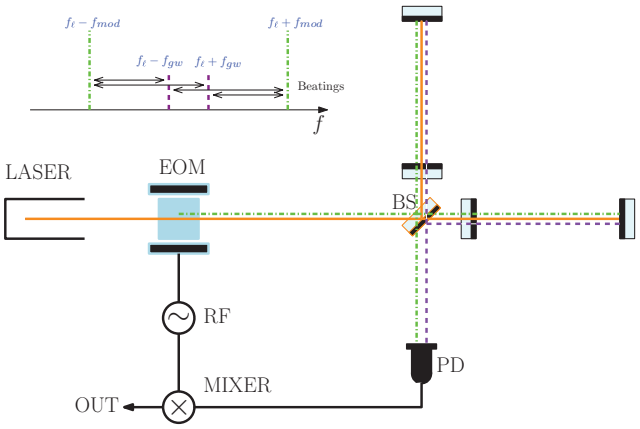


FIG. 14. (Color) The heterodyne detection technique. The continuous lines corresponds to the carrier field, the dashed ones to the modulation sidebands induced by the differential motion of the cavities, the dotted-dashed ones to the radio frequency sidebands generated by the EOM. The radio frequency sidebands must be transmitted by the interferometer, so a small asymmetry is introduced between the two arms. The photo-diode senses the beat between the signal sidebands and the modulation sidebands (black arrows). The resulting radio frequency signal is further demodulated in the mixer.

A disadvantage of this solution is that additional optical noise is introduced. This can be understood by observing that the intensity of the detected field is of the form

$$I[\delta\underline{o}_2 + \underline{m}](\Omega) = 2\underline{\mu} \star \delta\underline{o}_2 + 2\underline{\mu} \star \delta\underline{m}, \tag{97}$$

where the second term is proportional to the fluctuation of the modulation field $\underline{m}$, a contribution which is absent from the corresponding Eq. (96) appropriate for the Homodyne detection.

Conceptually, the simplest way of reading the output of an interferometer is a variation of the Homodyne scheme called dc readout,[78] which was used also by Michelson and Morley with their first interferometer.[79] The optical scheme is depicted in Figure 15 and it is really quite trivial: there are no modulations, and the output photo-diode reads directly the

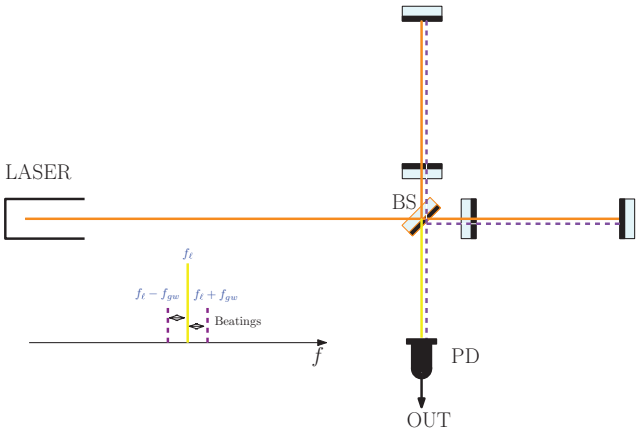


FIG. 15. (Color online) The dc detection technique. The continuous line represents the carrier field, the dashed one to the modulation sidebands induced by the differential motion of the cavities. In the output the sidebands at the frequencies $f_\ell \pm f_{gw}$ are present, together with some carrier field at a frequency f_ℓ. In order to allow the transmission of the carrier a small offset from the "dark fringe" working point is introduced.

Downloaded 02 Nov 2011 to 180.149.51.196. Redistribution subject to AIP license or copyright; see http://rsi.aip.org/about/rights_and_permissions

beatings between the carrier field and the signal sidebands. Of course, this means that the carrier entering the interferometer must partially be transmitted, and a small offset from the "dark fringe" working point is introduced in order to allow for this.

The reason why this has not been the first choice for gravitational waves detectors has already been discussed, namely, that if we move from the "dark fringe" working point we couple the output to laser fluctuations. However, the increased stability of today's laser sources now makes it possible to adopt this solution and to obtain performance comparable with other schemes,[80] with several advantages, in particular,

- the additional shot noise contribution of modulation sidebands is absent.[81]
- Several "technical" noises could be reduced by the absence of modulations at the output. We note that modulations can be introduced in the input laser light for other purposes, for example, in order to lock the cavities, but can be filtered out at the output using a filter cavity similar to the *OMC* depicted in Figure 2.
- The use of squeezed light for the reduction of quantum noise, that will be discussed in the following (see in particular Subsection II E 1) is simplified.[82]

There are also some disadvantages: we mentioned the increased coupling with laser noise. Also, the response of the system is less linear than in an heterodyne scheme. However, the feasibility of this technique in interferometers with suspended mirrors has been demonstrated[83,84] and dc readout will be the chosen solution in the next generation of detectors.[85,86] We refer to Ref. 78 for a detailed discussion.

E. Beating the standard quantum limit

Comparing Eq. (11) with the sensitivity curves of current interferometers (see Eq. (5)) we see that a reduction of thermal noise of at least two orders of magnitude is mandatory before the standard quantum limit will become an issue.

In spite of that in recent years there has been a considerable activity around this subject. Many proposals for the evasion of standard quantum limit exist now, and in this subsection we will give a concise overview of some of these.

Before starting the discussion one may wonder if the standard quantum limit is a fundamental limit, as one could suspect considering that it is strictly connected to a fundamental principle of quantum mechanics. The answer is negative, because in detecting gravitational waves we are not really trying to measure the position of the test masses, but instead to get information about a (classical) force which acts on them.

We refer to Ref. 55 for a detailed analysis of this point. However, as we will see the final sensitivity of a detector will depend on an interplay between the dynamics of the optical degrees of freedom (the relevant modes of the laser) and the mechanical ones (the mirrors). These are not independent, as they are coupled by radiation pressure effects. Radiation pressure acts in a dual way.

- It can modify the dynamic of the mirrors, inducing an effective mechanical stiffness of the cavity. This is the so-called *optical spring*[87–92] effect which is discussed in Subsection (II E 4).
- It induces a modification of the quantum state of the optical modes, through the back action of the mirrors' mechanical response. This is the *ponderomotive squeezing*[93–95] effect which can be exploited in several ways (see Subsections (II E 1) and (II E 5)) in order to improve the sensitivity.

No direct evidence of ponderomotive squeezing exists, though experimental investigations have been proposed,[96] the main reason being the intrinsic weakness of the radiation pressure fluctuations with respect to classical noise sources.

1. Modification of input and/or output

The basic starting point of this kind of approach is the observation that the interaction of the laser beam with the free masses of the mirror generates *ponderomotive squeezing*. Put in simple terms, this means that as the mirror recoils in response to a fluctuation of the laser's amplitude, a fluctuation of the beam's phase is generated. Phase and amplitude quantum fluctuations are no longer uncorrelated, as it is the case for a coherent state, and there is an appropriate quadrature of the relevant mode of the electromagnetic field which sees reduced quantum fluctuations.

Using the relation (85) between quadrature operators of input and output modes we can calculate the full covariance array for output quadratures, which can be written as

$$\boldsymbol{S} = \frac{1}{2}\begin{pmatrix} 1 & -\mathcal{K} \\ -\mathcal{K} & 1+\mathcal{K}^2 \end{pmatrix}, \tag{98}$$

where the out of diagonal element being non-zero is a clear signature of the correlation introduced between amplitude and phase fluctuations. It is common to represent $\boldsymbol{S}$ as an "error ellipse," defined as the ellipse whose principal axes are oriented in the direction of the eigenvectors of $\boldsymbol{S}$ and have a length equal to the square root of corresponding eigenvalues, namely, the locus of vectors ρ such that

$$\rho^T \boldsymbol{S}^{-1} \rho = 1. \tag{99}$$

However, the matrix $\boldsymbol{S}$ must be interpreted with care, because quadrature operators do not commute (see Eq. (60)) and cannot be measured at the same time with arbitrary precision. This means that it is not possible to define a probability distribution in quadrature space.

A consistent description of quadratures' quantum fluctuations can be given using a quasiprobability distribution, for example, the Wigner function (see Ref. 97). It turns out that it is legitimate to use $\boldsymbol{S}$ to evaluate the fluctuation for a single quadrature at a given angle θ. We can represent graphically the noise coupled to a quadrature in direction θ

$$\sigma^2(\theta) = \hat{n}^T(\theta)\boldsymbol{S}\hat{n}(\theta) = \frac{1}{2}\left[1+\mathcal{K}^2\sin^2\theta - 2\mathcal{K}\sin\theta\cos\theta\right] \tag{100}$$

with a polar plot (see Figure 16). The angles of maximum and minimum fluctuations correspond to the eigenvectors of

Downloaded 02 Nov 2011 to 180.149.51.196. Redistribution subject to AIP license or copyright; see http://rsi.aip.org/about/rights_and_permissions

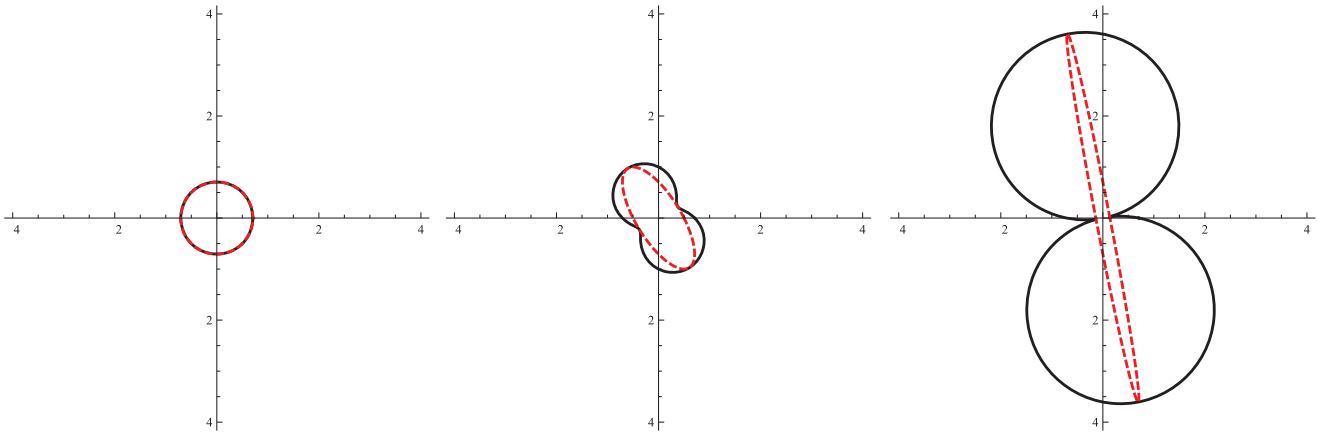


FIG. 16. (Color online) Polar plot of the quadrature error $\sigma(\theta)$ defined in Eq. (100) (continuous line) compared with the corresponding error ellipse (dashed line). The plots correspond to $\mathcal{K} = 0, 1, 5$ (from left to right).

$\boldsymbol{S}$, with eigenvalues given for large $\mathcal{K}$ by

$$(\lambda_+, \lambda_-) \sim \left(\frac{\mathcal{K}^2}{2}, \frac{1}{2\mathcal{K}^2}\right), \tag{101}$$

so there is a particular quadrature which has a reduced fluctuation, at the expense of the fluctuation of the orthogonal one which are amplified. In other words, the ponderomotive effect produced a squeezed state of light.

It follows that when we measure it we get a squared signal to noise ratio given by

$$\mathrm{SNR}(\theta)^2 = \left(\frac{\mathrm{h}}{\mathrm{S_h}}\right)^2 \frac{\sigma^2(\pi/2)}{\sigma^2(\theta)} \sin^2\theta \le \left(\frac{\mathrm{h}}{\mathrm{S_h}}\right)^2 (1+\mathcal{K}^2), \tag{102}$$

where we used the fact that in a conventional interferometer the information about the signal is aligned with the $\theta = \pi/2$ quadrature.

We can exploit this result measuring at the output the quadrature with the best SNR ratio. In Figure 17, we plotted the square root of Eq. (102) in units $h/\sqrt{S_h}$ for different values of the parameter $\mathcal{K}$. In the usual case the quadrature $\pi/2$ is measured, and it is apparent that no improvement is obtained by increasing $\mathcal{K}$. By choosing an optimized quadrature we saturate the upper limit in Eq. (102) and we obtain

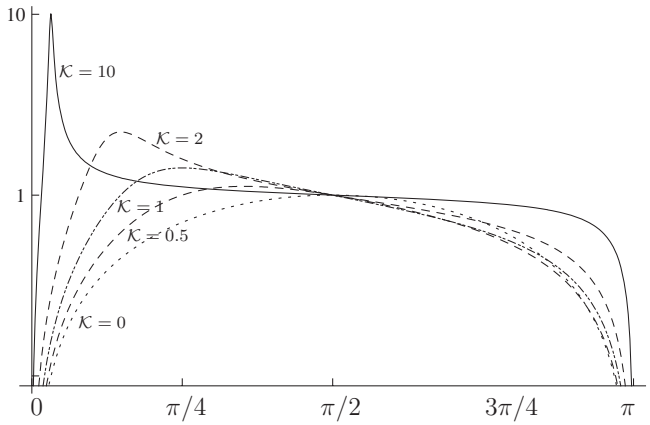


FIG. 17. Signal-to-noise ratio in units of $h/\sqrt{S_h}$, for different values of the parameter $\mathcal{K}$ (0, 1/2, 1, 2, 10) as a function of the measured quadrature angle.

an improvement of the sensitivity proportional to the level of ponderomotive squeezing. Note that, as $\mathcal{K}$ is a frequency dependent parameter, the optimal quadrature will depend on frequency also and appropriate measurement strategies must be devised.[73]

Another observation is that as the parameter $\mathcal{K}$ becomes large and the SNR gain becomes a very sensitive function of the quadrature angle.

An alternative possibility is the injection of a squeezed state in the dark port of the interferometer (the only one which contribute to the output quantum noise). To see the effect of this option we simply reevaluate the covariance array (98) using a squeezed state as input state in Eq. (85).

By choosing an appropriate (frequency dependent) squeezing angle we find a quantum noise amplitude spectrum given by

$$S_h = \frac{1}{2} S_h^{SQL} \left(\frac{1}{\mathcal{K}} + \mathcal{K}\right) e^{-2r}, \tag{103}$$

which is reduced from the expression in Eq. (86) exponentially in the squeezing parameter r, which is related to the maximum and minimum quadrature error *of the injected state* by

$$\begin{pmatrix} \sigma_{\max} \\ \sigma_{\min} \end{pmatrix} = \frac{1}{\sqrt{2}} \begin{pmatrix} e^{r} \\ e^{-r} \end{pmatrix}. \tag{104}$$

From Eq. (103) it follows that the improvement obtainable injecting squeezed light depends on the degree of squeezing available.

All these possibilities and their combinations are discussed in details in Ref. 73. It is possible in principle to suppress completely radiation pressure noise, which means that there are no obstructions, in principle, to reduce shot noise also by increasing laser power.

2. Measurement of quantum non demolition observables

Instead of measuring the distance between the mirrors, we can look at their relative velocity. Repeating the phase space considerations we did previously, we look again at

Downloaded 02 Nov 2011 to 180.149.51.196. Redistribution subject to AIP license or copyright; see http://rsi.aip.org/about/rights_and_permissions

Figure 12. A first measurement of give as a value $m^{-1}\delta P(t_1)$ with some small uncertainty $\Delta\delta P(t_1)$ and leave the system is in a state with a large δL uncertainty, as shown in Figure 12(b.1). Now the momentum of a free mass is conserved, so $\Delta\delta P(t_1)$ is not changed by the evolution, i.e., (Figure 12(b.2), compare with Eq. (89))

$$\Delta\delta P(t_2) = \Delta\delta P(t_1). \tag{105}$$

It follows that we can make $\Delta\delta P(t_1)$ as small as we want, and this will not have consequences on the accuracy of the velocity measurements that will follows. Another way to look at this is to evaluate the two times commutator between the momentum operators, which gives (compare with Eq. (91))

$$[\delta\hat{P}(t_1), \delta\hat{P}(t_2)] = 0. \tag{106}$$

There is no quantum limit to the precision obtainable in a repeated measurement of the mirror's velocity. The velocity of a free mass is an example of a *quantum non-demolition* observable: more generally a conserved quantity is QND also (see Ref. 57 for a general discussion).

A very schematic representation of a detector which provides a measurement connected with the speed of the mirrors is represented on the right in Figure 18.

This is just a Sagnac interferometer. The output signal is the superposition of a beam which follows the dashed path in the clockwise direction, with another which moves in the opposite direction, with a final phase shift given by

$$\begin{aligned}\delta\phi(t) &= x_E(t) + x_N(t+\tau) - x_N(t) - x_E(t+\tau)\\ &\simeq \tau v_N(t) - \tau v_E(t),\end{aligned} \tag{107}$$

where in the last equality we discarded contributions proportional to higher powers of $\tau d/dt$. This is a good approximation if we are interested in frequencies $\Omega \ll \tau^{-1}$.

The original idea of a device measuring the momentum of a test mass was initially proposed by Braginsky and Khalili.[99] and further developed in Ref. 100. The main problem of this initial design was the extremely large amount of input ($\gtrsim$300 MW) and circulating power ($\sim$8 MW) needed to achieve an order of magnitude reduction of noise power compared with the standard quantum limit.

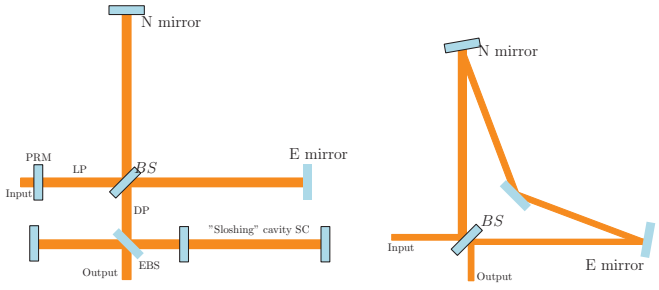


FIG. 18. (Color online) (Left) A simplified version of the speed meter proposed in Ref. 98. The input laser light passes through the power recycling mirror *PRM*, and enters into a standard Michelson interferometer built with the beams splitter *BS* and the *N* and the *E* mirrors. The dark port of this interferometer is coupled with an additional "sloshing" cavity. See the text for explanations. (Right) The schematic of a Sagnac interferometer. The input beam incoming from the left is split in two by the semitransparent mirror BS and recombined on it after a round trip.

Alternative optical schemes have been proposed,[98,101] in an effort to evade these limitations and obtain a practically realizable detector.

A simplified scheme of one of these proposals[98] is represented on the left in Figure 18. Here the input laser light feeds the light port *LP* of a standard Michelson interferometer formed by the beam splitter *BS* and by the two mirrors *N* and *E* (in the picture we can see also a power recycling mirror *PRM* which we will ignore in the analysis) which is locked on the usual dark fringe working point. As we noticed when we discussed the general features of a Michelson interferometer in this configuration the light entering through a port is completely reflected back (see Eq. (2)), so there is no power exiting the dark port, *DP*.

This is no longer true when the mirrors are moved, and some light will exit through *DP*. This is not detected directly as the dark port is coupled to a resonant "sloshing" cavity, *SC*. The real output will be the result of the interference between the fraction of the output light transmitted directly by the extraction beam splitter, *EBS*, and a fraction filtered by the *SC*. In steady state the two contributions just cancel out, owing to the π phase shift induced by the cavity. But for a time varying input the system will be controlled by the frequency scale

$$\Omega = \frac{c}{L}\sqrt{\frac{\pi}{2\mathcal{F}}}, \tag{108}$$

where $\mathcal{F}$ is the finesse of the *SC* and *L* its length, which is also the length of the Michelson's arms. When the typical frequency of the signal $h(t)$ is much lower that Ω the output is proportional to the relative speed of the Michelson's mirrors. More generally it will be a combination of all odd time derivatives of $h(t)$.

This scheme permits an evasion of the standard quantum limit with reasonable input powers, though other refinements are needed to reduce the circulating power. It is also possible to implement the variational readout scheme and the squeezing vacuum injection discussed in Subsection II E 1, at the price of a greater complexity of the optical scheme. We refer to Refs. 98, 101 for a detailed discussion.

3. Signal recycling

By putting a partially reflecting mirror after the dark port of a standard interferometer we modify the optical transfer function.[102] With an appropriate tuning of the parameters this can give advantages in term of sensitivity. The relevant transfer functions can be evaluated mapping the detector to an equivalent detuned cavity,[103] and parametrized in terms of three parameters, the normalized intensity

$$\iota_c = \frac{8\omega_c}{\mu L c}\sqrt{\frac{\pi}{2\mathcal{F}}}I_0, \tag{109}$$

and the real and imaginary part of the optical resonant frequency $\Omega_R = -\lambda - i\epsilon$. The mirror "recycles" the signal which is reflected back inside the interferometer's arms. One consequence of this is that the quadrature which carries the signal becomes frequency dependent, and if the detection is done at a fixed homodyne angle the enhancement of the sensitivity can become selective in frequency. With a traditional

Downloaded 02 Nov 2011 to 180.149.51.196. Redistribution subject to AIP license or copyright; see http://rsi.aip.org/about/rights_and_permissions

detection scheme an additional parameter is needed, namely, the angle ξ of the quadrature which is detected. As an example we show in Figure 19 the ratio $(S_h/S_h^{SQL})^{1/2}$ as a function of the frequency for a particular set of parameters.

The gray band corresponds to the region forbidden in a traditional detector by the standard quantum limit, and we see that this can be evaded using this technique. In principle, the parameters of a detector of this kind can be changed quite easily. This has the advantage of being able to "tune" the experiment to a particular kind of search, for example, enhancing the sensitivity around the frequency of an expected monochromatic source.

It is also possible to combine the signal recycling techniques with the injection of a squeezed vacuum and/or with a variational homodyne detection, improving both the best sensitivity and the bandwidth of the standard quantum limit evasion, as discussed in Refs. 92 and 104. The sensitivity of this class of detectors is given by the relatively compact expressions

$$S_h = \frac{h_{SQL}^2}{2\mathcal{K}} \frac{e^{-2r}\left(C_{11}\sin\zeta + C_{21}\cos\zeta\right)^2 + e^{2r}\left(C_{12}\sin\zeta + C_{22}\cos\zeta\right)^2}{\tau^2\left|\left(\rho e^{2i(\beta+\theta)}+1\right)\sin\phi\sin\zeta + \left(\rho e^{2i(\beta+\theta)}-1\right)\cos\phi\cos\zeta\right|^2} \tag{110}$$

with

$$\begin{pmatrix} C_{11} & C_{12} \\ C_{21} & C_{22} \end{pmatrix} = \begin{pmatrix} (1+\rho^2)\left(\cos 2\phi + \frac{\mathcal{K}}{2}\sin 2\phi\right) - 2\rho\cos 2(\beta+\theta) & -\tau^2\left(\sin 2\phi + \mathcal{K}\sin^2\phi\right) \\ \tau^2\left(\sin 2\phi - \mathcal{K}\cos^2\phi\right) & (1+\rho^2)\left(\cos 2\phi + \frac{\mathcal{K}}{2}\sin 2\phi\right) - 2\rho\cos 2(\beta+\theta) \end{pmatrix} \boldsymbol{R}(\lambda). \tag{111}$$

Here r is the squeezing parameter and λ is the squeezing angle of the input vacuum state, ζ is the angle of the measured quadrature, ρ and τ are the reflectivity and transmissivity of the signal recycling mirror. The parameters ϕ and θ characterize the signal recycling cavity. In detail, ϕ is the cavity detuning and θ the phase shift induced by the cavity in a single pass.[104] Finally, $\boldsymbol{R}(\lambda)$ is a matrix which describes a rotation by an angle λ.

4. Modification of the test mass dynamics

In a resonant cavity the cavity power is maximized, and in the linearized approximation pressure does not change when the mirrors are moved. This is easy to understand looking at Eq. (8) which gives the ratio between the cavity power and the input one, which is proportional to the radiation pressure. In this regime, information about the signal is encoded only in the phase of the output beam.[88]

Out of resonance, or in presence of a more complicated optical scheme (notably if a signal recycling mirror is present) this is no longer true: part of the signal is present also in the intensity quadrature, and a restoring force proportional to the mirrors' displacement is present. This is called the "optical spring" effect originally discovered by Braginsky and colleagues[105] and has been observed.[106,107]

An equivalent way to describe the situation is the following: when radiation pressure effects are negligible, the dynamics of an interferometer is determined by two "resonances"

- a purely optical one at $\Omega = -i\Omega_p$. Here Ω_p is just given by Eq. (73), and is equal to the inverse storage time of the cavities and
- a purely mechanical one at $\Omega = 0$, or more precisely at the angular frequency of the equivalent pendulum which describes the free dynamics of the difference between the two cavities length.

Radiation pressure introduces a coupling between these. We obtain two optomechanical modes which are more and more different from the original ones when the laser power increases. The modified dynamics can be exploited to evade the standard quantum limit.[89–91,103]

It comes out that not all the optomechanical modes are stable, an effect which is analogous to the instability induced by radiation pressure in a detuned Fabry-Perot cavity,[108–110] and an appropriate active control strategy must be devised.[81]

5. Quantum feedback

It is possible to monitor the movement of a test mass with an auxiliary cavity. Using a carefully implemented feedback strategy, which exploits the light squeezing generated by ponderomotive effects, this test mass can be controlled in principle at the quantum level, subtracting completely radiation pressure noise.[111–114]

This subtraction does not reduce the gravitational signal because the measurement is done locally with a short cavity, insensitive to the wave's strain. The effect of other sources of noise, for example, thermal ones, has been studied in Ref. 115.

Downloaded 02 Nov 2011 to 180.149.51.196. Redistribution subject to AIP license or copyright; see http://rsi.aip.org/about/rights_and_permissions

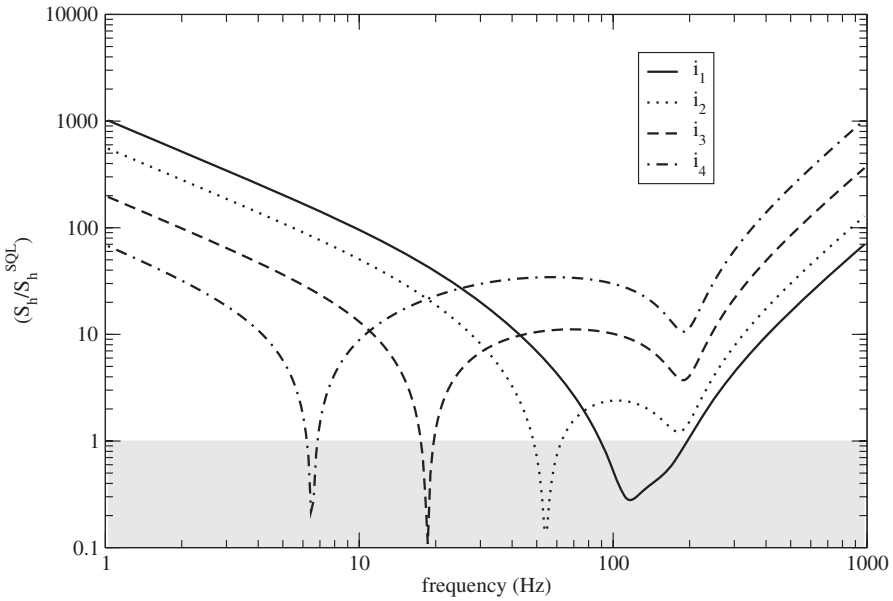


FIG. 19. The ratio between the strain equivalent noise amplitude and its standard quantum limit for a traditional interferometer. Here $\lambda = 2\pi \times 123.2$ Hz, $\varepsilon = 2\pi \times 13.8$ Hz, and $\xi = 0$. The different plots correspond to $\imath_c = i_1 = (2\pi \times 120\ \text{Hz})^3$, $\imath_c = i_2 = (2\pi \times 80\text{Hz})^3$, $\imath_c = i_3 = (2\pi \times 40\ \text{Hz})^3$, and $\imath_c = i_4 = (2\pi \times 20\ \text{Hz})^3$.

It is also possible to devise a feedback strategy appropriate for a complete resonant cavity, using a single error signal.[116]

A possible scheme is given in Figure 20. Starting from it we can write the variation of the length of the cavity A as

$$\Delta_{21} = \frac{1}{2} h L_A + (\chi_2 g_2 - \chi_1 g_1) F + \Delta_{21}^{(th)} + \hbar[(\chi_1 + \chi_2)\xi_A \hat{a}_0 - \chi_2 \xi_B \hat{b}_0], \tag{112}$$

where χ_i are the mechanical susceptibilities of the mirrors, g_i are the feedback gains, and ξ_K is the optomechanical coupling of the Kth cavity which is given by

$$\xi_K^2 = \frac{8\omega_0^{(K)} I_0^{(K)}}{\hbar c^2} \frac{F^{(K)}}{\pi}. \tag{113}$$

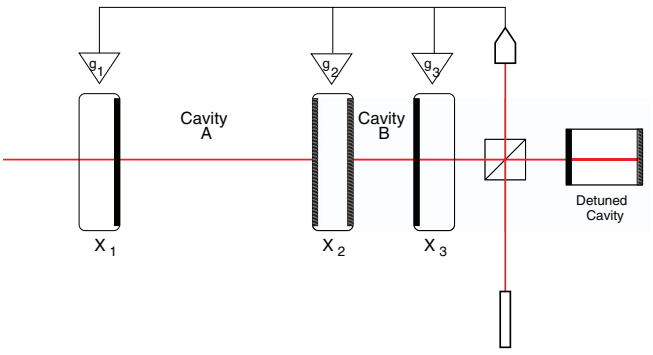


FIG. 20. (Color online) A possible scheme for the subtraction of radiation pressure noise in a cavity. Cavity A of unperturbed length L_A is the main one, while cavity B of unperturbed length L_B is used to monitor the position of the central mirror. The g_i are gains for the actuators driven by the error signal and the detuned cavity is used to measure the appropriate quadrature of the output beam. The variation of the length of the two cavities used in the text are given by $\Delta_{21} = \Delta X_2 - \Delta X_1$ and by $\Delta_{32} = \Delta X_3 - \Delta X_2$, where X_i are the coordinates of the mirrors.

The first term in Eq. (112) describes the changes induced by the gravitational wave's strain h, and the second the action of the feedback force F. We inserted also a piece $\Delta_{21}^{(th)}$ proportional to the thermally induced motion.

The second row contains the motion induced by the radiation pressure fluctuations: $\hat{b}_0$ is the $\theta = 0$ quadrature of the field entering in the cavity B, $\hat{a}_0$ is the same for the field entering in the cavity A.

If we use as a feedback force an appropriate quadrature of the field exiting from the cavity B, which we can parameterize with the quadrature angle θ as

$$F = \hat{b}_\theta + 2\xi_B \Delta_{32} \sin\theta, \tag{114}$$

we can rewrite Eq. (112) in the form

$$\Delta_{21} = \frac{1}{2} h\,(L_A + 2G\xi_B L_B \sin\theta) + \Delta_{21}^{(th)} + 2G\xi_B \Delta_{32}^{(th)} + G\sin\theta \hat{b}_{\pi/2} + \left[G\left(\cos\theta + 2\hbar\xi_B^2(\chi_2 + \chi_3)\sin\theta\right) - \chi_2 \hbar \xi_B\right]\hat{b}_0 + \hbar\xi_A\left[(\chi_1 + \chi_2) - 2G\xi_B \chi_2 \sin\theta\right]\hat{a}_0, \tag{115}$$

where

$$G = \frac{\chi_2 g_2 - \chi_1 g_1}{1 - 2\xi_B \sin\theta\,(\chi_3 g_3 - \chi_2 g_2)}. \tag{116}$$

From the first row we see that as we anticipated the effect of the feedback on the coupling of the cavity to the gravitational strain is negligible, as soon as $L_A \gg L_B$.

By choosing appropriately the measured quadrature and the gain it is possible to set to zero the last two rows in Eq. (115), which contain the effect of radiation pressure fluctuations.

Downloaded 02 Nov 2011 to 180.149.51.196. Redistribution subject to AIP license or copyright; see http://rsi.aip.org/about/rights_and_permissions

It comes out that when the mirrors behave as free masses the quadrature angle must be

$$\cot\theta = \frac{3\hbar\xi_B^2}{\mu\Omega^2}, \tag{117}$$

where μ is a function of the mirrors' masses. This kind of frequency dependent measurement can be implemented by filtering the output beam in a cavity with an appropriately chosen detuning, as the one showed in Figure 20.

The gains must be also frequency dependent, more precisely the condition

$$\frac{g_1+g_2}{M_1+M_2} - \frac{g_3}{M_3} = \frac{1}{2\xi_B}\sqrt{\Omega^4 + \frac{4\hbar^2\xi_B^4}{\mu^2}} \tag{118}$$

must be satisfied.

To evaluate the sensitivity in the presence of feedback we observe that the measured output quadrature of the cavity A is given by $\hat{a}_{\pi/2} + 2\xi_A\Delta_{12}$ and gives us an estimator for the gravitational strain

$$\hat{h} = h + \frac{2\Delta_{21}^{(th)} + 4\rho\Delta_{32}^{(th)} + 2\rho\xi_B^{-1}\hat{b}_{\pi/2} + \xi_A^{-1}\hat{a}_{\pi/2}}{L_A + 2\rho L_B}, \tag{119}$$

where $\rho = (1 + M_1/M_2)/2$.

From this expression we verify explicitly the complete cancellation of the back action forces. We can also evaluate the power spectrum of the quantum noise, which contains only shot noise contributions and is given by

$$S_h = \frac{4}{(L_A + 2\rho L_B)^2}\left(\frac{1}{4\xi_A^2} + \frac{\rho^2}{\xi_B^2}\right). \tag{120}$$

Note that the shot noise in the cavity B reduces the apparatus sensitivity through the feedback, so that in order to improve it we need to increase the field in both the cavities to increase the optomechanical couplings. A side effect of the feedback procedure is the enhancement of thermal noise. This can be deduced by looking at Eq. (119) and comparing the contribution proportional to the thermal displacements $\Delta_{ij}^{(th)}$ with the $2\Delta_{21}^{(th)}/L_A$, which would be obtained without feedback (see Eq. (112)).

6. Optical losses

A connected point is the reduction of losses inside the apparatus, because a loss is equivalent to the introduction of a source of non squeezed quantum fluctuations.

To understand better this point we observe that if losses are present in an optical element the "naive" connection between the input and the output quantum operators

$$\hat{a}_{out} = \lambda\hat{a}_{in}, \quad |\lambda| < 1 \tag{121}$$

is not compatible with the canonical commutation rules.

The simpler solution to preserve these is to introduce another input and output mode, and to couple it in such a way to preserve unitarity,[117] for example,

$$\begin{aligned}\hat{a}_{out} &= \lambda\hat{a}_{in} - \sqrt{1-\lambda^2}\hat{b}_{in},\\ \hat{b}_{out} &= \sqrt{1-\lambda^2}\hat{a}_{in} + \lambda\hat{b}_{in}.\end{aligned} \tag{122}$$

If we suppose now that the input mode $\hat{a}_{in}$ is squeezed, there is usually no reason to suppose that $\hat{b}_{in}$ is squeezed also. If we calculate the minimum variance output quadrature we obtain

$$\Delta q_{min}^2 = \lambda e^{-2r} + (1-\lambda), \tag{123}$$

which shows that squeezing is rapidly destroyed by losses. An optical loss can have different origins, in particular

- the electromagnetic field in the mode we are interested to, for example, the fundamental resonant mode of a cavity, can be scattered in another one. This can be caused also by imperfections of the optical elements, but also by incorrect optical parameters such as the curvature of the mirrors and their alignment and
- light can be adsorbed by imperfections of the optical elements, and converted to ordered excitations such as excitation of elastic modes[118–120] or directly to heat.

Whatever the case, we can always imagine conceptually our optical mode interacting with a beam splitter which couples it to another one, which is exactly what is described by Eqs. (122).

As a concrete example we can model a photo-diode with a given quantum efficiency $\eta = \lambda^2$ as an ideal one with a beam splitter inserted before, as in Figure 21. Here the laser beam is described by $\hat{a}$, and a fraction $\sqrt{\eta}$ of its amplitude is extracted. It is not important what happens after the extraction: the light can simply propagate away in the new mode (scattering) or converted to a different kind of excitation (adsorption). The key point is that unavoidably a source of quantum fluctuations (the mode described with $\hat{b}$) is coupled to the beam.

7. Perspectives

Two of the techniques discussed, namely, signal recycling and squeezed light, will surely play an important role in the next generation of interferometric detectors. In particular, signal recycling has already been implemented in GEO600, which in spite of its reduced overall sensitivity is playing a very important role as a test bed of advanced optical configurations.

It is now possible to produce squeezed light in the low frequency region, which is the interesting one from

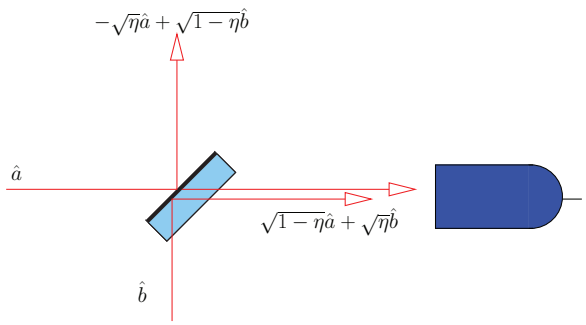


FIG. 21. (Color online) The simple model of photo-diode with quantum efficiency η discussed in Subsection II E 6. Only a fraction η of the incoming energy is converted in photoelectrons, and this is equivalent to an amplitude loss $\sqrt{\eta}$ in the input beam. The beam incoming on the detector gets an additional contribution from fluctuations.

Downloaded 02 Nov 2011 to 180.149.51.196. Redistribution subject to AIP license or copyright; see http://rsi.aip.org/about/rights_and_permissions

the point of view of gravitational waves' detectors.[121,122] GEO600 tested a working non-classical light source,[123,124] and a squeezing level of up to 9 dB in the detection band between 10 Hz and 10 kHz was observed. Noise reduction connected to injection of squeezed light has been demonstrated in interferometers with suspended mass,[125] in particular in GEO600 (Ref. 126) with a reduction level currently of 3.5 dB.[127]

The standard way to produce squeezed light is by using nonlinear crystals,[128] i.e., materials with a polarization P which is related in a nonlinear way to the electric field,

$$\mathcal{P} = \varepsilon_0(\chi^{(1)}E + \chi^{(2)}E^2 + \chi^{(3)}E^3 + \cdots). \tag{124}$$

The term proportional to $\chi^{(1)}$ in Eq. (124) induces a quadratic term in the Hamiltonian of the electromagnetic field, which gives the usual change in the light propagation speed, even in a linear medium. The term proportional to $\chi^{(2)}$ induces a cubic interaction: a single photon of angular frequency ω_0 can be converted into a pair of photons with angular frequencies ω_1, ω_2 with $\omega_0 = \omega_1 + \omega_2$ owing to the energy conservation (down conversion). Analogously a pair of photons can merge in a single one (up conversion).

The two most successful techniques used today are based on optical parametric oscillators and optical parametric amplifiers (OPA).[129,130]

In degenerate, OPA a down conversion with $\omega_1 = \omega_2 = \omega_0/2$ is implemented. This process can be described by the interaction Hamiltonian,

$$H_{\text{int}} = \frac{i\hbar\varepsilon}{2}[\hat{b}\hat{a}^+\hat{a}^+ - \hat{b}^+\hat{a}\hat{a}], \tag{125}$$

where $\hat{a}$ is the destruction operator for the mode we want to squeeze and $\hat{b} \simeq \beta + \delta\hat{b}$ describes a "pump" field with a large classical amplitude β, provided by a laser source. Working in the large β regime we see that the evolution operator will be something like

$$\hat{S}(\varepsilon) = \exp\left[\frac{1}{2}(\gamma^*\hat{a}\hat{a} - \gamma\hat{a}^+\hat{a}^+)\right], \tag{126}$$

where the parameter γ depends on the amplitude β of the pump field and on the interaction parameter ϵ related to $\chi^{(2)}$ factor which appears in Eq. (125). It depends also on the geometry of the region where the pump field will interact with the nonlinear medium, which can be a resonant cavity in order to increase the interaction time. But Eq. (126) is just a squeezing operator, so the mode described by $\hat{a}$ will evolve to a squeezed state.

As we observed previously in order to use squeezed light to beat the standard quantum limit an accurate frequency dependent control of the squeezing angle is needed. This is not an easy task, and would require additional optics and small losses. However, squeezed light can be used also in a different and easier way to reduce shot noise at higher frequencies. The basic idea is to introduce squeezed light, with a fixed squeezing angle, just in the high frequency region. In this way the phase noise can be reduced without increasing the laser power. This is important because higher power lasers can induce several problems, mainly thermal lensing effects (see Sec. IV C). A squeezed light source will be used in this way in second generation interferometers, like advanced LIGO and advanced VIRGO.

We said in Subsection II E 1 that a squeezed state is produced spontaneously inside the cavities of an interferometer by the mechanical response of the mirrors. The idea of using this ponderomotive effect to produce squeezed light has been proposed.[131] Conceptually, the ponderomotive effect should be enhanced at low frequencies, which is the region most important for gravitational waves detectors.

III. ENVIRONMENTAL NOISES

In this section, we will discuss the need to isolate the experimental apparatus from environmental noise. This is important by itself, and some ideas that will be introduced will be used again in discussing other issues, in particular thermal noise.

A. Seismic isolation

In an earthbound environment the ground is in continuous motion, with a typical spectral amplitude which can be represented above 10 Hz by the approximate power law $S^{1/2}_{seism}(f) = [\mathcal{A}f^{-2}]m/\sqrt{\text{Hz}}$ where $\mathcal{A}$ is a site dependent constant[132–135] ($\mathcal{A} \simeq 10^{-7}$ at the Virgo site[136]). As this displacement is orders of magnitude larger than the one which could be generated by a gravitational wave, it is necessary to isolate the test masses in an appropriate way.

In order to do this it is possible to take advantage of the mechanical transfer function of a simple harmonic oscillator. The basic building block for this kind of approach is the vibrating string, which can be modeled in the frequency domain by the simplified Lagrangian[137]

$$\mathcal{L}_{string} = \int dx \left(\frac{1}{2}\rho_m\omega^2\tilde{u}^*\tilde{u} - \frac{1}{2}T\tilde{u}^*_x\tilde{u}_x\right). \tag{127}$$

Here $\tilde{u}(x,\omega)$ describes the horizontal displacement of a point of the string from its equilibrium position, ρ_m is the linear mass density, T is the tension.

The Lagrangian (127) gives the equation of motion

$$\tilde{u}_{xx} + K^2\tilde{u} = 0, \quad K^2 = \frac{\rho_m\omega^2}{T} \equiv \frac{\omega^2}{c_S^2}, \tag{128}$$

which we can solve in terms of the boundary conditions $\tilde{u}(0)$, $\tilde{u}(L)$:

$$\tilde{u}(x,\omega) = u(0)\cos Kx + \frac{u(L) - u(0)\cos kL}{\sin kL}\sin Kx. \tag{129}$$

If we substitute the solutions inside Eq. (127) we find an effective Lagrangian for the boundary variables which incorporate the full dynamics of the string. The result is given by a quadratic form in the boundary variables $w = (\tilde{u}_0, \tilde{u}_1)$ (we set here $\tilde{u}_0 = \tilde{u}(0)$, $\tilde{u}_1 = \tilde{u}(L)$) which we can write as

$$\mathcal{L}_{string} = -\frac{1}{2}w^+\Lambda w, \tag{130}$$

$$\Lambda = \frac{TK}{\sin KL}\begin{pmatrix}\cos KL & -1\\ -1 & \cos KL\end{pmatrix}. \tag{131}$$

Downloaded 02 Nov 2011 to 180.149.51.196. Redistribution subject to AIP license or copyright; see http://rsi.aip.org/about/rights_and_permissions

We can use this Lagrangian to get the quantity which is of main interest for us, namely, the transfer function between the top and the bottom. First, we append a mass M at the bottom of the string, in such a way that $T = Mg$. Now we add the kinetic mass term to obtain the full Lagrangian of this prototype suspension,

$$\mathcal{L}_{pendulum} = \mathcal{L}_{string} + \frac{1}{2} M\omega^2 \tilde{u}_1^* \tilde{u}_1 \tag{132}$$

to obtain immediately

$$\tilde{u}_1 = \frac{1}{\cos\left(\frac{f}{\gamma f_p}\right) - \gamma \frac{f}{f_p} \sin\left(\frac{f}{\gamma f_p}\right)} \tilde{u}_0, \tag{133}$$

where γ is the square root of the ratio M and the total mass of the string, and $f_p = (2\pi)^{-1}\sqrt{g/L}$ is the frequency of a pendulum with the same length. This transfer function is plotted in Figure (22) for selected values of γ.

Note that the frequency on the horizontal axis is normalized to f_p. The dotted plot corresponds to $\gamma = 1$. Note that the first peak of the transfer function, which corresponds to the pendular motion, is slightly reduced by the non-negligible inertia of the string. Moving to higher frequency we observe a decrease in the transfer function. This is exactly the effect that is used in a seismic attenuator.

This reduction stops quite early, owing to the second peak which correspond to another resonance of the system. However, in a real application $\gamma \gg 1$, and as can be seen looking at the dashed and continuous plot in this regime the second resonance is pushed to higher frequencies and the region where the transfer function decreases becomes wider. The important point here is that when γ is large the first peak is of order $f \simeq f_p$, while the higher resonances are pushed to $f \simeq k\pi\gamma f_p$ for $k \in \mathbb{N}^+$.

The main problem is that the decrease is not fast enough. With a low frequency expansion of Eq. (133) it can be realized that below the second peak the transfer function is essentially the same of a simple pendulum, which gives a factor $\propto (f_p/f)^2$ above the first peak. This is solved mounting N of these systems in a chain. In this case the Lagrangian is given by

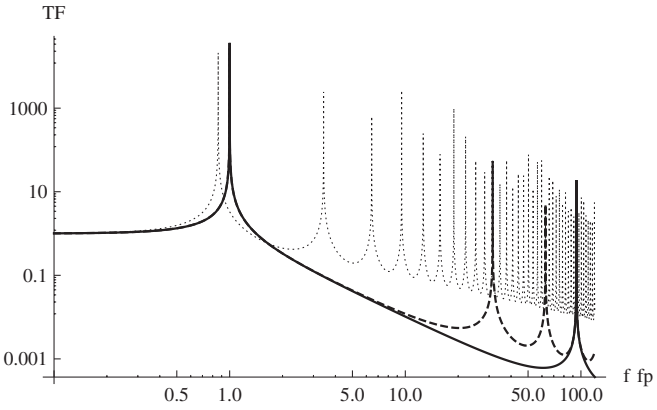


FIG. 22. The modulus of the transfer function of Eq. (133) for $\gamma = 1$ (dotted line), $\gamma = 10$ (dashed line), and $\gamma = 30$ (continuous line). The frequency on the horizontal axis is expressed in unit of $f_p = (2\pi)^{-1}\sqrt{g/L}$.

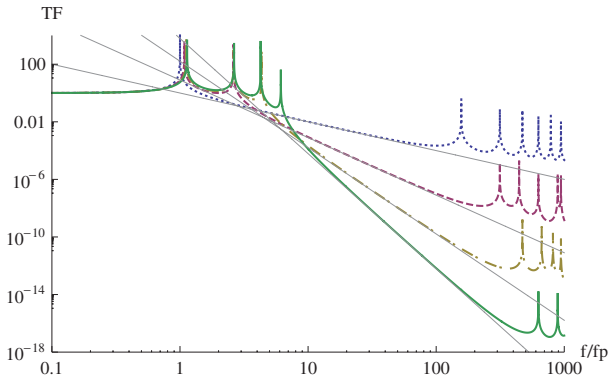


FIG. 23. (Color) The modulus of the transfer function for a chain of N physical pendula for $N = 1$ (dotted line), $N = 2$ (dashed line), $N = 3$ (dotted-dashed line), and $N = 4$ (continuous line) for $\gamma = 60$. The frequency on the horizontal axis is expressed in unit of $f_p = (2\pi)^{-1}\sqrt{g/L}$, where L is the total length of the chain. All the pendula have the same mass and length. The functions $N!(\sqrt{N} f_p/f)^{2N}$ are plotted (thin lines) for reference.

$$\mathcal{L}_{chain} = \sum_{k=1}^{N} \frac{1}{2} M_k \omega^2 \tilde{u}_k^* \tilde{u}_k - \frac{1}{2} w_k^+ \Lambda_k w_k, \tag{134}$$

where $w_k = (\tilde{u}_{k-1}, \tilde{u}_k)$ and Λ_k is given by Eq. (131) evaluated with the appropriate values for T, K, and L. In Figure 23 we plot the result in the particular case of equal masses and lengths, for $N = 1, 2, 3, 4$.

The relevant feature is that the transfer function decreases after the first N peaks as $\mathrm{TF} \simeq (-1)^N N!(\sqrt{N} f_p/f)^{2N}$ until the $N + 1$-th peak is reached. This expression can be written in the general case as

$$TF \simeq (-1)^N \left(\frac{f_p}{f}\right)^{2N} \prod_{m=1}^{N} \left[\frac{L}{L_m} \sum_{k=m}^{N} \frac{M_k}{M_m}\right], \tag{135}$$

where M_k and L_k are the mass and the length of the kth pendulum.

In the $\gamma \gg 1$ regime we are interested in the first group of resonances (the so-called rigid body modes) which correspond to the normal modes of the chain in which the inertia of the strings has a negligible effect. The chain behaves as a multiple pendulum, and each string is only a geometrical constraint.

There are two methods that can be used to obtain good attenuation performance at low frequency. The first is to increase the total length of the chain. In this way the f_p will decrease and the rigid body mode peaks will move to lower frequencies. In this way the attenuation scales as $L^{-N/2}$, but too long chain can create practical problems.

The second possibility is to increase the number of stages. Here there will be an advantage as long as $N!(Nf_p/f)^N$ is a decreasing function of N, which is the case especially at higher frequencies. At some point this decrease will stop, or in other words the peaks of the rigid body modes "invade" the frequency window of interest.

At the beginning of year 1980 a group in Pisa was investigating techniques for improving sensitivity of interferometric detectors of gravitational waves at low frequency with

Downloaded 02 Nov 2011 to 180.149.51.196. Redistribution subject to AIP license or copyright; see http://rsi.aip.org/about/rights_and_permissions

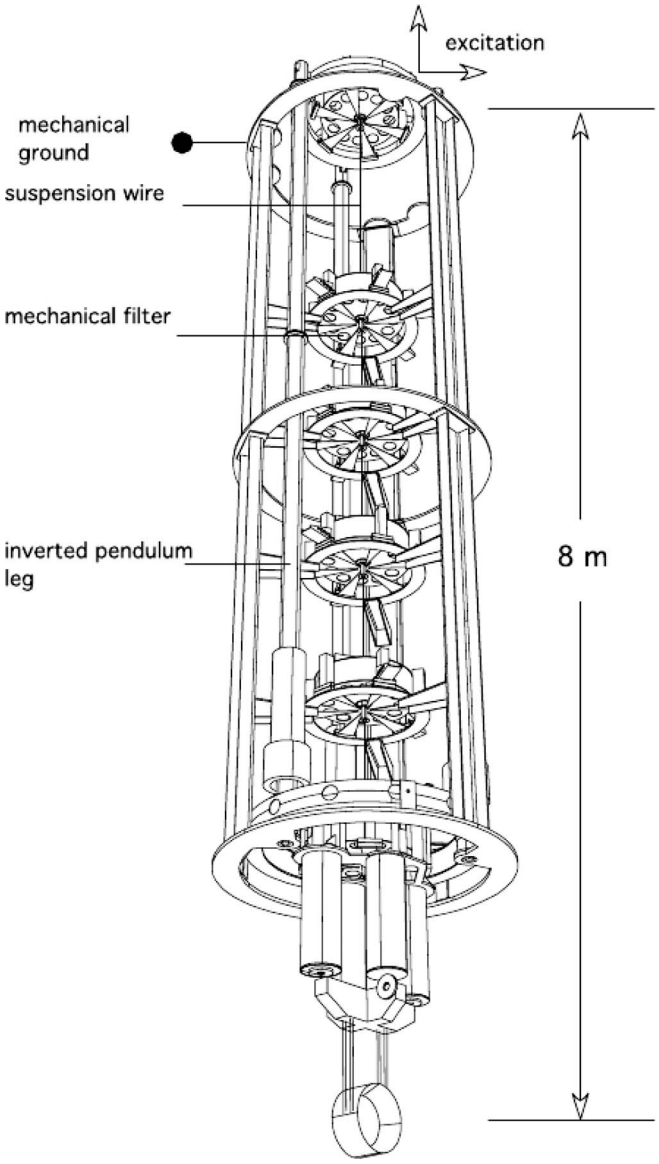


FIG. 24. The scheme of a Virgo superattenuator (see Ref. 138).

the purpose of detecting gravitational wave emission from Pulsars and other slowly rotating objects. The test devices were chains of mechanical filters having very soft compliance in the vertical direction, suspending a heavy mass. A very fundamental point was understood: each chain filter should be able to isolate vibrations along the six coordinates of a rigid body, i.e., x, y, z and θ_x, θ_y, θ_z. Two 8 m tall chains composed of seven gas spring filters were put under vacuum and the remnant of seismic noise between two 400 kg masses appended to each chain was measured.[139] This experiment showed for the first time that it was possible to obtain mirror seismic noise attenuation, at the level of 10^{-10} at 10 Hz.[140] Gas spring filters, being affected by instability due to excessive thermal gas expansion, were abandoned and substituted with mechanical filters.[141]

Virgo was initially designed with an attenuation chain with 7 stages,[138] which were reduced to 5 afterward. A complete attenuation stage is depicted in Fig. 24. We schematized the "mechanical filters" as point masses in our model. The mirror is suspended at the bottom through an intermediate device (called "marionetta") which provides the actuation points that are needed to control the test mass position (See Sec. II A).

The pendula chain is mounted over a three leg structure which provides additional attenuation using the "inverted pendulum" principle.[142] The basic idea can be explained looking at a very simple model: a rigid rod fixed at the bottom with a flexible joint, with a mass at its top. The small oscillation behavior of this system around its equilibrium point can be described by the Lagrangian

$$\mathcal{L} = \frac{1}{2}mL^2\dot{\theta}^2 + \frac{1}{2}(mgL - K)\theta^2, \tag{136}$$

where K parameterizes the restoring momentum of the joint. Clearly, the equilibrium is stable if $K > mgL$, but the interesting point is the frequency of the small oscillations, given by

$$f_{IP} = \frac{1}{2\pi}\sqrt{\frac{K - mgL}{mL^2}}, \tag{137}$$

which can be tuned at least in principle to very small values. We can see the inverted pendulum as another stage of the attenuation chain, depicting it as a normal pendulum with a very large length: in Virgo its resonance frequency is tuned to 40 mHz.

The inverted pendulum stage of the suspensions gives several benefits. First of all it provides a pre-attenuation in the frequency band which is populated by the rigid body modes (confined between 0.3 Hz and 2.5 Hz in Virgo) which gives a relevant contribution to the residual rms.

Another important point is that the top of the attenuation chain is "soft," and it is possible to control its position with low forces, using low dissipation electromagnetic actuators. This possibility is exploited by the so-called *inertial damping* system, which is used to damp with an active feedback the internal modes of the chain connected to the horizontal motion of the top stage. In this way, the residual rms horizontal motion of the mirror is reduced to few tenths of micrometers per second,[143] and the additional forces which must be applied to maintain its correct position are strongly reduced.

In the current LIGO detectors the approach to seismic attenuation is a bit different from Virgo.[144] The main idea is the same, namely, to stack several stages of oscillators to provide the required attenuation. But these oscillators were obtained building from the bottom, alternating rigid platforms and stages of multiple springs of metal and rubber the rubber providing the damping needed to avoid strong noise amplification at the frequencies of the internal resonances. The stack is supported by an external fine actuation system which can give positioning at the $\pm 10^{-4}$ m level in the laser beam direction, and can be used to attenuate partially the noise in an active way.

In LIGO the mirror is suspended as a simple pendulum, mounted over three attenuation stages which provides an

Downloaded 02 Nov 2011 to 180.149.51.196. Redistribution subject to AIP license or copyright; see http://rsi.aip.org/about/rights_and_permissions

attenuation proportional to f^{-6} above the resonance frequencies, which are in the $1 - 14$ Hz region. The design is simpler than the Virgo's one, but it revealed some drawbacks in the low frequency region. It is difficult to push the resonances of the many internal modes of the structure toward low frequencies, and also to build a system with good symmetry. For these reason the lower frequency cutoff in LIGO is one order of magnitude above Virgo's one (around 40 Hz).

In order to meet the overall isolation and alignment requirements for the optics in the next generation detector (advanced LIGO), the attenuation subsystem was redesigned in a quite radical way.[145] It will be composed of three stages.

- An hydraulic external pre-isolator[146] for low frequency alignment and control, which will substitute the previous actuation system and will be able to act in all the six degrees of freedom. In order to avoid injection of noise produced by low frequency hydraulic resonances the working fluid (mineral oil) is maintained in a continuous laminar flow, and the actuation is done with a differential scheme which is the hydraulic equivalent of a Wheatstone bridge.[145]
- A two stage active isolation platform designed to give a factor of $\sim 10^3$ attenuation at 10 Hz. This will have the capability of acting both with a force feedback based on signal obtained from sensors mounted on the payload, and with a *feedforward* action[147] based on measurement on the ground.
- A multiple pendulum suspension system that provides passive isolation above a few Hz.[148,149]

One of the basic limit of this active scheme is the noise of the sensors. We refer to Ref. 145 for details.

Some aspects of the suspension system are more related to thermal noise suppression than to seismic noise, and will be discussed in Subsection IV B. This is particularly true for the last stage of the suspension.

1. Effective mirror mass

The Lagrangian (134) can be used to understand better in which sense the mirror can be considered a free mass. If we couple it to an external force

$$\mathcal{L} = \mathcal{L}_{chain} + \tilde{f}\tilde{u}_N^*, \tag{138}$$

we can solve for $\tilde{u}_N$, obtaining a relation of the form

$$-\mathcal{M}(\omega)\omega^2\tilde{u}_N = \tilde{f}, \tag{139}$$

where $\mathcal{M}(\omega)$ can be considered an effective mirror mass. It follows that the mass behave as a free one if $\mathcal{M}(\omega)$ is constant with a good enough approximation in the frequency interval of interest. As an example, for the single stage suspension described by Eq. (132) we find

$$\mathcal{M}(\omega) = M\left[1 - \frac{g}{L\omega^2}\frac{(\omega L/c_s)}{\tan(\omega L/c_s)}\right], \tag{140}$$

which is approximately constant inside the interval $\sqrt{g/L} < \omega < \pi c_s/(2L)$ where the lower limit corresponds to the pendulum oscillation, and the upper one to the first mode of vibration of the wire.

2. Vertical attenuation

In the linear approximation only the motion of the mirror in the direction of the laser beam is coupled to the phase shift sensed by the detector. It seems that we need to worry only about the attenuation of seismic motion in the horizontal direction. But this is not strictly true, for several reasons.

If we analyze an attenuation chain such as the one depicted in Eq. (24), and we describe the Ith rigid body (a filter mass or the mirror) using the small linear $(x^{(I)}, y^{(I)}, z^{(I)})$ and angular $(\theta_x^{(I)}, \theta_y^{(I)}, \theta_z^{(I)})$ variations from their equilibrium position we can group these in the four sets $\{x^{(1)}, \ldots, x^{(N)}, \theta_y^{(1)}, \ldots, \theta_y^{(N)}\}$, $\{z^{(1)}, \ldots, z^{(N)}, \theta_x^{(1)}, \ldots, \theta_x^{(N)}\}$, $\{z^{(1)}, \ldots, z^{(N)}\}$, and $\{z^{(1)}, \ldots, z^{(N)}\}$. The members of each set are unavoidably coupled: for example, $x^{(I)}$ and $\theta_y^{(I)}$ are coupled by the flexural stiffness of the wires. But in the ideal case we can argue on the basis of symmetry arguments that, for example, z's and x's could be completely decoupled.

In a real attenuator it will not be possible to avoid mechanical asymmetries, so there will be small cross couplings between all the previous sets. The common experience is that with a careful design and with experimental tuning it is possible to reduce these cross couplings to a 1% level, which can be understood as a conservative estimate. This means that the vertical attenuation performance of the attenuator should be comparable at this level with the horizontal one.

There are other effects. Owing to the curvature of the earth's surface the local vertical at the bottom and at the end mirror of a cavity is not the same. This means that there is an unavoidable coupling to the vertical motion, which or a 4 km arm length is $L/R_{earth} \simeq 8 \times 10^{-4}$. Also, optical wedges and mirror orientation can give contribute.

To achieve vertical attenuation performances comparable (up to a factor of about 10^{-2}) to that obtainable in the horizontal direction is one of the major difficulties in designing a seismic attenuation system. In the actual LIGO system, the vertical attenuation is directly provided by the layers of oscillators in the design, using the same principle as the horizontal one. If good attenuation is required in the low frequency region the vertical resonance frequencies of the suspension system must be lowered as much as possible.

There is a basic difficulty here. While the stiffness in the horizontal direction of a pendulum can be reduced quite easily simply by increasing its length without affecting the sustainable load, this is not the case for vertical displacements. This can easily be understood: suppose we use a spring with rest length ℓ_0 and stiffness constant k to sustain a large mass M. In order to do that the spring deformation at the working point must be

$$\frac{Mg}{k} = \frac{g}{\omega^2} = |\ell - \ell_0| \lessapprox \ell_0, \tag{141}$$

which means that the typical dimensions of the system are proportional to the inverse of the square of the desired resonance angular frequency ω, which is quite unpractical (for ω

Downloaded 02 Nov 2011 to 180.149.51.196. Redistribution subject to AIP license or copyright; see http://rsi.aip.org/about/rights_and_permissions

$= 2\pi 10^{-1}$ Hz, which could be a typical reference value, we get $\ell_0 \sim 25$ m).

A possible solution to the problem, which has been implemented in the VIRGO superattenuators represented in Eq. (24), is based on the magnetic anti-spring concept.[150] The idea was to obtain a negative stiffness using interactions between magnets and use it to nearly cancel the mechanical one. In this way we get an oscillator with a very low resonance frequency which attenuates seismic noise in the vertical degree of freedom.

A considerable improvement to the magnetic anti-spring is the geometric anti-spring concept (GAS),[151,152] which allows significant increases in the vertical attenuation and thermal stability of a seismic attenuation system (seismic filter). The monolithic geometric anti-spring concept[153] is essentially an evolution of the GAS concept capable to significantly improve the GAS system performance.

3. The tilt problem

In a real attenuation system it is important to control not only vertical and horizontal displacements, but also angular ones. A first reason is that there are always conversions between angular motions and displacements along the attenuation chain.

Beyond this, it must be realized that in the implementation of an attenuation strategy there is always active feedback applied to the system. This is true for the LIGO system discussed previously, which is mainly active, but also for the Virgo one which is mainly passive. Let us suppose that we want to use an accelerometer to measure the horizontal acceleration of a particular point in the attenuation chain. The sensor will not be able to distinguish a true horizontal acceleration from the effect of the gravity which couples to it if its angular orientation is changed. In order to disentangle the contribution of angular motion an independent *tiltmeter* is needed.

The implementation of a device with good enough sensitivity and manageable size is not trivial, and it is the subject of current research activity.[154,155]

B. Gravity gradient noise

Seismically induced fluctuating gravitational fields directly couple to the test masses themselves, bypassing all attenuation stages. This limitation is called gravity gradient noise (or Newtonian noise). Looking at Figure 5 we see that this noise is more important at low frequencies, but it is not an issue for current detectors.[156–158] It will become a fundamental limitation for the planned sensitivity of third generation detectors.[159]

Gravity gradient noise originates from both seismic and atmospheric density fluctuation, generating a varying gravitational force on the test mass, which is in practice indistinguishable from GW. In general, seismic waves originate from crustal creep, human induced activities (cultural seismic noise), ocean and ground water dynamics, slow gravity drifts, and atmospheric influences. Since no filter or shield can be built for gravitational coupling, suppressing this noise source is difficult and low seismicity sites should be identified.

Possible ways to mitigate gravity gradient noise are currently under study. A possibility is to build the detector underground, taking advantage of reduced seismic activity, as proposed for the future large-scale cryogenic gravitational wave telescope (LCGT) (Ref. 45) and the Einstein Telescope (ET) (Ref. 159) detectors.

Another possible approach is the offline subtraction of the noise,[160–163] using information from auxiliary sensors coupled to seismic motion.

IV. THERMAL NOISE

Thermal noise represents a fundamental limiting noise for gravitational wave detectors. When the laser beam inside an interferometer is reflected by a mirror, it is modulated by the thermal motion of the surface, and this random modulation generates an effective change of the cavity length.

We can describe the thermal motion of the surface of a mirror looking at it as a elastic body. In the linear approximation which is appropriate for the small deformation regime we are interested to the mirror motion can be described by an appropriate set of coordinates Q_n which correspond to normal modes. It can be quite difficult to determine normal modes from a mathematical point of view, however, in principle each Q_n is governed by an equation which can be written as

$$\frac{d^2Q_n}{dt^2} + \gamma_n \frac{dQ_n}{dt} + \omega_n^2 Q_n = \frac{1}{M_n} F(t), \tag{142}$$

which is the equation of a forced harmonic oscillator of (mode dependent) frequency ω_n and mass M_n. We introduced a (small) viscous damping force proportional to γ_n. The force $F(t)$ describes the coupling of the oscillator to the environment, which can be modeled by an heat bath at the temperature T.

For a first rough estimate we can use the equipartition theorem, which tell us the average value of the potential energy,

$$\left\langle \frac{1}{2} M_n \omega_n^2 Q_n^2 \right\rangle = \frac{k_B T}{2}. \tag{143}$$

It follows that the standard deviation σ_n of the coordinate Q_n is given by

$$\sigma_n = \sqrt{\frac{k_B T}{M_n \omega_n^2}}, \tag{144}$$

which for a mode with an eigenfrequency $f_n = 10^3$ Hz and an equivalent mass $M_n = 10$ kg is given at room temperature by $\sigma_n \simeq 3 \times 10^{-15}$ m. This is three orders of magnitudes larger than the typical displacement we want to detect, and it seems that the detection of a gravitational wave is a quite hopeless task.

However, our simple estimate did not take into account the frequency distribution of the noise. Coming back to the Eq. (142) and taking the Fourier transform we can obtain the relation between the power spectrum S_Q of Q_n and the power

Downloaded 02 Nov 2011 to 180.149.51.196. Redistribution subject to AIP license or copyright; see http://rsi.aip.org/about/rights_and_permissions

spectrum S_F of the force, namely,

$$S_Q(\omega) = \frac{1}{M_n^2} \frac{1}{\left(\omega^2 - \omega_n^2\right)^2 + \gamma_n^2 \omega^2} S_F(\omega), \tag{145}$$

which tells us that the larger part of the displacement is connected to fluctuations with frequency around $\omega_n/(2\pi)$, especially when γ_n is small. Assuming that the power spectrum of the force is frequency independent, which means that the force is a white noise stochastic process, and using the fact that the variance σ_n^2 is just the integral of S_Q over all the frequencies we get the final expression

$$S_Q(\omega) = \frac{1}{M_n Q_n} \frac{4k_B T \omega_n}{\left(\omega^2 - \omega_n^2\right)^2 + \frac{\omega^2 \omega_n^2}{Q_n^2}}, \tag{146}$$

where we defined the *quality factor* $Q_n = \omega_n/\gamma_n$ of the mode. When $\left|\omega^2 - \omega_n^2\right| \gg \omega_n^2/Q_n$ the second term in the denominator can be neglected and the noise will be suppressed, more explicitly

$$S_Q(\omega) = \begin{cases} \dfrac{4k_B T}{M_n Q_n \omega_n^3} & (\omega \ll \omega_n) \\ \dfrac{4k_B T \omega_0}{M_n Q_n \omega^4} & (\omega \gg \omega_n) \end{cases}. \tag{147}$$

We conclude that though the standard deviation of the noise is always given by Eq. (144), if we manage to have high values for the quality factors of the normal modes it is possible to confine a large fraction of the noise in a small frequency window around the mode eigenfrequency.

A more general derivation of this result can be obtained from the fluctuation-dissipation theorem,[164] which gives us S_Q in term of the mechanical impedance Z of the mechanical system,

$$S_Q(\omega) = \frac{4k_B T}{\omega^2} \mathrm{Re}\,(Z), \tag{148}$$

where Z is defined as the ratio $Z = \tilde{v}/\tilde{F}$ between the driving force $\tilde{F}$ and the velocity of the system $\tilde{v}$ evaluated in the frequency domain. An advantage of this formulation is that it allows to study systems with more general damping mechanisms.

It is also possible to bypass completely the decomposition in normal modes. Using a very useful reformulation of the fluctuation-dissipation theorem due to Levin[165] it is possible to show that the power spectrum of the equivalent thermal displacement of the mirror can be written as

$$S_x(f) = \frac{2k_B T}{\pi^2 f^2} W_{diss}, \tag{149}$$

where W_{diss} is the average power dissipated in it when an oscillatory pressure

$$P(\vec{r}, t) = f(\vec{r}) \cos 2\pi f t \tag{150}$$

is applied on the surface. Here k_B is the Boltzmann's constant and T is the temperature. The form factor $f(\vec{r})$ is proportional to the intensity profile of the laser beam, and is normalized in such a way that its integral over all the surface is equal to one. The influence of the beam shape can be understood remembering that the thermal noise which affects the detector is an appropriate average over the beam of the random surface motion.

The avoiding of normal mode expansion is important for several reasons.

- The usual way to estimate of the total thermal noise requires a sum over the contributions of all the normal modes. In practice, this sum must be truncated, but it is not always clear how the accuracy of the estimate depends on the truncation.
- Sometimes the concept of normal modes is ill defined, for instance when the damping mechanism is not homogeneous over all the mirror.[165] This is a very important case in fact: as we will see the mirror substrate must be covered by a coating layer, and the two parts have quite different dissipations.
- The evaluation of the dissipated power W_{diss} which appears in Eq. (149) can be analytically quite difficult, but it can be done easily using numerical finite element methods.

In early generation GW detectors, cryogenic aluminum bars, the temperature was brought to a mK region in order to reduce thermal noise. In present high sensitivity interferometric detectors working at room temperature, the more direct way to suppress thermal noise effects is to try to reduce W_{diss}, which is of course equivalent to increasing the quality factor of the normal modes where a description in term of these is applicable. This can be done using materials having extremely low losses for both the mirrors and the wires which suspend them. Research for high Q materials[166,167] and mechanical arrangements[168,169,171] is currently actively pursued by several groups.

There are other possibilities. The first one is to increase gravitational wave's Riemann force by making mirror separation $O(10^4$ m). Note that trying to increase the "effective separation" using Fabry-Perot resonant cavities on the interferometer's arms does not help in this case. The reason is that both the "effective length" and the number of interactions between the beam and the mirrors is increased by the same finesse factor $\mathcal{F}$.

Finally, it should be mentioned that in order to reach the planned sensitivities for third generation detectors probably the use of cryogenics will be needed.[45,159]

A. Mirror thermal noise

The evaluation of thermal noise amounts to the estimation of the dissipated energy W_{diss} in Eq. (149). There can be several dissipation mechanisms, which will correspond to distinct contributions to the total noise budget.[170]

The simplest one comes from the fact that mirror material can have some intrinsic losses, which are usually parameterized by giving the Young's modulus E a small imaginary part $E\phi(f)$, where $\phi(f)$ is named loss angle. Applying the Levine's recipe we find the noise power spectrum for this *structural damping* or *Brownian* contribution, obtaining[165]

$$S_{x,SD}^{Bulk} = \frac{4}{(2\pi)^{3/2}} \frac{k_B T}{f} \frac{1 - \sigma^2}{r_0 E} \phi(f). \tag{151}$$

Downloaded 02 Nov 2011 to 180.149.51.196. Redistribution subject to AIP license or copyright; see http://rsi.aip.org/about/rights_and_permissions

In the estimate given in Eq. (151) and in following ones, we assume a Gaussian beam in its fundamental mode, with beam radius r_0, and neglect the effect of the finite size of the mirror. Also, a quasistatic approximation for the response of the mirror to the pressure (150) is used, which is appropriate below the resonance frequencies of the internal elastic modes. This is the reason why these estimates cannot reproduce the peak at several kHz which is evident in Figure 5 (*tnMir* contributions).

If the beam radius r_0 increases then the surface fluctuations are averaged over a larger area and the noise is suppressed. We see that $S_{x,SD}^{Bulk}$ scales as $T^{1/2}$ with the temperature, so a cryogenic reduction is not in principle very effective. However, we should take into account that in several materials a reduction of the loss angle $\phi(f)$ with the temperature is observed.

This is not the end of the story. If we imagine an ideal material with $\phi = 0$, we will not be able to eliminate its temperature fluctuations. Owing to the thermal expansion these will generate a surface fluctuation also, which can be evaluated in the Levin's approach by considering the losses induced by the irreversible transport of heat between regions compressed in different ways by the pressure (150). The so-called *thermoelastic* contribution will be[174]

$$S_{x,TE}^{Bulk} = \frac{8}{(2\pi)^{5/2}} \frac{\alpha^2 (1+\sigma)^2 \kappa}{(\rho C_v)^2 r_0^3} \frac{k_B T^2}{f^2}, \tag{152}$$

where α is the thermal expansion coefficient, κ is the thermal conductivity, ρ is the density, and C_v is the specific heat at constant volume. Note that the noise scales with $f^{-1} r_0^{-3}$, so it could beat the Brownian contribution in the low frequency regime and for smaller laser spot beam.

Currently in LIGO, VIRGO, and GEO600 mirrors of fused silica are used. Fused silica has quite low intrinsic mechanical losses and excellent optical qualities. Very high quality surfaces can be obtained by applying an appropriate polishing method. Fused silica has also a very low thermal expansion coefficient: as a consequence the thermoelastic noise is quite low and the $S_{x,SD}^{Bulk}$ contribution is the dominant one.

In principle other kind of substrates could be used. In particular Sapphire[172] (a single cristal of Al_2O_3) has quite good optical properties, such as perfect transparency for light with $\lambda = 1064$ nm, and low dependence of the refraction index from the temperature. Sapphire main problem was a large thermal expansion coefficient, 10 times larger that that of the fused silica at room temperature, which makes the thermoelastic thermal noise too large. For this reason it has not been choosen either for advanced detectors. Sapphire seems to have remarkable mechanical properties at cryogenic temperatures, such as an high thermal conductivity which is an important parameter when it is needed to remove heath efficiently. Extensive studies has been done in Japan as a part of the proposal for a LCGT,[45] which suggest, however, only moderate performance.[173]

1. The coating thermal noise

In an interferometric detector of gravitational waves low optical losses are necessary, and this means that mirrors with very high reflectivities are needed. The common strategy used to improve reflectivity is to cover the mirror's surface with a variable number of dielectric layers with alternate values of the refraction index, the standard choice being silica (SiO_2) and tantala (TiO_2). This is the so-called coating, and in this way it is possible to suppress by interference the transmission of light.

The price to pay is that the mechanical losses in the coating are usually quite large, and this has a negative impact on thermal noise.[175–178] Considering the intrinsic losses of the materials the coating contribution to Brownian thermal noise will be[179]

$$S_{x,SD}^{Coat}(f) = \sqrt{\frac{2}{\pi}} \frac{d}{r_0 (1-\sigma^2)} \frac{\phi_c}{\phi} \times S_{x,SD}^{Coat}(f). \tag{153}$$

Here ϕ_c is the loss angle for the coating, and d is his thickness. The factor $d/r_0 \simeq 10^{-4}$ can be understood by considering that it is proportional to the ratio E_C/E_B of the elastic energies which are stored in the coating and in the bulk of the mirror when the pressure (150) is applied (see Fig. 25 and its caption for an intuitive explanation).

Silica is considered today the best material conjugating very good optical properties and extremely low mechanical losses. Recent mechanical losses measurements on coated silica mirrors have shown that mirror coatings are source of high mechanical losses; even if the multilayer coatings have thickness of order $d = 10-15$ μm, their low mechanical quality factor can heavily spoil the overall mirror bulk high mechanical quality factor. The loss angle, which can reach 10^{-8} in the mirror silica bulk, in the coating remains close to $3–4 \times 10^{-4}$ even at low temperature,[180,181] as shown in Figure 26.

We can estimate the effect of the high losses in the coating using the previous values,

$$\phi_{Total} = \phi + \frac{E_C}{E_B}\phi_c \sim \frac{E_C}{E_B}\phi_c \sim 4 \times 10^{-8}. \tag{154}$$

The total loss angle for a coated silica mirror is approximately given by Eq. (154), which corresponds to a mechanical Q of the order

$$Q = \phi_{Total}^{-1} \sim 2.5 \times 10^7. \tag{155}$$

By assuming $T = 300$ K, $E = 71$ GPa, $w_0 = 3 \times 10^{-2}$, from Eq. (153) it follows:

$$\sqrt{S_x(f)} \sim \frac{0.4 \times 10^{-17}}{\sqrt{f}} \frac{\text{m}}{\sqrt{\text{Hz}}}. \tag{156}$$

At 10 Hz $\sqrt{S_x(f)} \sim 10^{-18}$ m/$\sqrt{\text{Hz}}$; if the interferometer has 10 km long arms at 10 Hz the limiting sensitivity will be $\tilde{h} \sim 10^{-22}/\sqrt{\text{Hz}}$, not very good indeed. The coating thermoelastic contribution is also present, but somewhat less important, together with the *thermorefractive* contribution, which is connected to the temperature induced fluctuations of the refraction index inside the coating.

Previously we commented Figure 26 which shows no evidence of reduction of the loss angle ϕ with the temperature. It seems that this sensitivity will improve reducing the temperature only owing to the thermodynamical factor $\sqrt{k_B T}$,

Downloaded 02 Nov 2011 to 180.149.51.196. Redistribution subject to AIP license or copyright; see http://rsi.aip.org/about/rights_and_permissions

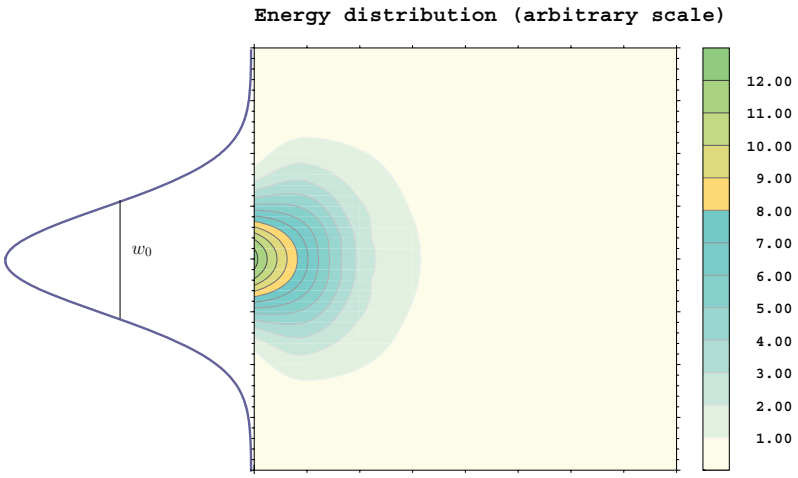


FIG. 25. (Color) The distribution of elastic energy inside an infinite half space, when a pressure is applied on its boundary surface, in the static limit. The shape of the pressure distribution is a Gaussian with spot size r_0 depicted on the left. It is evident that the energy is localized in a region of typical linear size r_0. It follows that the ratio between the total energy stored in the coating and in the bulk region is given approximately by $E_C/E_B \sim d/r_0$. In each region the dissipated energy will be proportional to the stored one multiplied by the appropriate loss angle. For a real mirror there will be corrections when the mirror's dimension becomes comparable with r_0.

which decreases quite slowly. This very limited improvement at low temperature shows that different light reflection techniques should be explored.

A possibility that has been suggested is to explore coatings built with several dielectric layers of not equal thicknesses, organized in such a way to maintain a good reflectivity but optimized from the point of view of thermal noise.[182] This is possible because there is evidence that the main dissipation source is in the bulk of tantala's layers,[177] and a search for reflective configurations which minimize them can be done.

Another option is to optimize the form factor $f(\vec{r})$ which appears in Eq. (150) using higher order Gaussian[183] or non-Gaussian[184] laser modes. In both cases one of the problems to be solved is the generation with good efficiency of a mode which is not contaminated by spurious contributions. In the non-Gaussian case the profile of the mirror's surface must be redesigned also.

A less conservative option is to eliminate completely the coatings. This is possible using diffraction gratings[185–189] or total internal reflection[179] in a prism. In the last case, the main problem is connected to the fact that the light beam moves inside the material, and could get a large thermorefractive noise contribution. This can also be evaluated using the Levin's approach,[190] obtaining

$$S_{x,TR}^{Bulk}(f) = \beta^2 \frac{4k_B T^2 \kappa}{(\rho C_v)^2} \frac{\ell}{4\pi^3 r_0^4}, \tag{157}$$

where $\beta = dn/dT$ and ℓ is the length of the path inside the material.

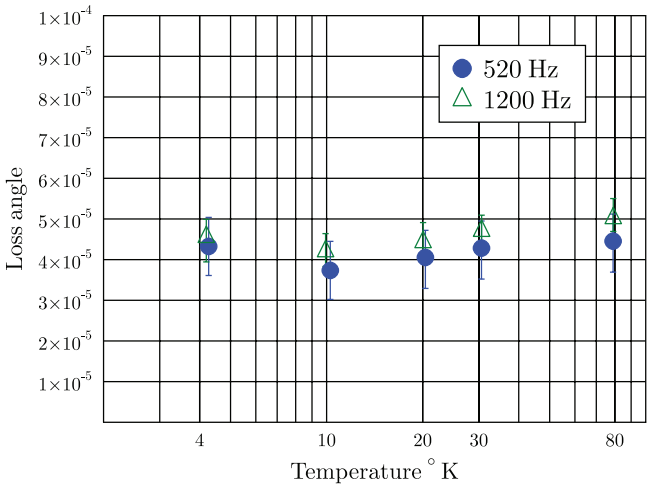


FIG. 26. (Color online) Mechanical loss angle for a mirror coating at different temperatures (see Refs. 180 and 181). The data corresponds to the mirror "sample 1" in Ref. 181. The loss angle is measured at the frequencies specified, which correspond to the first and third internal modes of the mirror. The usual reduction of loss angle at low temperature occurring in many materials unfortunately is absent here.

B. Suspension thermal noise

The contributions of the mirror to thermal noise we discussed decrease slowly with the frequency. For this reason they dominate the sensitivity above 50 Hz, until they are surpassed by the shot noise around 100 Hz. The mechanical suspension system is also subjected to thermal fluctuations, and it turns out that their spectrum decreases much faster, and is the dominant one between 2 Hz and 50 Hz. The intuitive reason is the effect of a stochastic force applied at a given point along the attenuation chain is filtered by the stages below.

In principle, there is no reason to separate the suspension and the mirror thermal noise. We could apply the Levin's approach to the complete mechanical system, evaluating the response of the suspended mirror to the pressure (150). However, we expect that this will be a good approximation, at least when the magnitude of the two effects is very different.

With a direct application of the fluctuation-dissipation theorem to the mirror, considered as a rigid body, we obtain

$$S_{x,SUS}(f) = \frac{k_B T}{2\pi^3 f^3} \mathrm{Im}\left(\frac{1}{\mathcal{M}}\right), \tag{158}$$

Downloaded 02 Nov 2011 to 180.149.51.196. Redistribution subject to AIP license or copyright; see http://rsi.aip.org/about/rights_and_permissions

where $\mathcal{M}$ is the effective mirror mass introduced in Subsection (III A 1). In order to get a useful result we must insert mechanical losses into the model, otherwise the imaginary part of $\mathcal{M}$ will be zero. The suspension should be carefully designed in order to reduce these. Most critical issues are connected to the contact point between different pieces of the apparatus, for example, the junction between suspension wires and the mirror. In this particular case a large improvement is expected by the use of the so-called *monolithic suspensions*.[191] The idea is to use fused silica fibers for the suspension, which are attached to the mirror with the silicate bonding technique.[42]

Also in the ideal case of a totally monolithic suspension, the material of the wires will be subject to deformation. For a wire, the dissipation must depend on the curvature, which is negligible at low frequency for the ideal string described by the Lagrangian (127). The reason is that if we neglect the inertia of the wire, its shape will be always a line. This is the main reason that makes a pendulum a mechanical system with in principle a very low dissipation.

The dominant effect is connected to the flexural stiffness of the wire, which can be described adding to the Lagrangian in Eq. (127) the term

$$\mathcal{L}_{flexural} = -\frac{1}{2} E I \tilde{u}^*_{xx} \tilde{u}_{xx}, \tag{159}$$

where $I = \pi r^4/4$ is the second moment of area of the wire[192] and r is its radius. The equation for the wire which is obtained can be written in the limit $\omega \to 0$ as

$$E I u_{xxxx} - T u_{xx} = 0, \tag{160}$$

and typically $\lambda = \sqrt{EI/T} \ll L$, so u_{xx} will be different from zero in a significant way only in a small region of the order λ near the boundaries. The dissipated energy will be proportional to the one stored in this region, which is a small fraction of the total potential energy if we take into account the gravitational one. A detailed calculation[193] shows that the loss angle of the pendulum is connected to the one of the material by the relation

$$\phi_{pendulum} = \frac{\lambda}{2L} \phi_{material} \ll \phi_{material}. \tag{161}$$

This *dilution factor* λ/L makes possible to build oscillator chains with very low dissipation. However, a pendulum does not give useful vertical attenuation, and noise in the vertical direction will be larger, though suppressed by the small cross coupling factor.

C. High power lasers and thermal lensing

As we saw the most direct way to reduce shot noise is to increase the laser power. However, this is not a free lunch, as a higher power inside the cavities induces several problems.

One issue is connected with the so-called thermal lensing effect. The absorption of the mirrors used in interferometric detectors is kept very small, as an example, less that 10^{-6} for VIRGO mirrors. This is quite impressive, and difficult to obtain, however, for next generation detectors lasers of few 10^2 W are foreseen, and taking into account power recycling and cavity finesse we see that mirror heating will not be negligible.

Thermal lensing effects have been extensively studied from a theoretical point of view:[194,195] the heat absorbed by the mirror can induce both geometrical distortions proportional to the thermal expansion coefficient and purely optical ones mediated by the temperature dependent refraction index.

In order to resonate inside the cavity an optical mode must have equal phase surfaces matched to the mirror profile. Optical distortions can destroy this matching both directly, changing the curvature radius of the mirrors, and indirectly focusing the beam.

Several strategies have been proposed to reduce thermal lensing effect. We can roughly separate them into correction strategies and heat extraction ones. In the first case typically the curvature radius of the mirror is controlled with an external source of heat.[196] This can be an auxiliary laser, which can easily be shaped to obtain the required correction. In the second case heat is extracted from the mirror with several techniques. An interesting possibility is to focus a heat sink (a cold body) with a reflector on the mirror,[197] obtaining a system capable of extracting heat with a given spatial pattern.

It is interesting to note that these thermal compensation techniques are very useful also in the current generation of detectors, as they give a way to tune the optical parameters (mainly the mirror's curvature radius) independently from thermal lensing effects.

Another issue connected to high power inside cavities is the parametric instability problem. The beam's photons interact with the phonons which describe the normal mode oscillations of the mirror.[118,120] If the beam power and the Q factor of the optical cavity is high enough these modes can become unstable, giving an upper limit for the storable energy. A suggested solution is the use of thermal tuning to change the mirror radius of curvature, putting unstable modes out of resonance. Another possibility is the reduction of the Q factor of the mirror with the application of a lossy coating. Obviously this must be done without increasing the thermal noise, which is possible because we saw (see Figure 25) that the fraction of the elastic energy which is important for it is localized near the mirror surface, so it should be enough to induce losses far from it. Finally, it is possible to attempt a stabilization obtained with an external feedback. This could be obtained using an external auxiliary cavity, by applying a force directly to the mirror or by injecting higher order modes of the laser with an appropriate phase.

We end this section mentioning the technique of resonant sideband extraction (RSE) proposed originally by Mizuno.[198,199] One of its main advantages is the reduction of thermal absorption of optical substrates.

The optical scheme requires the addiction of a partially reflecting mirror on the dark port, in complete analogy with the setup used for signal recycling. While the purpose of signal recycling as is commonly understood is to increase the storage time of signal sidebands inside the interferometer, in the RSE technique the parameters are tuned in such a way to obtain the opposite effect. In this way it is possible to increase the storage time of the carrier inside the cavities, without doing the same for the signal. A large storage time for the

Downloaded 02 Nov 2011 to 180.149.51.196. Redistribution subject to AIP license or copyright; see http://rsi.aip.org/about/rights_and_permissions

carrier allows the power inside the cavity to be increased without increasing the injected power, which must pass through the optical elements. At the same time the storage time for the signal is not increased, and there is no sensitivity reduction at higher frequencies.

A detailed description of the technique can be found in Ref. 200. The more complex optical setup requires an appropriate control strategy, and it will be probably implemented in the next generation of interferometric detectors.

V. CONCLUSIONS

The prediction of the existence of gravitational waves is more that a century old. However, their direct detection still remains elusive. Estimates about the strength of the signal generation by different mechanisms has changed in recent years[201,202] and the same is true for the rate of some classes of events expected to generate them.[37] In part this can be seen as a side effect of the current experimental activity, which also started to generate physically interesting upper limits.[11]

A very large effort is currently put into exploring and implementing ways of enhancing the sensibility of detectors. The noises to beat are at the moment the thermal and optical ones. In the future seismic noise could also play a role, allowing for an enlargement of the sensitivity window in the low frequency region. However, it does not seem that it will be possible to go below 1 Hz in an earthbound detector. Starting from the next generation of detectors other noises will start to play a major role, namely, quantum and gravity gradient noise.

Apart from these fundamental noise sources, the real work which allows for a detector to be commissioned is the continuous effort of scientists and engineers who continuously try to understand the "real object." This means fighting against unforeseen noise sources, often poorly understood, and against intricate unpredicted effects. It is really difficult to describe this enormous activity in a systematic way, and to give justice to all the people involved.

An interferometric detector, though based on a simple basic principle, is really a quite complicated instrument. Only the joint work of a large scientific collaboration will make it possible to obtain a first detection, which we expect confidently with the next generation of detectors or, with some luck, with the current one.

ACKNOWLEDGMENTS

We are grateful to Lee Holloway for a careful reading of the manuscript. The authors want to thank the editor for the patience and the kindness he showed in allowing several delays in the completion of this work.

APPENDIX: COUPLING BETWEEN DETECTOR AND GRAVITATIONAL WAVES BEYOND THE LOW FREQUENCY APPROXIMATION

In the expressions used during the discussions presented in the review we worked under the hypothesis of a wavelength λ_{gw} much larger that the typical size L of the detector. Here we present an analysis of the coupling between the detector and the gravitational wave beyond this approximation. We start again from the generic scheme in Figure 1.

The simplest possibility is the Michelson interferometer: in this case the transfer functions $\mathcal{P}_{N,W}$ are just defined by

$$\mathcal{P}A(t) = A\left[t - \tau_{RT}(t)\right], \tag{A1}$$

where $\tau_{RT}(t)$ is the time needed by the field to move back and forth between the beam splitter and the terminal mirrors, and we omit an index which labels the arm considered for simplicity. This τ_{RT} is a function of the time when a gravity wave is present, or when the terminal mirrors move. Its calculation is simpler in the TT gauge. The motion of the terminal mirrors is determined by the geodesic equation, and if they are initially at rest the spatial part of their quadrivelocity will be zero so that

$$\frac{du^{\mu}}{d\tau} = -\Gamma^{\mu}_{00}u^0u^0 = 0 \tag{A2}$$

but then as in the TT gauge

$$\Gamma^{\mu}_{00} = \frac{1}{2}\eta^{\mu\alpha}\left(2h_{\alpha 0,0} - h_{00,\alpha}\right) = 0, \tag{A3}$$

there will be no quadriacceleration and the mirrors will remain at rest forever. In other words, the reference frame associated with the TT gauge is adapted to a system of free falling masses at rest.

We determine now the motion of a photon which moves along an arm of the interferometer. For the first half round trip in absence of gravitational waves we have simply

$$X^{\mu}_0 = \begin{pmatrix} t_0 + \lambda \\ \hat{n}\lambda \end{pmatrix}, \tag{A4}$$

where t_0 is the time of the first arrival of the photon at the beam splitter, the three dimensional versor $\hat{n}$ specify the direction of the arm and $0 < \lambda < L$. We determine now the $O(h)$ correction X^{μ}_1 using the geodesic equation

$$\frac{d^2X^{\mu}_1}{d\lambda^2} + \frac{1}{2}\eta^{\mu\alpha}(h_{\alpha\rho,\nu} + h_{\alpha\nu,\rho} - h_{\rho\nu,\alpha})\frac{dX^{\rho}_0}{d\lambda}\frac{dX^{\nu}_0}{d\lambda} = 0. \tag{A5}$$

When a gravitational wave moving in the $\hat{u}$ direction is present we can write

$$h_{\mu\nu} = \varepsilon_{\mu\nu}h\left(t - \hat{u}\cdot\vec{x}\right). \tag{A6}$$

The geodesic equation becomes

$$\frac{d^2T_1}{d\lambda^2} + \frac{1}{2}\frac{\varepsilon_{ij}n^in^j}{(1-\hat{u}\cdot\hat{n})}\frac{dh}{d\lambda}(s) = 0 \tag{A7}$$

for the time and

$$\frac{d^2}{d\lambda^2}\hat{n}\cdot\vec{X} + \varepsilon_{ij}n^in^j\left[1 + \frac{1}{2}\frac{\hat{u}\cdot\hat{n}}{(1-\hat{u}\cdot\hat{n})}\right]\frac{dh}{d\lambda}(s) = 0 \tag{A8}$$

for the displacement along the interferometer arm. Equation (A8) can be integrated to obtain the λ value at the arrival on the mirror

$$\lambda = L + \varepsilon_{ij}n^in^j\left[1 + \frac{1}{2}\frac{\hat{u}\cdot\hat{n}}{(1-\hat{u}\cdot\hat{n})^2}\right]\int_{t_0}^{t_0+L(1-\hat{u}\cdot\hat{n})} h(s)ds \tag{A9}$$

Downloaded 02 Nov 2011 to 180.149.51.196. Redistribution subject to AIP license or copyright; see http://rsi.aip.org/about/rights_and_permissions

then we can integrate Eq. (A7) to get

$$T = L + \varepsilon_{ij} n^i n^j \left[1 - \frac{1}{2(1-\hat{u}\cdot\hat{n})}\right] \int_{t_0}^{t_0+L(1-\hat{u}\cdot\hat{n})} h(s)ds. \tag{A10}$$

We can repeat the same calculation for the second half round trip (inverting $\hat{n}$) to get the total delay

$$\tau_{RT} = 2L + \frac{1}{2}\varepsilon_{ij} n^i n^j \left\{ \int_{t_0}^{t_0+L(1-\hat{u}\cdot\hat{n})} \frac{1-2\hat{u}\cdot\hat{n}}{1-\hat{u}\cdot\hat{n}} h(s)ds + \int_{t_0+L(1-\hat{u}\cdot\hat{n})}^{t_0+2L} \frac{1+2\hat{u}\cdot\hat{n}}{1+\hat{u}\cdot\hat{n}} h(s)ds \right\}. \tag{A11}$$

It is convenient to consider a monochromatic complex wave,

$$h_{ij} = h\varepsilon_{ij} \exp[i\Omega(t - \hat{u}\cdot\vec{x})], \tag{A12}$$

remembering that the general case can be constructed by superposition. From now on we will use a capital Ω for the frequency of a gravitational wave. In this particular case Eq. (A11) becomes

$$\tau_{RT}(t) = 2L + Lh\varepsilon_{ij} n^i n^j e^{i\Omega(t-2L)} \Upsilon_X(\Omega), \tag{A13}$$

where

$$\Upsilon_X(\Omega) = \frac{1}{2} e^{i\Omega L_X(1-\hat{u}\cdot\hat{n}_X)} \left\{ (1-2\hat{u}\cdot\hat{n}_X) e^{-i\frac{\Omega L_X}{2}(1-\hat{u}\cdot\hat{n}_X)} \times j_0\left[\frac{\Omega L_X}{2}(1-\hat{u}\cdot\hat{n}_X)\right] + (1+2\hat{u}\cdot\hat{n}_X) \times e^{i\frac{\Omega L_X}{2}(1+\hat{u}\cdot\hat{n}_X)} j_0\left[\frac{\Omega L_X}{2}(1+\hat{u}\cdot\hat{n}_X)\right] \right\}, \tag{A14}$$

and we reparameterized τ_{RT} in terms of the final time. If we substitute this result in Eq. (A1) we can conclude that the output field is phase modulated.

Similar considerations can be done for an interferometer with resonant Fabry-Perot cavities. We can recover the final expression remembering that the output field of a resonant cavity is a coherent sum over all the possible paths. For a single cavity the output amplitude will be given by[203]

$$A_{out}[t] = -RA_{in}[t] + T^2 \sum_{k=1}^{\infty} R^{k-1} A_{in}\left[t - \tau_{RT}^{(k)}(t)\right]. \tag{A15}$$

In this expression $\tau_{RT}^{(k)}(t)$ is the time spent inside the cavity by a photon which exited from it at time t after k round trips. It can be obtained from Eq. (A13) summing over each trip, with the result

$$\tau_{RT}^{(k)}(t) = 2kL + Lh\varepsilon_{ij} n^i n^j \Upsilon(\Omega) e^{i\Omega(t-2L/c)} \frac{1-e^{-2ik\Omega L/c}}{1-e^{-2i\Omega L/c}}. \tag{A16}$$

We can now write the transfer function of the cavity, which up to $O(h)$ terms becomes a simple linear relation most conveniently written in the frequency domain

$$\mathcal{P}\tilde{A}_{in}(\omega) = e^{i\beta(\omega)} \tilde{A}_{in}(\omega) - i\omega\Gamma(\Omega,\omega) Lh\varepsilon_{ij} n^i n^j \Upsilon(\Omega) \tilde{A}_{in}(\omega - \Omega). \tag{A17}$$

The first term can be interpreted as the input field filtered by a static cavity, which in our simple modelization has a single input and no losses. For this reason the filtering action is simply described by a frequency dependent phase factor

$$e^{2i\beta(\omega)} = \frac{e^{-2i\omega L/c} - R}{1 - Re^{-2i\omega L/c}} \tag{A18}$$

The term in the second row gives the contribution of the phase modulated input field, the modulation being induced by the gravitational wave. The factor $\Gamma(\Omega, \omega)$ is defined by

$$\Gamma(\Omega,\omega) = \frac{(1-R)(1+R) e^{-2i(\Omega+\omega)L/c}}{(1-Re^{-2i\omega L/c})(1-Re^{-2i(\Omega+\omega)L/c})}. \tag{A19}$$

We obtain the final result for an interferometer by recombining at the beam splitter the beams filtered by the cavity of each arm, getting (we set $R_{BS}T_{BS} = 1/2$ from now on, and we reinsert the arm labels N and W)

$$\tilde{A}_{out}^{(2)}(\omega) = \frac{1}{2}(e^{2i\beta_N(\omega)} - e^{2i\beta_W(\omega)})\tilde{A}_{in}^{(1)}(\omega) - i\omega h\varepsilon_{ij}\mathcal{D}_-^{ij}(\Omega,\omega)\tilde{A}_{in}^{(1)}(\omega-\Omega) + \frac{1}{2}(e^{2i\beta_N(\omega)} + e^{2i\beta_W(\omega)})\tilde{A}_{in}^{(2)}(\omega) - i\omega h\varepsilon_{ij}\mathcal{D}_+^{ij}(\Omega,\omega)\tilde{A}_{in}^{(2)}(\omega-\Omega). \tag{A20}$$

We can interpret Eq. (A20) in the following way. In the general case, the field of the output beam 2 (see Figure 1) receives contributions from the both the input beams 1 and 2.

In each case the coupling between a gravitational wave and the detector is proportional to the contraction between the gravitational field evaluated at the beam splitter and $\mathcal{D}_-^{ij}$ (input 1) or $\mathcal{D}_+^{ij}$ (input 2). When a gravity wave of frequency Ω is present, it generates sidebands of the laser field, at a frequency $\omega_c + \Omega$. In a real gravitational wave the component at frequency $-\Omega$ will be present, so the sideband $\omega - \Omega$ will also be generated.

In the typical configuration a strong field (the input laser beam) will be present only in the input 1, so from the point of view of the signal we can neglect $\tilde{A}_{in}^{(2)}$ and only $\mathcal{D}_-^{ij}$ is relevant. As we will see this is not the case when we are interested to evaluate the detector's optical noise.

The factors $\mathcal{D}_\pm^{ij}$ which completely describes the dependence of the output field by the polarization and by the direction of the wave are defined by

$$\mathcal{D}_\pm^{ij}(\Omega,\omega) = \frac{1}{2}\left[L_W n_W^i n_W^j \Upsilon_W(\Omega)\Gamma_W(\Omega,\omega) \mp L_N n_N^i n_N^j \Upsilon_N(\Omega)\Gamma_N(\Omega,\omega)\right]. \tag{A21}$$

If for simplicity we assume the same optical behavior for the two optical cavities, which means $\Gamma_W = \Gamma_N = \Gamma$ and $\beta_W = \beta_N$, the frequency factor factorizes, $\mathcal{D}_\pm^{ij} = \Gamma D_\pm^{ij}$ and we can study the dependence of the coupling from the direction and the frequency of a gravitational wave by looking at the square modulus of $\varepsilon_{ij} D_-^{ij}$.

Expanding D_-^{ij} in powers of $\Omega L/c$ we see that at the first order the correction is a time delay which is different for the

Downloaded 02 Nov 2011 to 180.149.51.196. Redistribution subject to AIP license or copyright; see http://rsi.aip.org/about/rights_and_permissions

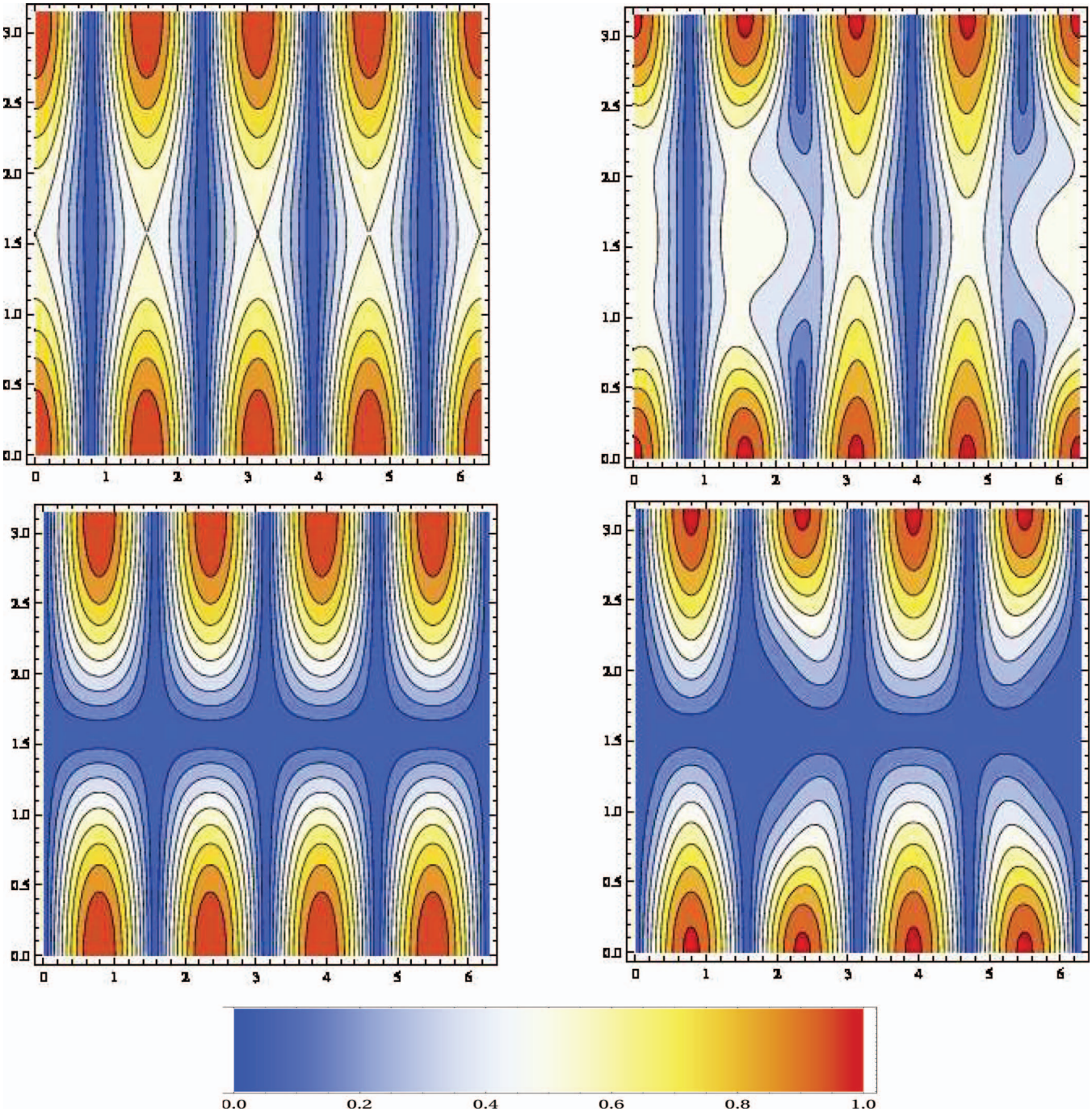


FIG. 27. (Color) Plots of the dependence of the coupling between a gravitational wave and an interferometer with an arm length $L = 4$ km. The functions plotted are $|D_-^{ij}\varepsilon_{ij}^{+}(\theta,\phi)|$ (top) and $|D_-^{ij}\varepsilon_{ij}^{\times}(\theta,\phi)|$ (bottom) for $f = 0$ (left) and $f = 16$ kHz (right). The angles θ (vertical axis) and ϕ (horizontal axis), both given in radians, are spherical coordinates parameterizing the direction of the gravitational wave. The polarization tensors are defined as in Ref. 2. The arms of the detector are in the x and y direction.

two different arms

$$D_-^{ij} = \frac{e^{i\Omega L}}{2}\left(n_W^i n_W^j e^{i\frac{\Omega L}{2}\hat{u}\cdot\hat{n}_W} - n_N^i n_N^j e^{i\frac{\Omega L}{2}\hat{u}\cdot\hat{n}_N}\right). \qquad \text{(A22)}$$

In Figure 27 we show a polar plot of this dependence for the two conventional choices of the polarization tensor ϵ_{ij} (see, for instance, Ref. 2). Frequency corrections to the angular dependence start to be relevant when $\Omega L/c$ is not small, which for a 4 km detector means $f \simeq 20$ kHz. As we will see $\Omega L/c$ is quite small in the sensitivity window of the current interferometric detectors.

1. Locally Lorentzian coordinates

Mirrors do not really behave as free falling test masses, as they are subjected to several external forces, the most obvious ones being the elastic forces needed to suspend the mirrors in a practical experimental setup. They are also unavoidably coupled to the environment. As discussed in the review

Downloaded 02 Nov 2011 to 180.149.51.196. Redistribution subject to AIP license or copyright; see http://rsi.aip.org/about/rights_and_permissions

the coupling to microscopic degrees of freedom of the system generates thermal noise, the coupling to the laser used to monitor the mirrors' positions generates radiation pressure noise, the coupling to the seismic fluctuation of the ground generates seismic noise.

For this reason mirrors will not really move along geodesics, and additional external force terms should be added to the equation of motion. While it is completely legitimate to do this in the TT gauge, the description of an external force can be tricky, and a coordinate system which is adapted to our Newtonian intuition can be very useful.

This *proper detector frame* can be obtained with two conceptual steps. First, we can consider the Fermi normal coordinates associated with a given geodesic γ.[204,205] These have the property that near γ the metric differs from $\eta_{\mu\nu}$ only at the second order in the coordinate separation, namely, external forces can be described using their Newtonian expressions in the neighborhood of the geodesic. The second step is to change coordinates from this frame to the one attached to the laboratory.

The metric will be given by[2,206]

$$\frac{1}{c^2}g_{00} = -1 + \frac{2}{c^2}\vec{g}\cdot\vec{x} - \frac{1}{c^4}(\vec{g}\cdot\vec{x})^2 + \frac{1}{c^2}(\vec{\Omega}\wedge\vec{x})^2 - R_{0i0j}x^i x^j, \tag{A23}$$

$$\frac{1}{c}g_{0i} = \frac{1}{c}(\vec{\Omega}\wedge\vec{x})_i - \frac{2}{3}R_{0jik}x^j x^k, \tag{A24}$$

$$g_{ij} = \delta_{ij} - \frac{1}{3}R_{ikjl}x^k x^l, \tag{A25}$$

neglecting $O(x^3)$ terms. Here $\vec{g}$ is the gravity acceleration and $\vec{\Omega}$ is the angular velocity of the laboratory. The effect of gravitational waves and local variations of the gravitational fields, both in time and space, are encoded in the components of the Riemann's tensor (which are evaluated at $x = 0$).

The biggest advantage of this frame is that we can describe additional forces using a Newtonian formalism. This means that the equation of motion for a mirror can be written simply as

$$\frac{d^2x^\mu}{d\tau^2} + \Gamma^\mu{}_{\nu\rho}\frac{dx^\nu}{d\tau}\frac{dx^\rho}{d\tau} = \frac{F^\mu}{m}, \tag{A26}$$

where the left side is simply the geodesic equation and F^μ is a quadrivector which describes external forces. On the other hand, the metric (A25) is a good approximation only when x is small compared with the curvature scale of the gravitational field, which for a gravitational wave of wavelength λ_{gw} means $x \ll \lambda_{gw}/2\pi$. The description will be accurate only when λ_{gw} is large compared with the detector size. As we said this is currently a reasonable approximation.

If we write the explicit expression of this equation of motion, we recognize that the terms proportional to $\vec{\Omega}$ in $\Gamma^\mu{}_{\nu\rho}$ give rise to the usual centrifugal and Coriolis forces, plus relativistic corrections. In the same way terms proportional to $\vec{g}$ generate a Newtonian gravitational force (plus a gravitational red shift).

We are mainly interested here in the contributions proportional to the Riemann tensor. If we neglect relativistic effect only $\Gamma^i{}_{00}$ is relevant, and it is given by

$$\Gamma^i_{00} = -\frac{1}{2}h^{TT}_{ij,00}x^j, \tag{A27}$$

where we used the fact that the linearized Riemann tensor is invariant under coordinate changes. The main conclusion is that in the proper detector frame we can use Newtonian physics, and describe the effect of a gravitational wave by applying to each mirror a force which is given by

$$F^i_{GW} = \frac{1}{2}m\ddot{h}^{TT}_{ij}x^j, \tag{A28}$$

where m is the mirror's mass and x^j is its coordinate. This means that the effect of the gravitational wave can be described entirely by a fluctuation of the length of the cavity given by

$$\delta L = \frac{L}{2}h^{TT}_{ij}n^i n^j. \tag{A29}$$

To simplify the presentation from now on we will work in the low frequency regime, setting $\Upsilon_X = 1$ inside Eq. (A21), and we will suppose also that $L_W\Gamma_W = L_N\Gamma_N \equiv L\Gamma$. Under these assumptions $\mathcal{D}^{ij}_\pm = L\Gamma D^{ij}_\pm$ where the frequency independent factor

$$D^{ij}_\pm = \frac{1}{2}\left(n^i_W n^j_W - n^i_N n^j_N\right) \tag{A30}$$

is named *detector tensor* and completely describes the direction dependence of the coupling between detector and gravitational waves.

An interesting discussion about the use of the proper detector frame in the high frequency regime can be found in Ref. 207.

[1] C. M. Will, "The Confrontation between General Relativity and Experiment," Living Rev. Relativity **9**, (2006), 3. URL: http://www.livingreviews.org/lrr-2006-3.
[2] M. Maggiore, *Gravitational Waves* (Oxford University Press, Oxfordshire, England, 2008).
[3] B. Allen, Phys. Rev. D **56**, 545 (1997); e-print arXiv:gr-qc/9604033.
[4] E. Komatsu, J. Dunkley, M. R. Nolta, C. L. Bennett, B. Gold, G. Hinshaw, N. Jarosik, D. Larson, M. Limon, L. Page, D. N. Spergel, M. Halpern, R. S. Hill, A. Kogut, S. S. Meyer, G. S. Tucker, J. L. Weiland, E. Wollack, and E. L. Wright, Astrophys. J., Suppl. Ser. **180**, 330 (2009).
[5] F. A. Jenet, G. B. Hobbs, W. van Straten, R. N. Manchester, M. Bailes, J. P.W. Verbiest, R. T. Edwards, A. W. Hotan, J. M. Sarkissian, and S. M. Ord, Astrophys. J. **653**, 1571 (2006); e-print arXiv:astro-ph/0609013.
[6] J. W. Armstrong, "Low-Frequency Gravitational Wave Searches Using Spacecraft Doppler Tracking," Living Rev. Relativity **9**, (2006), 1. URL: http://www.livingreviews.org/lrr-2006-1.
[7] S. Babak, J. R. Gair, A. Petiteau, and A. Sesana, e-print arXiv:cond-mat/1011.2062.
[8] R. Ballantini, P. Bernard, E. Chiaveri, A. Chincarini, G. Gemme, R. Losito, R. Parodi, and E. Picasso, Class. Quantum Grav. **20**, 3505 (2003).
[9] F.-Y. Li and M.-X. Tang, Int. J. Mod. Phys. D **11**, 1049 (2002).
[10] A. M. Cruise, Class. Quantum Grav. **17**, 2525 (2000).
[11] The LIGO scientific collaboration and the Virgo collaboration, Nature (London) **460**, 990 (2009).
[12] The LIGO scientific collaboration and the Virgo scientific collaboration (the LIGO scientific and the Virgo), Phys. Rev. D **81**, 102001 (2010); e-print arXiv:1002.1036.

Downloaded 02 Nov 2011 to 180.149.51.196. Redistribution subject to AIP license or copyright; see http://rsi.aip.org/about/rights_and_permissions

[13]The LIGO scientific collaboration and the Virgo scientific collaboration (LIGO scientific), Phys. Rev. D **82**, 102001 (2010); e-print arXiv:1005.4655.
[14]The LIGO scientific collaboration and the Virgo scientific collaboration (the Virgo), Astrophys. J. **713**, 671 (2010); e-print arXiv:0909.3583.
[15]B. S. Sathyaprakash and Bernard F. Schutz, "Physics, Astrophysics and Cosmology with Gravitational Waves," Living Rev. Relativity **12**, (2009), 2. URL: http://www.livingreviews.org/lrr-2009-2.
[16]L. P. Grishchuk, V. M. Lipunov, K. A. Postnov, M. E. Prokhorov, and B. S. Sathyaprakash, Phys. Usp. **44**, 1 (2001); e-print arXiv:astro-ph/0008481.
[17]M. Pössel, "The wave nature of simple gravitational waves," Einstein Online **2**, 1008 (2006).
[18]R. A. Hulse and J. H. Taylor, Astrophys. J. **195**, L51 (1975).
[19]J. Levine, Phys. Perspect. **6**(1), 42 (2004).
[20]M. Bonaldi, D. Carlesso, E. Cavallini, S. Caruso, A. Colombo, P. Falferi, G. Fontana, P. L. Fortini, R. Mezzena, A. Ortolan, G. A. Prodi, L. Taffarello, G. Vedovato, S. Vitale, and J. P. Zendri, Class. Quantum Grav. **14**, 1491 (1997).
[21]J. Weber, Phys. Rev. Lett. **22**, 1320 (1969).
[22]M. E. Gertsenshtein and V. I. Pustovoit, Sov. Phys. JETP **16**, 433 (1963).
[23]R. Weiss, Q. Prog. Rep. Res. Lab. MIT **105**, 54 (1972).
[24]G. E. Moss, L. R. Miller, and R. L. Forward, Appl. Opt. **10**, 2495 (1971).
[25]J. Hough, S. Rowan, and B. Sathyaprakash, J. Phys. B **38**, S497 (2005).
[26]C. M. Caves, Phys. Rev. D **23**, 1693 (1981).
[27]S. Marka, "Transient multimessenger astronomy with gravitational waves," Class. Quantum Grav. **28**, 114013 (2011).
[28]N. L. Christensen, "Multimessenger Astronomy," eprint arXiv:1105.5843v1.
[29]F. Cavalier, M. Barsuglia, M.-A. Bizouard, V. Brisson, A.-C. Clapson, M. Davier, P. Hello, S. Kreckelbergh, N. Leroy, and M. Varvella, Phys. Rev. D **74** 082004 (2006).
[30]S. Fairhurst, New J. Phys. **11**, 123006 (2009); e-print arXiv:0908.2356.
[31]C. Cutler and J. L. Hernandez-Pastora, *Accuracy of Parameter Estimation within a Network of Gravitational-Wave Detectors*, In Salamanca 1998, Relativity and Gravitation in General (World Scientific, Singapore, 1999), pp. 219–223.
[32]S. V. Dhurandhar and M. Tinto, in *Proceedings of Recent Developments in Theoretical and Experimental General Relativity, Gravitation, and Relativistic Field Theories* (World Scientific, Perth, 1988), pp. 1811–1814.
[33]A. Abramovici, W. E. Althouse, R. W.P. Drever, Y. Gürsel, S. Kawamura, F. J. Raab, D. Shoemaker, L. Sievers, R. E. Spero, K. S. Thorne, R. E. Vogt, R. Weiss, S. E. Whitcomb, and M. E. Zucker, Science **256**, 325 (1992).
[34]C. Bradaschia, R. Del Fabbro, E. Calloni, A. Di Virgilio, R. Flaminio, S. Galeotti, A. Giazotto, L. E. Holloway, H. Kautzky, V. Montelatici, M. Morganti, and D. Passuello, Nucl. Phys. B (Proc. Suppl.) **28A**, 54 (1992).
[35]L. E. Holloway, Nucl. Phys. B (Proc. Suppl.) **54B**, 176 (1997).
[36]H. Kogelink and T. Li, Appl. Opt. **5**, 1550 (1966).
[37]F. Acernese, P. Amico, M. Al-Shourbagy, S. Aoudia, S. Avino, D. Babusci, G. Ballardin, R. Barillé, F. Barone, L. Barsotti, M. Barsuglia, F. Beauville, M. A. Bizouard, C. Boccara, F. Bondu, L. Bosi, C. Bradaschia, S. Braccini, A. Brillet, V. Brisson, L. Brocco, D. Buskulic, E. Calloni, E. Campagna, F. Cavalier, R. Cavalieri, G. Cella, E. Chassande-Mottin, C. Corda, A.-C. Clapson, F. Cleva, J.-P. Coulon, E. Cuoco, V. Dattilo, M. Davier, R. D. Rosa, L. D. Fiore, A. D. Virgilio, B. Dujardin, A. Eleuteri, D. Enard, I. Ferrante, F. Fidecaro, I. Fiori, R. Flaminio, J.-D. Fournier, S. Frasca, F. Frasconi, A. Freise, L. Gammaitoni, A. Gennai, A. Giazotto, G. Giordano, L. Giordano, R. Gouaty, D. Grosjean, G. Guidi, S. Hebri, H. Heitmann, P. Hello, L. Holloway, S. Kreckelbergh, P. L. Penna, V. Loriette, M. Loupias, G. Losurdo, J.-M. Mackowski, E. Majorana, C. N. Man, M. Mantovani, F. Marchesoni, F. Marion, J. Marque, F. Martelli, A. Masserot, M. Mazzoni, L. Milano, C. Moins, J. Moreau, N. Morgado, B. Mours, A. Pai, C. Palomba, F. Paoletti, S. Pardi, A. Pasqualetti, R. Passaquieti, D. Passuello, B. Perniola, F. Piergiovanni, L. Pinard, R. Poggiani, M. Punturo, P. Puppo, K. Qipiani, P. Rapagnani, V. Reita, A. Remillieux, F. Ricci, I. Ricciardi, P. Ruggi, G. Russo, S. Solimeno, A. Spallicci, R. Stanga, R. Taddei, D. Tombolato, M. Tonelli, A. Toncelli, E. Tournefier, F. Travasso, G. Vajente, D. Verkindt, F. Vetrano, A. Viceré, J.-Y. Vinet, H. Vocca, M. Yvert, and Z. Zhang, Class. Quantum Grav. **23**, S91 (2006).
[38]H. Lück, M. Hewitson, P. Ajith, B. Allen, P. Aufmuth, C. Aulbert, S. Babak, R. Balasubramanian, B. W. Barr, S. Berukoff, A. Bunkowski, G. Cagnoli, C. A. Cantley, M. M. Casey, S. Chelkowski, Y. Chen, D. Churches, T. Cokelaer, C. N. Colacino, D. R. M. Crooks, C. Cutler, K. Danzmann, R. J. Dupuis, E. Elliffe, C. Fallnich, A. Franzen, A. Freise, I. Gholami, S. Goßler, A. Grant, H. Grote, S. Grunewald, J. Harms, B. Hage, G. Heinzel, I. S. Heng, A. Hepstonstall, M. Heurs, S. Hild, J. Hough, Y. Itoh, G. Jones, R. Jones, S. H. Huttner, K. Kötter, B. Krishnan, P. Kwee, M. Luna, B. Machenschalk, M. Malec, R. A. Mercer, T. Meier, C. Messenger, S. Mohanty, K. Mossavi, S. Mukherjee, P. Murray, G. P. Newton, M. A. Papa, M. Perreur-Lloyd, M. Pitkin, M. V. Plissi, R. Prix, V. Quetschke, V. Re, T. Regimbau, H. Rehbein, S. Reid, L. Ribichini, D. I. Robertson, N. A. Robertson, C. Robinson, J. D. Romano, S. Rowan, A. Rüdiger, B. S. Sathyaprakash, R. Schilling, R. Schnabel, B. F. Schutz, F. Seifert, A. M. Sintes, J. R. Smith1, P. H. Sneddon, K. A. Strain, I. Taylor, R. Taylor, A. Thüring, C. Ungarelli, H. Vahlbruch, A. Vecchio, J. Veitch, H. Ward, U. Weiland, H. Welling, L. Wen, P. Williams, B. Willke, W. Winkler, G. Woan, and R. Zhu, Class. Quantum Grav. **23**, S71 (2006).
[39]I. Zawischa, M. Brendel, K. Danzmann, C. Fallnich, M. Heurs, S. Nagano, V. Quetschke, H. Welling, and B. Willke, Class. Quantum Grav. **19**, 1775 (2002).
[40]H. Grote, A. Freise, M. Malec, G. Heinzel, B. Willke, H. Lück, K. A. Strain, J. Hough, and K. Danzmann, Class. Quantum Grav. **21**, S473 (2004).
[41]J. E. Logan, J. Hough, and R. D. Thomson, Phys. Lett. A **218**, 181 (1996).
[42]M. Lorenzini, E. Cesarini, G. Cagnoli, E. Campagna, K. Haughian, J. Hough, G. Losurdo, F. Martelli, I. Martin, F. Piergiovanni, S. Reid, S. Rowan, A. A. van Veggel, and F. Vetrano, J. Phys.: Conf. Ser. **228**, 012019 (2010).
[43]K. Arai, J. Phys.: Conf. Ser. **120**, 032010 (2008).
[44]F. Kawazoe, K. Kokeyama, S. Sato, O. Miyakawa, K. Somiya, M. Fukushima, N. Arai, S. Kawamura, and A. Sugamoto, J. Phys.: Conf. Ser. **32**, 380 (2006).
[45]K. Kuroda, Class. Quantum Grav. **27**, 084004 (2010).
[46]A. Einstein, Sitzungsber. Preuss. Akad. Wiss., Phys. Math. Kl. **1916**, 688.
[47]H. Bondi, Nature (London) **179**, 1072 (1957).
[48]A. Nishizawa, A. Taruya, K. Hayama, S. Kawamura, and M.-a. Sakagami, Phys. Rev. D **79**, 082002 (2009).
[49]In fact, in this case the coupling is exactly zero for a wave which propagates in a direction orthogonal to the plane defined by the interferometer arms. However, this is not true for a generic direction.
[50]G. Heinzel, A. Freise, H. Grote, K. Strain, and K. Danzmann, Class. Quantum Grav. **19**, 1547 (2002).
[51]M. Landry, AIP Conf. Proc. **983**, 627 (2008).
[52]K. Kotter, I. S. Heng, M. Hewitson, K. Strain, G. Woan, and H. Ward, Class. Quantum Grav. **20**, S895 (2003).
[53]K. Ishidoshiro, M. Ando, K. Tsubono, N. Kanda, and H. Takahashi, Class. Quantum Grav. **24**, S405 (2007).
[54]F. Barone, R. De Rosa, A. Eleuteri, L. Milano, and K. Qipiani, IEEE Trans. Nucl. Sci. **49**, 405 (2002).
[55]C. M. Caves, K. S. Thorne, R. W.P. Drever, V. D. Sandberg, and M. Zimmermann, Rev. Mod. Phys. **52**, 341 (1980).
[56]K. S. Thorne, R. W. P. Drever, C. M. Caves, M. Zimmermann, and V. D. Sandberg, Phys. Rev. Lett. **40**, 667 (1978).
[57]V. B. Braginsky and F. Y. Khalili, *Quantum Measurement* (Cambridge University Press, Cambridge, England, 1995).
[58]E. Black, Am. J. Phys. **69**, 79 (2001).
[59]R. W.P. Drever, J. L. Hall, F. V. Kowalski, J. Hough, G. M. Ford, A. J. Munley, and H. Ward, Appl. Phys. B **31**, 97 (1983).
[60]D. S. N. Mavalvala and D. Sigg, Appl. Opt. **37**, 7743 (1998).
[61]D. Babusci, H. Fang, G. Giordano, G. Matone, L. Matone, and V. Sannibale, Phys. Lett. A **226**, 31 (1997).
[62]D. Z. Anderson, Appl. Opt. **23**, 2944 (1984).
[63]E. Morrison, B. J. Meers, D. I. Robertson, and H. Ward, Appl. Opt. **33**, 5041 (1994).
[64]F. Cavalier, *Le Controle Globale de Virgo*, These d'habilitation a diriger de reserches (Universitè de Paris Sud, Paris, 2001).
[65]M. Evans, N. Mavalvala, P. Fritschel, R. Bork, B. Bhawal, R. Gustafson, W. Kells, M. Landry, D. Sigg, R. Weiss, S. Whitcomb, and H. Yamamoto, Opt. Lett. **27**, 598 (2002).
[66]F. Acernese, P. Amico, M. Al-Shourbagy, S. Aoudia, S. Avino, D. Babusci, G. Ballardin, R. Barillé, F. Barone, L. Barsotti, M.

Downloaded 02 Nov 2011 to 180.149.51.196. Redistribution subject to AIP license or copyright; see http://rsi.aip.org/about/rights_and_permissions

Barsuglia, F. Beauville, M. A. Bizouard, C. Boccara, F. Bondu, L. Bosi, C. Bradaschia, S. Braccini, A. Brillet, V. Brisson, L. Brocco, D. Buskulic, E. Calloni, E. Campagna, F. Cavalier, R. Cavalieri, G. Cella, E. Chassande-Mottin, C. Corda, A.-C. Clapson, F. Cleva, J.-P. Coulon, E. Cuoco, V. Dattilo, M. Davier, R. D. Rosa, L. D. Fiore, A. D. Virgilio, B. Dujardin, A. Eleuteri, D. Enard, I. Ferrante, F. Fidecaro, I. Fiori, R. Flaminio, J.-D. Fournier, S. Frasca, F. Frasconi, A. Freise, L. Gammaitoni, A. Gennai, A. Giazotto, G. Giordano, L. Giordano, R. Gouaty, D. Grosjean, G. Guidi, S. Hebri, H. Heitmann, P. Hello, L. Holloway, S. Kreckelbergh, P. L. Penna, V. Loriette, M. Loupias, G. Losurdo, J.-M. Mackowski, E. Majorana, C. N. Man, M. Mantovani, F. Marchesoni, F. Marion, J. Marque, F. Martelli, A. Masserot, M. Mazzoni, L. Milano, C. Moins, J. Moreau, N. Morgado, B. Mours, A. Pai, C. Palomba, F. Paoletti, S. Pardi, A. Pasqualetti, R. Passaquieti, D. Passuello, B. Perniola, F. Piergiovanni, L. Pinard, R. Poggiani, M. Punturo, P. Puppo, K. Qipiani, P. Rapagnani, V. Reita, A. Remillieux, F. Ricci, I. Ricciardi, P. Ruggi, G. Russo, S. Solimeno, A. Spallicci, R. Stanga, R. Taddei, D. Tombolato, M. Tonelli, A. Toncelli, E. Tournefier, F. Travasso, G. Vajente, D. Verkindt, F. Vetrano, A. Viceré, J.-Y. Vinet, H. Vocca, M. Yvert, Z. Zhang, and M. Evans, Class. Quantum Grav. **23**, S85 (2006).

[67] A. E. Siegman, *Lasers* (University Science Book, Sausalito, 1986).

[68] C. N. Man, J. Phys. IV France **04**, C4-311-C4-319 (1994).

[69] A. Araya, N. Mio, K. Tsubono, K. Suehiro, S. Telada, M. Ohashi, and M.-K. Fujimoto, Appl. Opt. **36**, 1446 (1997).

[70] S. Vyatchanin and A. B. Matsko, JETP **83**, 690 (1996).

[71] C. M. Caves and B. L. Schumaker, Phys. Rev. A **31**, 3068 (1985).

[72] B. L. Schumaker and C. M. Caves, Phys. Rev. A **31**, 3093 (1985).

[73] H. J. Kimble, Y. Levin, A. B. Matsko, K. S. Thorne, and S. P. Vyatchanin, Phys. Rev. D **65**, 022002 (2002); e-print arXiv:gr-qc/0008026.

[74] It can be objected that quantum uncertainties forbid the introduction of a probability distribution in phase space. This is true, and our considerations must be understood in a semiclassical sense. It is also possible to reformulate them in a more rigorous way using a quantum quasiprobability distribution, for example, the Wigner function. See also, for example, Ref. 97.

[75] V. B. Braginsky, M. L. Gorodetsky, F. Y. Khalili, A. B. Matsko, K. S. Thorne, and S. P. Vyatchanin, Phys. Rev. D **67**, 082001 (2003); e-print arXiv:gr-qc/0109003.

[76] L. Schnupp, in *Proceedings at a European Collaboration Meeting on Interferometric Detection of Gravitational Waves* (Sorrento, Italy, 1988).

[77] R. Takahashi, J. Mizuno, S. Miyoki, and N. Kawashima, Phys. Lett. A **187**, 157 (1994).

[78] S. Hild, H. Grote, J. Degallaix, S. Chelkowski, K. Danzmann, A. Freise, M. Hewitson, J. Hough, H. Lueck, M. Prijatelj, K. A. Strain, J. R. Smith, and B. Willke, Class. Quantum Grav. **26**, 055012 (2009); e-print arXiv:0811.3242.

[79] A. A. Michelson and E. W. Morley, Am. J. Sci. **34**, 333 (1887).

[80] P. Fritschel, *Technical Plenary Session of the LSC Meeting Hannover*, Technical Report No. LIGO-GEO30460-00 R, 2003/lIGO-GEO30460-00.

[81] A. Buonanno, Y.-b. Chen, and N. Mavalvala, Phys. Rev. D **67**, 122005 (2003); e-print arXiv:gr-qc/0302041.

[82] V. Chickarmane, S. V. Dhurandhar, T. C. Ralph, M. Gray, H.-A. Bachor, and D. E. McClelland, Phys. Rev. A **57**, 3898 (1998).

[83] R. L. Ward, R. Adhikari, B. Abbott, R. Abbott, D. Barron, R. Bork, T. Fricke, V. Frolov, J. Heefner, A. Ivanov, O. Miyakawa, K. McKenzie, B. Slagmolen, M. Smith, R. Taylor, S. Vass, S. Waldman, and A. Weinstein, Class. Quantum Grav. **25**, 114030 (2008).

[84] H. Grote and the LIGO scientific collaboration, Class. Quantum Grav. **27**, 084003 (2010).

[85] K. Somiya, Y. Chen, S. Kawamura, and N. Mio, Phys. Rev. D **73**, 122005 (2006).

[86] A. Weinstein, Class. Quantum Grav. **19**, 1575 (2002).

[87] A. Di Virgilio, L. Barsotti, S. Braccini, C. Bradaschia, G. Cella, C. Corda, V. Dattilo, I. Ferrante, F. Fidecaro, I. Fiori, F. Frasconi, A. Gennai, A. Giazotto, P. La Penna, G. Losurdo, E. Majorana, M. Mantovani, A. Pasqualetti, D. Passuello, F. Piergiovanni, A. Porzio, P. Puppo, P. Rapagnani, F. Ricci, S. Solimeno, G. Vajente, and F. Vetrano, Phys. Rev. A **74**, 013813 (2006).

[88] A. Buonanno and Y. Chen, Class. Quantum Grav. **18**, L95 (2001); e-print arXiv:gr-qc/0010011.

[89] A. Buonanno and Y.-b. Chen, Phys. Rev. D **64**, 042006 (2001); e-print arXiv:gr-qc/0102012.

[90] A. Buonanno and Y. Chen, Phys. Rev. D **65**, 042001 (2002); e-print arXiv:gr-qc/0107021.

[91] A. Buonanno and Y.-b. Chen, Class. Quantum Grav. **19**, 1569 (2002); e-print arXiv:gr-qc/0201063.

[92] J. Harms, Y. Chen, S. Chelkowski, A. Franzen, H. Vahlbruch, K. Danzmann, and R. Schnabel, Phys. Rev. D **68**, 042001 (2003).

[93] S. Mancini and P. Tombesi, Phys. Rev. A **49**, 4055 (1994).

[94] C. Fabre, M. Pinard, S. Bourzeix, A. Heidmann, E. Giacobino, and S. Reynaud, Phys. Rev. A **49**, 1337 (1994).

[95] S. Bose, K. Jacobs, and P. L. Knight, Phys. Rev. A **56**, 4175 (1997).

[96] T. Corbitt, Y. Chen, F. Khalili, D. Ottaway, S. Vyatchanin, S. Whitcomb, and N. Mavalvala, Phys. Rev. A **73**, 023801 (2006).

[97] W. Schleich, *Quantum Optics in Phase Space* (Wiley VCH, Weinheim, 2001).

[98] P. Purdue and Y.-b. Chen, Phys. Rev. D **66**, 122004 (2002); e-print arXiv:gr-qc/0208049.

[99] V. B. Braginsky and F. Y. Khalili, Phys. Lett. A **147**, 251 (1990).

[100] V. B. Braginsky, M. L. Gorodetsky, F. Y. Khalili, and K. S. Thorne, Phys. Rev. D **61**, 044002 (2000); e-print arXiv:gr-qc/9906108.

[101] Y.-b. Chen, Phys. Rev. D **67**, 122004 (2003); e-print arXiv:gr-qc/0208051.

[102] B. J. Meers, Phys. Rev. **D 38**, 2317 (1988).

[103] A. Buonanno and Y.-b. Chen, Phys. Rev. D **67**, 062002 (2003); e-print arXiv:gr-qc/0208048.

[104] A. Buonanno and Y.-b. Chen, Phys. Rev. D **69**, 102004 (2004); e-print arXiv:gr-qc/0310026.

[105] V. B. Braginsky, M. L. Gorodetsky, and F. Y. Khalili, Phys. Lett. **A232**, 340 (1997).

[106] B. S. Sheard, M. B. Gray, C. M. Mow-Lowry, D. E. McClelland, and S. E. Whitcomb, Phys. Rev. A **69**, 051801 (2004).

[107] V. B. Braginsky and F. Y. Khalili, Phys. Lett. A **257**, 241 (1999).

[108] A. Dorsel, J. D. McCullen, P. Meystre, E. Vignes, and H. Walther, Phys. Rev. Lett. **51**, 1550 (1983).

[109] P. Meystre, E. M. Wright, J. D. McCullen, and E. Vignes, J. Opt. Soc. Am. B **2**, 1830 (1985).

[110] A. Pai, S. Dhurandhar, P. Hello, and J. Vinet, Eur. Phys. J. D **8**, 333 (2000).

[111] J.-M. Courty, A. Heidmann, and M. Pinard, Phys. Rev. Lett. **90**, 083601 (2003); e-print arXiv:gr-qc/0212081.

[112] J. M. Courty, A. Heidmann, and M. Pinard, Europhys. Lett. **63**, 226 (2003); e-print arXiv:gr-qc/0301068.

[113] A. Heidmann, J.-M. Courty, M. Pinard, and J. Lebars, J. Opt. B: Quantum Semiclassical Opt. **6**, S684 (2004); e-print arXiv:quant-ph/0311167.

[114] A. Heidmann, J. M. Courty, and M. Pinard, Class. Quantum Grav. **21**, S1053 (2004).

[115] D. Vitali, S. Mancini, P. Tombesi, M. Punturo, and P. Amico, J. Opt. B: Quantum Semiclassical Opt. **6**, S691 (2004); e-print arXiv:gr-qc/0311061.

[116] A. Giazotto and G. Cella, Class. Quantum Grav. **21**, S1183 (2004).

[117] U. Leonhardt, *Essential Quantum Optics* (Cambridge University Press, Cambridge, England, 2010).

[118] V. B. Braginsky, A. Gurkovsky, S. E. Strigin, and S. P. Vyatchanin, Phys. Lett. A **362**, 91 (2007); e-print arXiv:gr-qc/0608007.

[119] V. B. Braginsky, S. E. Strigin, and S. P. Vyatchanin, Phys. Lett. A **305**, 111 (2002); e-print arXiv:gr-qc/0209064.

[120] V. B. Braginsky, S. E. Strigin, and S. P. Vyatchanin, Phys. Lett. A **287**, 331 (2001); e-print arXiv:gr-qc/0107079.

[121] K. McKenzie, N. Grosse, W. P. Bowen, S. E. Whitcomb, M. B. Gray, D. E. McClelland, and P. K. Lam, Phys. Rev. Lett. **93**, 161105 (2004); e-print arXiv:quant-ph/0405137.

[122] K. Mckenzie, D. A. Shaddock, D. E. McClelland, B. C. Buchler, and P. K. Lam, Phys. Rev. Lett. **88**, 231102 (2002); e-print arXiv:quant-ph/0205043.

[123] H. Vahlbruch, A. Khalaidovski, N. Lastzka, C. Graef, K. Danzmann, and R. Schnabel, Class. Quantum Grav. **27**, 084027 (2010); e-print arXiv:1004.4975.

[124] S. Chelkowski, "*Squeezed Light and Laser Interferometric Gravitational Wave Detectors*," Ph.D. Dissertation, Gottfried Wilhelm Leibniz Universität Hannover (2007).

[125] K. Goda, O. Miyakawa, E. E. Mikhailov, S. Saraf, R. Adhikari, K. McKenzie, R. Ward, S. Vass, A. J. Weinstein, and N. Mavalvala, Nat. Phys. **4**, 472 (2008).

[126] H. Vahlbruch, Squeezing geo600, (2010), lIGO Document G1000870-v1, LSC-Virgo September 2010 Meeting held on 20 Sept. 2010 in Cracow, Poland.

[127] H. Grote, Geo600 status, LIGO Document G1100206-v1.

Downloaded 02 Nov 2011 to 180.149.51.196. Redistribution subject to AIP license or copyright; see http://rsi.aip.org/about/rights_and_permissions

[128]R. Schnabel, J. Harms, K. A. Strain, and K. Danzmann, Class. Quantum Grav. **21**, S1045 (2004); e-print arXiv:gr-qc/0401119.
[129]P. K. Lam, T. C. Ralph, B. C. Buchler, D. E. McClelland, H.-A. Bachor, and J. Gao, J. Opt. B: Quantum Semiclassical Opt. **1**, 469 (1999).
[130]M. Xiao, L.-A. Wu, and H. J. Kimble, Phys. Rev. Lett. **59**, 278 (1987).
[131]T. Corbitt, Y. Chen, F. Khalili, D. Ottaway, S. Vyatchanin, S. Whitcomb, and N. Mavalvala, Phys. Rev. A **73**, 023801 (2006).
[132]F. Acernese, R. De Rosa, R. De Salvo, F. Garufi, G. Giordano, J. Harms, V. Mandic, A. Sajeva, T. Trancynger, and F. Barone, J. Phys.: Conf. Ser. **228**, 012036 (2010).
[133]H. Hoffmann, J. Winterflood, Y. Cheng, and D. G. Blair, Class. Quantum Grav. **19**, 1709 (2002).
[134]E. J. Daw, J. A. Giaime, D. Lormand, M. Lubinski, and J. Zweizig, Class. Quantum Grav. **21**, 2255 (2004); e-print arXiv:gr-qc/0403046.
[135]J. Harms, F. Acernese, F. Barone, I. Bartos, M. Beker, J. F. J. van den Brand, N. Christensen, M. Coughlin, R. DeSalvo, S. Dorsher, J. Heise, S. Kandhasamy, V. Mandic, S. Márka, G. Mueller, L. Naticchioni, T. O'Keefe, D. S. Rabeling, A. Sajeva, T. Trancynger, and V. Wand, Class. Quantum Grav. **27**, 225011 (2010).
[136]The VIRGO collaboration, Class. Quantum Grav. **21**, S433 (2004).
[137]A. Vicere, paper presented at the*International Summer School on Experimental Physics of Gravitational Waves*, Urbino, Italy, 6–18 September 1999.
[138]S. Braccini, L. Barsotti, C. Bradaschia, G. Cella, A. D. Virgilio, I. Ferrante, F. Fidecaro, I. Fiori, F. Frasconi, A. Gennai, A. Giazotto, F. Paoletti, R. Passaquieti, D. Passuello, R. Poggiani, E. Campagna, G. Guidi, G. Losurdo, F. Martelli, M. Mazzoni, B. Perniola, F. Piergiovanni, R. Stanga, F. Vetrano, A. Viceré, L. Brocco, S. Frasca, E. Majorana, A. Pai, C. Palomba, P. Puppo, P. Rapagnani, F. Ricci, G. Ballardin, R. Barillé, R. Cavalieri, E. Cuoco, V. Dattilo, D. Enard, R. Flaminio, A. Freise, S. Hebri, L. Holloway, P. L. Penna, M. Loupias, J. Marque, C. Moins, A. Pasqualetti, P. Ruggi, R. Taddei, Z. Zhang, F. Acernese, S. Avino, F. Barone, E. Calloni, R. D. Rosa, L. D. Fiore, A. Eleuteri, L. Giordano, L. Milano, S. Pardi, K. Qipiani, I. Ricciardi, G. Russo, S. Solimeno, D. Babusci, G. Giordano, P. Amico, L. Bosi, L. Gammaitoni, F. Marchesoni, M. Punturo, F. Travasso, H. Vocca, C. Boccara, J. Moreau, V. Loriette, V. Reita, J. Mackowski, N. Morgado, L. Pinard, A. Remillieux, M. Barsuglia, M. Bizouard, V. Brisson, F. Cavalier, A. Clapson, M. Davier, P. Hello, S. Krecklbergh, F. Beauville, D. Buskulic, R. Gouaty, D. Grosjean, F. Marion, A. Masserot, B. Mours, E. Tournefier, D. Tombolato, D. Verkindt, M. Yvert, S. Aoudia, F. Bondu, A. Brillet, E. Chassande-Mottin, F. Cleva, J. Coulon, B. Dujardin, J. Fournier, H. Heitmann, C. Man, A. Spallicci, and J. Vinet, Astropart. Phys. **23**, 557 (2005).
[139]R. D. Fabbro, A. D. Virgilio, A. Giazotto, H. Kautzky, V. Montelatici, and D. Passuello, Phys. Lett. A **132**, 237 (1988).
[140]A. Giazotto, Phys. Rep. **182**, 365 (1989).
[141]E. Bougleux, S. Braccini, C. Bradaschia, C. Casciano, G. Cella, V. Dattilo, R. DeSalvo, A. D. Virgilio, G. T. Feng, F. Fidecaro, F. Frasconi, A. Gaddi, A. Giazotto, L. Holloway, P. L. Penna, G. Losurdo, S. Malik, F. Palla, R. Passaquieti, F. Raffaelli, R. Stanga, R. Valentini, and A. Vicere, Nucl. Instrum. Methods Phys. Res. A **409**, 480 (1998).
[142]R. DeSalvo, A. DiVirgilio, A. Errico, F. Guotong, I. Ferrante, F. Frasconi, A. Gaddi, A. Gennai, G. Gennaro, A. Giazotto, L. Holloway, G. Losurdo, M. Maggiore, S. Mancini, M. Mazzoni, F. Palla, P. H. Bao, F. Paoletti, A. Pasqualetti, R. Passaquieti, D. Passuello, R. Poggiani, P. Popolizio, F. Raffaelli, D. Righetti, R. Ruberti, V. Rubino, P. Ruggi, R. Stanga, R. Taddei, R. Valentini, A. Vicere, J. Winterflood, Z. Zhou, M. Bernardini, A. Bozzi, S. Braccini, C. Bradaschia, C. Casciano, G. C. Cella, A. Ciampa, G. Curci, E. D'Ambrosio, V. Dattilo, G. C. DeCarolis, and A. Delapierre, Nucl. Instrum. Meth. A **420**, 316 (1999).
[143]G. Losurdo, G. Calamai, E. Cuoco, L. Fabbroni, G. Guidi, M. Mazzoni, R. Stanga, F. Vetrano, L. Holloway, D. Passuello, G. Ballardin, S. Braccini, C. Bradaschia, R. Cavalieri, R. Cecchi, G. Cella, V. Dattilo, A. D. Virgilio, F. Fidecaro, F. Frasconi, A. Gennai, A. Giazotto, I. Ferrante, P. L. Penna, F. Lelli, T. Lomtadze, A. Marin, S. Mancini, F. Paoletti, A. Pasqualetti, R. Passaquieti, R. Poggiani, R. Taddei, A. Vicere, and Z. Zhang, Rev. Sci. Instrum. **72**, 3653 (2001).
[144]J. Giaime, P. Saha, D. Shoemaker, and L. Sievers, Rev. Sci. Instrum. **67**, 208 (1999).
[145]J. Giaime, B. Lantz, C. Hardham, W. Hua, R. Adhikari, D. DeBra, G. Hammond, J. How, S. Richman, J. Rollins, G. Stapfer, and R. Stebbins, *Advanced Ligo Seismic Isolation System Conceptual Design*, LIGO report LIGO-E010016-00-D (2001). URL: http://www.ligo.caltech.edu/docs/E/E010016-00.pdf.
[146]C. Hardham, G. Allen, D. DeBra, W. Hua, B. Lantz, and J. Nichol, in *Proceedings of Control of Precision Systems, ASPE Topical Meeting* (American Society for Precision Engineering, Raleigh, 2001).
[147]J. Giaime, E. J. Daw, M. Weitz, R. Adhikari, R. Abbott, R. Bork, and J. Heefner, Rev. Sci. Instrum. **74**, 218 (2003).
[148]R. Abbott, R. Adhikari, G. Allen, D. Baglino, C. Campbell, D. Coyne, E. Daw, D. DeBra, J. Faludi, P. Fritschel, A. Ganguli, J. Giaime, M. Hammond, C. Hardham, G. Harry, W. Hua, L. Jones, J. Kern, B. Lantz, K. Lilienkamp, K. Mailand, K. Mason, R. Mittleman, S. Nayfe, D. Ottaway, J. Phinney, W. Rankin, N. Robertson, R. Scheffler, D. H. Shoemaker, S. Wen, M. Zucker, and L. Zuo, Class. Quantum Grav. **21**, S915 (2004).
[149]R. Abbott, R. Adhikari, G. Allen, S. Cowley, E. Daw, D. DeBra, J. Giaime, G. Hammond, M. Hammond, C. Hardham, J. How, W. Hua, W. Johnson, B. Lantz, K. Mason, R. Mittleman, J. Nichol, S. Richman, J. Rollins, D. Shoemaker, G. Stapfer, and R. Stebbins, Class. Quantum Grav. **19**, 1591 (2002).
[150]M. Beccaria, M. Bernardini, E. Bougleux, S. Braccini, C. Bradaschia, C. Casciano, G. Cella, E. Cuoco, E. D'Ambrosio, G. D. Carolis, R. D. Fabbro, R. D. Salvo, A. D. Virgilio, I. Ferrante, F. Fidecaro, R. Flaminio, A. Gaddi, A. Gennai, G. Gennaro, A. Giazotto, L. Holloway, P. L. Penna, G. Losurdo, S. Malik, S. Mancini, J. Nicolas, F. Palla, H. B. Pan, F. Paoletti, A. Pasqualetti, D. Passuello, R. Poggiani, P. Popolizio, F. Raffaelli, A. Vicere, F. Waharte, and Z. Zhang, Nucl. Instrum. Methods Phys. Res. A **394**, 397 (1997).
[151]A. Bertolini, N. Beverini, G. Cella, R. DeSalvo, F. Fidecaro, M. Francesconi, and D. Simonetti, Nucl. Instrum. Methods Phys. Res. A **518**, 233 (2004); Frontier Detectors for Frontier Physics: Proceedings.
[152]A. Bertolini, G. Cella, W. Chenyang, R. de Salvo, J. Kovalik, S. Márka, V. Sannibale, A. Takamori, H. Tariq, and N. Viboud, Nucl. Instrum. Methods Phys. Res. A **461**, 300 (2001); 8th Pisa Meeting on Advanced Detectors.
[153]G. Cella, V. Sannibale, R. DeSalvo, S. Marka, and A. Takamori, Nucl. Instrum. Meth. A **540**, 502 (2005); e-print arXiv:gr-qc/0406091.
[154]B. Lantz, R. Schofield, B. O'Reilly, D. E. Clark, and D. DeBra, Bull. Seismol. Soc. Am. **99**, 980 (2009).
[155]J. Belfi, N. Beverini, F. Bosi, G. Carelli, A. di Virgilio, E. Maccioni, R. Passaquieti, and F. Stefani, Proc. SPIE **7993**, 79931H (2010).
[156]S. A. Hughes and K. S. Thorne, Phys. Rev. D **58**, 122002 (1998); e-print arXiv:gr-qc/9806018.
[157]M. Beccaria, M. Bernardini, S. Braccini, C. Bradaschia, A. Bozzi, C. Casciano, G. Cella, A. Ciampa, E. Cuoco, G. Curci, E. D'Ambrosio, V. Dattilo, G. D. Carolis, R. D. Salvo, A. D. Virgilio, A. Delapierre, D. Enard, A. Errico, G. Feng, I. Ferrante, F. Fidecaro, F. Frasconi, A. Gaddi, A. Gennai, G. Gennaro, A. Giazotto, P. L. Penna, G. Losurdo, M. Maggiore, S. Mancini, F. Palla, H. B. Pan, F. Paoletti, A. Pasqualetti, R. Passaquieti, D. Passuello, R. Poggiani, P. Popolizio, F. Raffaelli, S. Rapisarda, A. Viceré, and Z. Zhang, "Relevance of Newtonian seismic noise for the VIRGO interferometer sensitivity," Class. Quantum Grav. **15**, 3339 (1998).
[158]P. R. Saulson, Phys. Rev. D **30**, 732 (1984).
[159]J. F. J. van den Brand, M. G. Beker, M. Doets, E. Hennes, and D. S. Rabeling, J. Phys.: Conf. Ser. **203**, 012076 (2010).
[160]G. Cella, "Off-line Subtraction of Seismic Newtonian Noise," in Recent developments in general relativity," edited by B. Casciaro, D. Fortunato, M. Francaviglia, and A. Masiello (Springer, Milano, 2000), 495.
[161]J. Harms, R. DeSalvo, S. Dorsher, and V. Mandic, Phys. Rev. D **80**, 122001 (2009); e-print arXiv:0909.3341.
[162]M. G. Beker, J. F. J. van den Brand, E. Hennes, and D. S. Rabeling, J. Phys.: Conf. Ser. **228**, 012034 (2010).
[163]M. G. Beker, G. Cella, R. DeSalvo, M. Doets, H. Grote, J. Harms, E. Hennes, V. Mandic, D. S. Rabeling, J. F. J. van den Brand, and C. M. van Leeuwen, "Improving the sensitivity of future GW observatories in the 1-10 Hz band: Newtonian and seismic noise," Gen. Relativ. Gravit. **43**, 2 (2010).
[164]H. B. Callen and R. F. Greene, Phys. Rev. **86**, 702 (1952).
[165]Y. Levin, Phys. Rev. D **57**, 659 (1998); e-print arXiv:gr-qc/9707013.
[166]S. Rowan, J. Hough, and D. R. M. Crooks, Phys. Lett. A **347**, 25 (2005).
[167]K. Numata, G. Bertolotto Bianc, M. Tanaka, S. Otsuka, K. Kawabe, M. Ando, and K. Tsubono, Phys. Lett. A **284**, 162 (2001).
[168]M. Alshourbagy, P. Amico, L. Bosi, G. Cagnoli, E. Campagna, F. Cottone, A. Dari, L. Gammaitoni, M. Lorenzini, G. Losurdo, F. Marchesoni, F. Martelli, F. Piergiovanni, M. Punturo, A. Toncelli,

Downloaded 02 Nov 2011 to 180.149.51.196. Redistribution subject to AIP license or copyright; see http://rsi.aip.org/about/rights_and_permissions

M. Tonelli, F. Travasso, F. Vetrano, and H. Vocca, Rev. Sci. Instrum. **77**, 4 (2006).
[169]M. Alshourbagy, P. Amico, L. Bosi, G. Cagnoli, E. Campagna, F. Cottone, A. Dari, L. Gammaitoni, M. Lorenzini, G. Losurdo, F. Marchesoni, F. Martelli, F. Piergiovanni, M. Punturo, A. Toncelli, M. Tonelli, F. Travasso, F. Vetrano, and H. Vocca, Class. Quantum Grav. **23**, 8 (2006).
[170]M. L. Gorodetsky, Phys. Lett. A **372**, 6813 (2008).
[171]S. Reida, G. Cagnoli, D. R. M. Crooks, J. Houg, P. Murray, S. Rowan, M. M. Fejer, R. Route, and S. Zappe, Phys. Lett. A **351**, 205 (2006).
[172]E. D. Black and K. G. Libbrecht, Phys. Rev. Lett. **93**, 241101 (2004).
[173]T. Uchiyama, T. Tomaru, M. E. Tobar, D. Tatsumi, S. Miyoki, M. Ohashi, and K. Kuroda, Phys. Lett. A **261**, 5 (1999).
[174]Y. T. Liu and K. S. Thorne, Phys. Rev. **D 62**, 122002 (2000); e-print arXiv:gr-qc/0002055.
[175]D. R. M. Crooks, P. Sneddon, G. Cagnoli, J. Hough, S. Rowan, M. M. Fejer, E. Gustafson, R. Route, N. Nakagawa, D. Coyne, G. M. Harry, and A. M. Gretarsson, Class. Quantum Grav. **19**, 4229 (2002).
[176]G. M. Harry, A. M. Gretarsson, P. R. Saulson, S. E. Kittelberger, S. D. Penn, W. J. Startin, S. Rowan, M. M. Fejer, D. R. M. Crooks, G. Cagnoli, J. Hough, and N. Nakagawa, Class. Quantum Grav. **19**, 897 (2002).
[177]S. D. Penn, P. H. Sneddon, H. Armandula, J. C. Betzwieser, G. Cagnoli, J. Camp, D. R. M. Crooks, M. M. Fejer, A. M. Gretarsson, G. M. Harry, J. Hough, S. E. Kittelberger, M. J. Mortonson, R. Route, S. Rowan, and C. C. Vassiliou, Class. Quantum Grav. **20**, 2917 (2003).
[178]D. R. M. Crooks, G. Cagnoli, M. M. Fejer, A. Gretarsson, G. Harry, J. Hough, N. Nakagawa, S. Penn, R. Route, S. Rowan, and P. H. Sneddon, Class. Quantum Grav. **21**, S1059 (2004).
[179]G. Cella and A. Giazotto, Phys. Rev. D **74**, 042001 (2006).
[180]K. Numata, M. Ando, K. Yamamoto, S. Otsuka, and K. Tsubono, Phys. Rev. Lett. **91**, 260602 (2003).
[181]K. Yamamoto, S. Miyoki, T. Uchiyama, H. Ishitsuka, M. Ohashi, K. Kuroda, T. Tomaru, N. Sato, T. Suzuki, T. Haruyama, A. Yamamoto, T. Shintomi, K. Numata, K. Waseda, K. Ito, and K. Watanabe, Phys. Rev. D **74**, 022002 (2006).
[182]A. E. Villar, E. D. Black, R. DeSalvo, K. G. Libbrecht, C. Michel, N. Morgado, L. Pinard, I. M. Pinto, V. Pierro, V. Galdi, M. Principe, and I. Taurasi, Phys. Rev. D **81**, 122001 (2010).
[183]J.-Y. Vinet, Class. Quantum Grav. **24**, 3897 (2007).
[184]E. D'Ambrosio, R. O'shaugnessy, K. Thorne, P. Willems, S. Strigin, and S. Vyatchanin, Class. Quantum Grav. **21**, S867 (2004).
[185]R. W. P. Drever, in *Proceedings of the Seventh Marcel Grossman Meeting on Recent Developments in Theoretical and Experimental General Relativity, Gravitation, and Relativistic Field Theories*, edited by R. T. Jantzen, G. Mac Keiser, and R. Ruffini (World Scientific, Singapore, 1996), pp. 1401–1407.
[186]K. X. Sun and R. Byer, Opt. Lett. **15**, 567 (1998).
[187]J. Hallam, S. Chelkowski, A. Freise, B. W. Barr, S. Hild, K. A. Strain, O. Burmeister, and R. Schnabel, J. Phys.: Conf. Ser. **228**, 012022 (2010).
[188]J. Hallam, S. Chelkowski, A. Freise, S. Hild, B. Barr, K. A. Strain, O. Burmeister, and R. Schnabel, J. Opt. A, Pure Appl. Opt. **11**, 085502 (2009); e-print arXiv:0903.3324.
[189]A. Freise, A. Bunkowski, and R. Schnabel, New J. Phys. **9**, 433 (2007); e-print arXiv:0711.0291.
[190]Y. Levin, Phys. Lett. A **372**, 1941 (2008).
[191]G. Cagnoli, L. Gammaitoni, J. Hough, J. Kovalik, S. McIntosh, M. Punturo, and S. Rowan, Phys. Rev. Lett. **85**, 2442 (2000).
[192]L. D. Landau and L. P. Pitaevskii, *Theory of Elasticity* (Butterworth/Heinemann, Oxford, London, 1986), Vol. 7.
[193]G. Cagnoli, J. Hough, D. DeBra, M. M. Fejer, E. Gustafson, S. Rowan, and V. Mitrofanov, Phys. Lett. A **272**, 39 (2000).
[194]P. Hello and J. Vinet, J. Phys. (France) **51**, 1267 (1990).
[195]P. Hello and J. Y. Vinet, Phys. Lett. A **178**, 351 (1993).
[196]P. Hello, Eur. Phys. J. D **15**, 373 (2001); e-print arXiv:gr-qc/0104059.
[197]J. C. Kamp, H. Kawamura, R. Passaquieti, and R. DeSalvo, Nucl. Instrum. Meth. A **607**, 530 (2009).
[198]J. Mizuno, K. A. Strain, P. G. Nelson, J. M. Chen, R. Schilling, A. Rüdiger, W. Winkler, and K. Danzmann, Phys. Lett. A **175**, 273 (1993).
[199]G. Heinzel, J. Mizuno, R. Schilling, W. Winkler, A. Rüdiger, and K. Danzmann, Phys. Lett. A **217**, 305 (1996).
[200]S. Sato, S. Kawamura, K. Kokeyama, F. Kawazoe, and K. Somiya, Phys. Rev. D **75**, 082004 (2007).
[201]E. Müller, M. Rampp, R. Buras, H.-T. Janka, and D. H. Shoemaker, Astrophys. J. **603**, 221 (2004).
[202]C. J. Horowitz and K. Kadau, Phys. Rev. Lett. **102**, 191102 (2009).
[203]We neglect for simplicity the effect of the displacement of the front mirror on the field which is directly reflected by it, which is small if the finesse of the cavity is high enough.
[204]K.-P. Marzlin, Gen. Relativ. Gravit. **26**, 619 (1994); e-print arXiv:gr-qc/9402010.
[205]K.-P. Marzlin, Phys. Rev. D **50**, 888 (1994); e-print arXiv:gr-qc/9403044.
[206]K. S. Thorne, in *Gravitational Radiation*, edited by N. Deruelle and T. Piran (Elsevier, Oxford, 1983), pp. 1–57.
[207]M. Rakhmanov, Phys. Rev. D **71**, 084003 (2005).

Downloaded 02 Nov 2011 to 180.149.51.196. Redistribution subject to AIP license or copyright; see http://rsi.aip.org/about/rights_and_permissions